FATIGUE BEHAVIOUR OF COMPOSITES UNDER VIBRATION AND THERMAL LOADING

Georgios Voudouris

A dissertation submitted to the University of Bristol in accordance with the requirements for award of the degree of Doctor of Philosophy in the Faculty of Engineering.

University of Bristol

Faculty of Engineering

Department of Aerospace Engineering

June 2019

Word Count: 37000

Abstract

This thesis work examines the fatigue life of composite laminates under vibration fatigue loading and elevated ambient temperature conditions. Thus, the main objective of the current study is to pave the way on the rarely – discussed subject of vibration fatigue of composites under various exposure temperatures. This dissertation will guide the reader through the design of the testing method, which takes into account the environmental conditions while utilising a pre – defined failure criterion. Also, it focuses on the main aspects of the experimental procedure and highlights the common challenges associated with the procedure in order to achieve quality results and improve repeatability. Throughout the chapters, an overview on the accumulation of damage will support both the experimental and numerical investigations, aiming to generate insight regarding the physics that govern the fatigue behaviour of composites. Having identified the distinct stages of the mechanical and thermal responses and the size of fatigue damage accumulated at the respective stages during endurance, the outcomes of the novel testing method are discussed; aiming to link the two responses of composite laminates. The knowledge gathered, about the damage growth and its dependency to ambient thermal loads, is then employed in order to explore more complicated conditions such as the suspension of damage during endurance testing. Experimental results are supported by the numerical descriptions of the behaviour of composites, which can be captured by a FEA conducted in a synthetic dynamic environment. In the end, the conditions that govern vibration fatigue failure were unravelled, incorporating both experimental and numerical investigations. Finally, this dissertation will conclude highlighting the most interesting points that emerged throughout this project while suggesting how they can be exploited to pave the way for interesting future works.

Acknowledgements

First and foremost, I would like to thank Dr. Di Maio who gave me the opportunity to continue my studies and be a part of this project. Dario I would like to sincerely thank you for supporting and believing in me throughout all the stages of this project.

I would also like to express a big thank you to Dr. Sever for giving me the opportunity to work on this project and collaborate with a prestigious company as well as for his continuous support on this project.

Last but not least, I want to express my gratitude to Dr. Kawashita for all the constructive discussions and insightful guidance.

June 25, 2019

G. V

"I am indebted to my parents for living but to my teacher for living well"

- Alexander the Great - Ancient Greek King

Author’s Declaration

Publications

[1] G. Voudouris, D. Di Maio, and I. Sever, 'High Cycle Vibration Fatigue of CFRP under Elevated Ambient Temperatures', Submitted to 18th European Conference on Composite Materials, Athens, Greece, 2018.

[2] G. Voudouris, D. Di Maio, and I. Sever, 'Failure Behaviour of Composites Under Both Vibration Loading and Environmental Conditions', in *Model Validation and Uncertainty Quantification, Volume 3*, 2019, pp. 25–32.

Contents

List of Figures **9**

List of Tables **15**

Nomenclature **16**

1 Introduction **1**

1.1 Aim of the Research 1

1.2. Thesis Outline 3

2 Literature Review **6**

2.1. Introduction 6

2.2. Introduction to Composite Materials 8

2.2.1. From Metals to Composites 9

2.2.2. Introduction to Fibre Reinforced Polymers 10

2.3. Damage Mechanisms in Composites 13

2.3.1. The free – edge effect 15

2.4. Fatigue in Composites 16

2.4.1. Cyclic Loading 17

2.4.2. The phases of Fatigue Damage development 18

2.5. Overview on the Temperature Effects 20

2.5.1. Fracture Toughness 20

2.5.2. Fatigue Delamination Growth Rate 22

2.6. Overview on Vibration Fatigue 25

2.6.1. Introduction to Dynamics 25

2.6.2. Fatigue by vibration loading 27

2.7. The Self – Heating Effect 28

2.7.1. The Time – Temperature Superposition Principle 31

2.8. Fatigue Damage Modelling 32

2.8.1. Introduction in the Fatigue Damage Modelling 32

2.8.2. The Virtual Crack Closure Technique 33

2.8.3. The Paris' Law in Fatigue Damage Modelling 36

2.9. Conclusion 37

3 A New Approach for Vibration Testing at Elevated Temperatures 38

3.1. Background 38

3.2. Apparatus and Experimental Set Up 42

3.2.1. Acquisition Systems 44

3.2.2. The Fixture 45

3.2.3. Environmental Chamber 47

3.2.4. The Specimen 49

3.3. Vibration Testing Method 52

3.3.1. Experimental Procedure 54

3.3.2. Modal Analysis 59

3.3.3. Strain and Vibration Amplitude 60

3.4. Remarks 62

4 Experimental Investigation of Fatigue Life 63

4.1. Introduction 63

4.2. Mechanical and Thermal Responses during endurance 64

4.3. Fatigue Damage Evolution 67

4.3.1. The initial stage of Fatigue Testing 70

4.3.2. Development of Fatigue Damage 71

4.3.3. A Final Stage of Fatigue Testing 78

4.4. Fatigue Life at Elevated Temperatures 80

4.4.1. Self – Heating Temperatures 80

4.4.2. S – N Curve 83

4.4.3. Response Phase and Damage Propagation 85

4.5. The relationship between the Thermal and Mechanical Responses 87

4.6. Suspension of Fatigue Damage 92

4.7. Remarks 95

5 Simulating the Vibration Fatigue Testing 97

5.1. Introduction 97

5.2. Modelling the Dynamic Environment 99

5.3. Prediction of Damage Evolution 102

5.3.1. The Virtual Crack Closure Technique 103

5.3.2. Delamination in a 2D Model 105

5.3.3. Viscoelastic Temperature in a 3D Model 108

5.3.4. Simulation of Frictional Heat in 3D Model 116

5.4. Remarks 120

6 A Numerical Examination of the Fatigue Life 121

6.1. Introduction 121

6.2. The Mechanical Response by means of dynamic VCCT 122

6.2.1. The Effects of different Severity Levels 123

6.2.2. The Effects of different Environmental Temperature Levels 128

6.2.3. Suspension of Fatigue Damage 133

6.3. The Thermal Response by means of multi – physics FE Models 135

6.3.1. Self – Heating on Pristine Specimens 136

6.3.2. Self – Heating on Delaminated Specimens 137

6.3.3. Self – Heating and Damage Evolution 138

6.4. The relationship between the Thermal and Mechanical Responses 142

6.5. Discussion on the vibration Fatigue Testing 145

6.5.1. The Critical Event 145

6.5.2. Crack Growth Propagation Rate 148

6.6. Remarks 151

7 Conclusions 153

7.1. The novelties 153

7.2. Future Work 156

Bibliography 159

List of Figures

2.1 2.1 Prediction and observation of the amount of cracks in off – axis plies of a $[0, 90, \pm 45]_S$ laminate under fatigue loading at the two thirds of the ultimate tensile strength [8] 11

2.2 Development of damage in composites laminates [13] 12

2.3 Damage Mechanisms in impacted FRP [14] 13

2.4 Characteristic Modes of Separation [15] 14

2.5 Typical sinusoidal loading behaviour over time [19] 17

2.6 Schematic representation of Paris' Law [19] 19

2.7 Temperature effect on the Damage Growth Rate for a CFRP (HTA/6376C) [34] 23

2.8 Temperature effect on the Damage Growth Rate for a CFRP (IM7 /8552) [37] 24

2.9 Schematic representation of Mass – Spring – Damper System [19] 25

2.10 Schematic representation of Electromagnetic Shaker [43] 26

2.11 Typical Phase evolution during vibration fatigue testing [50] 28

2.12 Three – point bending DMA data for unidirectional IM7 / 8552. Storage Modulus a) and Loss Factor B) are zoomed – in around the testing temperatures [19] 29

2.13 a) Master curve for a temperature level Ti, b) Time – Temperature Shift Factor [63] 32

2.14 Two steps VCCT – a) The forces exerted at the node close the crack, b) crack is opened [67] 34

2.15 Single Step VCCT [67] 35

3.1 Specimen clamped for testing 39

3.2 Side & Top View of specimen with regions of interest 40

3.3 A comparison between the Fatigue Life Curves by means of Cycles to Failure (Top), Time to Failure (Bottom) 41

3.4 Test Set Up 43

3.5 Response Phase and Vibration Amplitude (0 to peak) Evolution for a test experiencing rotation 46

3.6 New Fixture used to clamp the components inside the environmental chamber 47

3.7 Surface Temperature of specimens exposed to 65 ℃ (left) and 75 ℃ (right) – no vibration load 48

3.8 Specimen's Lay Up (left) / Specimen clamped for testing 50

3.9 Simulated and Experimental ODS 51

3.10 Typical evolution of dynamic parameters of specimen (test at 25 ℃) 53

3.11 Schematic representation of specimen adapted to the clamp 55

3.12 Schematic representation of the experimental set – up 55

3.13 Transmissibility and Phase Response Functions before and after endurance 56

3.14 Monterverdi Process Flow Chart 58

3.15 Resonance Frequencies of specimens at different exposure temperatures 59

3.16 Structural Damping of specimens at different exposure temperatures 60

3.17 Variation in the rate of change of corelation curves due to ambient temperature 61

4.1 Typical Response Phase and Self – Heating Temperature evolutions during fatigue testing 65

4.2 Thermal Images of a specimen during fatigue testing (Top View) correspond to Figure 4.1 / Typical evolution of the temperature distribution 66

4.3 The three distinct regions of the phase and self – heating temperature evolutions 68

4.4 Response Phase and Self – Heating Temperature evolutions of the interrupted tests 69

4.5 Transient State of the Thermal and Dynamic Responses / Equilibrium Point A 70

4.6 Steady State of the Thermal and Dynamic Responses 71

4.7 Top – Thermal and Dynamic Responses of the 1st interrupted test (at 1.9 x10^5 cycles) / Middle – Top View of the respective CT Scan / Bottom – Side View of the respective CT Scan 72

4.8 Top – Thermal and Dynamic Responses of the 2nd interrupted test (at 5.6 x10^5 cycles) / Middle – Top View of the respective CT Scan / Bottom – Side View of the respective CT Scan 74

4.9 Top – Thermal and Dynamic Responses of the 3rd interrupted test (at 9 x10^5 cycles) / Middle – Top View of the respective CT Scan / Bottom – Side View of the respective CT Scan 75

4.10 Top – Thermal and Dynamic Responses of the 4th interrupted test (at 1.15 x10^6 cycles) / Middle – Top View of the respective CT Scan / Bottom – Side View of the respective CT Scan 77

4.11 Critical Event State of the Thermal and Dynamic Responses / Critical Event Point C 78

4.12 Top – Thermal and Dynamic Responses of the 5th interrupted test (at 1.7 x10^6 cycles) / Middle – Top View of the respective CT Scan / Bottom – Side View of the respective CT Scan 79

4.13 Thermal and Dynamic Responses of the test campaign at different ambient temperatures/ Data are colour coded according to their strain level 81

4.14 Top – Equilibrium Temperatures (Point A) over strain level / Bottom – Critical Event Temperatures (Point C) over strain level / The data correspond to the entirety of the test campaign and they are colour coded according to their ambient temperature 82

4.15 The occurrence of Critical Event at different ambient temperatures but at the same strain level 83

4.16 Fatigue Life curves at different ambient temperatures 84

4.17 Rate of Change of Phase at different ambient temperatures / Top – Before the Critical Event (Region B) / Bottom After the Critical Event (Region C) 86

4.18 Typical Hysteresis Loop 88

4.19 The Mechanical Response over the Thermal Response at different ambient temperatures for the entirety of the test campaign 91

4.20 Updated Experimental Set Up for the Fatigue Damage Suspension Tests 93

4.21 Fatigue Damage Suspension Tests at the same ambient temperature and strain levels / Top – Response Phase evolution of Cooled Tests / Middle – Response Phase evolution of the Cooled Tests compared to the original / Bottom – Self – Heating Temperature evolution of the Damage Suspension Tests 94

5.1 3D geometry of the component 99

5.2 Left – FE ply drop geometry / Right – Micrograph employed to partition the FE model 100

5.3 Flow Chart of the VCCT procedure 106

5.4 Flow Chart of the Viscoelastic Temperature Simulation Procedure 109

5.5 The effects of (a) through thickness conductivity, (b) transverse conductivity, (c) heat transfer coefficient over the self – heating temperature 111

5.6 Temperature distribution at Low (top) and High (bottom) Flow Rates in the FE environment 112

5.7 Comparison between the experimental (top) and FE (bottom) temperature distributions along the surface of a specimen 114

5.8 Numerical comparison between the experimental and FE temperature distributions along the length (top) and width (bottom) of a specimen 115

5.9 Flow Chart of the Frictional Temperature Simulation Procedure 117

5.10 Comparison between the experimental (top) and FE (bottom) Hot – Spot temperature distributions along the surface of a specimen / the Simulated Hot – Spot is depicted by the grey area 118

5.11 The effects of increasing Friction Coefficient over the Friction loads and temperature at the damaged region 119

6.1 Typical Damage Evolution as captured by VCCT 123

6.2 Typical Phase evolution as captured by VCCT 124

6.3 Comparison between Experimental and Simulated Phase evolutions at different severities and at 25 ℃ 125

6.4 Comparison between the increase in Damage Area and Phase decay for two strain levels, as captured by VCCT 126

6.5 Typical response Phase and crack growth rate as captured by VCCT 127

6.6 Comparison of the simulated crack growth rates at different severities 128

6.7 Comparison between Experimental and Simulated Phase evolutions at different ambient temperature levels and at the same severity (2.7×10^{-3}) 129

6.8 Comparison of the simulated crack growth rates at different ambient temperature levels 130

6.9 Simulated Fatigue Life curve at different ambient temperatures 131

6.10 Simulated Rate of Change of Phase at different ambient temperatures / Top – Before the Critical Event (Region B) / Bottom After the Critical Event (Region C) 132

6.11 Simulated Fatigue Damage Suspension Tests at the same ambient temperature and strain levels / Response Phase evolutions of the Cooled Test compared to original 133

6.12 The change in the Elastic Strain Energy and its respective viscoelastic Temperature due to the increase in the applied strain 135

6.13 Viscoelastic Temperature change due to the ambient Temperature 137

6.14 The change in the Friction Force and its respective frictional Temperature due to the increase in the applied strain 138

6.15 The change in the Elastic Strain Energy and its respective Correction Factor due to damage propagation 140

6.16 The increase in the Hot – Spot due to the damage propagation / the Hot – Spot is depicted by the grey area 141

6.17 Simulated Phase and Self – Heating Temperature Evolutions (based on the interrupted tests) at 25 ℃ 141

6.18 Experimental and Simulated Rate of change of the “Self – Heating over Phase” curves 142

6.19 A comparison between the final interrupted test and its simulated counterpart. 143

6.20 A comparison between the Experimental and Simulated “Phase over Self – Heating Temperature” Curves 144

6.21 Typical Phase and Modes of Separation Responses as captured by VCCT / Top – Mode Force Ratio / Bottom – Mode Displacement Ratio 146

6.22 Nodal Displacement at different stages of the simulated fatigue life (Number of Cycle) 147

6.23 Damage Growth Rate against Response Phase Decay 148

6.24 Simulated Damage Growth Rate against Response Phase Decay / Top – Same ambient Temperature but different strain levels / Bottom – Different ambient Temperatures but same severity 149

List of Tables

5.1 Physical and Mechanical Properties of UD laminate of IM7/8552..... 100

5.2 Physical, Mechanical and Thermal Properties of epoxy resin 8552 101

5.3 Thermal Properties of UD laminate of IM7/8552..... 101

5.4 Dynamic Parameters..... 101

5.5 Physical and Mechanical Properties of HTA/6376 [26], [34] 107

5.6 Fracture mechanics properties of HTA/6376 [26], [34]..... 107

Nomenclature

Acronyms

ASTM	American Society for Testing and Material
ASME	American Society of Mechanical Engineers
ACP	Asymmetric Cut Ply
CFRP	Carbon Fibre Reinforced Polymers
CMC	Ceramic Matrix Composites
CZM	Cohesive Zone Models
CT Scan	Computed Tomography Scan
ERR	Energy Release Rate
FRP	Fibre Reinforced Polymers
FE	Finite Elements
FLL	Frequency Lock Loop
FRF	Frequency Response Function
HCF	High Cycle Fatigue
IRC	Infrared Thermal Camera
IFT	Interlaminar Fracture Toughness
LEFM	Linear Elastic Fracture Mechanics
MMC	Metal Matrix Composites
ODS	Operating Deflection Shape
PvT	Response Phase against Self – Heating Temperature

PLL	Phase Lock Loop
PMC	Polymer Matrix Composites
RoC	Rate of Change
SLDV	Scanning Laser Vibrometer
SDOF	Single Degree of Freedom
SERR	Strain Energy Release Rate
UD	Unidirectional
VCCT	Virtual Crack Closure Technique

Geometric Properties	
a	Crack Length

Material Properties	
E	Young's Modulus
G, G_T, G_I, G_{II}	Strain Energy Release Rate: total, mode I and mode II
G_C, G_{IC}, G_{IIC}	Critical Strain Energy Release Rate: mode I and mode II
m	Mass
T_g	Glass Transition Temperature
T_s	Object’s Temperature

Dynamic Parameters

c	Damping Coefficient
f	Frequency
F	Excitation Force
k	Spring's Stiffness
T	Oscillation Period
$T(\omega)$	Transmissibility
X	Displacement of SDOF System
$\dot{X}$	Velocity of SDOF System
$\ddot{X}$	Acceleration of SDOF System
X_b	Displacement of the base
τ	Time Elapsed
φ	Phase Response
ω	Excitation Frequency

Mechanical Properties

h	Convection Coefficient
$K_{\max}$	Stress Intensity Factor
k_T	Thermal Conductivity
U	Elastic Strain Energy
$U_{\max}$	Reversible Strain Energy

Miscellaneous	
C, n	Paris Law Parameters
da / dN	Crack Growth Rate
N	Number of Cycles
Q_{sh}	Heat due to Hysteresis Loop
R	Stress Ratio
T_a	Ambient Temperature
ε	Strain
σ	Stress
$\sigma_{\max}$, $\sigma_{\min}$	Maximum, Minimum Stress

Chapter 1

INTRODUCTION

1.1. Aim of the Research

During the past decades, composite materials have found their way among a wide range of industrial sectors. The light weight of composite structures, commonly accompanied by a high material strength, as well as the capacity to tailor their mechanical and physical properties, are some of the advantages that led the aerospace industry to extensively use composite components. However, structural components are usually subjected to the combined effect of complex mechanical and thermal loads, during their lives. It is therefore crucial to understand the fatigue behaviour of composite materials in order to develop lightweight and reliable structures that work within safe operative conditions.

One of the major challenges that characterise fatigue testing, is attributed to its extreme time requirements. In fact, with an excitation frequency of a few cycles per second, traditional testing procedures are able to capture just a small picture of the fatigue life while studies are commonly aiming to avoid excessive self – heating associated with higher excitation frequencies. Furthermore, during the high frequency excitation, the issue of insufficient load transfer towards the specimens also emerges. For these reasons, a trend towards resonance fatigue testing can be observed in the recent years.

Additional factors, such as the ambient temperature effects, come into play when considering the actual operative conditions. In particular, structural components located at the first stage of a turbine can be subjected to a temperature range of – 50 °C to 100 °C during the length of a single flight. It is only natural that researchers wish to decouple the various factor that govern the fatigue life of specimens in order to simplify the investigation.

Even though, researchers naturally wish to decouple the various factors that govern the fatigue behaviour of composites, interesting information can emerge when analysing the overall phenomenon as it manifests. If environmental factors govern the fatigue behaviour of some components, it is necessary to include different ambient temperature conditions in the fatigue life investigation of those components. Obviously, the inducement of different variables in the experimental analysis is not always straightforward, but it can eventually provide useful answers to question such as “what is the effect of ambient temperatures on the fatigue damage mechanisms”, “is it possible to demonstrate a relationship between the mechanical and thermal responses of the system” and even “how can the application of different localised thermal loads can affect the fatigue life”.

To answer those questions, I will employ a common starting point. An existing experimental approach was adopted which is able to associate the fatigue failure to a specific moment in the life of dynamic parameters of a composite component, during vibration testing. This project was developed having the pre – requisite of incorporating this experimental approach, in order to investigate the effect of elevated ambient temperatures on the fatigue life of composite components. Thus, the first milestone of the current study is to introduce a testing method for studying the effect of ambient temperatures on the fatigue behaviour of rectangular CFRP specimens, employing a vibration testing technique. As a result, this thesis also aims to set the ground for an experimental investigation at different ambient condition, given that to date, there are no standardise procedures that exploit resonance fatigue testing.

Even though previous research was also conducted in the vibration fatigue of composites, the failure mechanisms that govern the fatigue damage were not studied. Thus, another objective of the current study is to analyse the experimental data in an effort to investigate, for the first time, the failure mechanisms that govern the fatigue failure. Additionally, this study is also aiming to express the relation between the mechanical and thermal responses of a CFRP specimen that undergoes resonance testing. Finally, the study will exploit the experimental observations in order to propose a method for delaying the propagation of damage, utilising different localised heat loads.

Despite the fact that high frequency fatigue testing is characterised by multiple advantages, certain limitations also are also present. It is easy to understand how challenging, it could be to capture certain parameters (e.g. damage accumulation) during high frequency excitation. For this reason, numerical models can be exploited, alongside the experimental investigation, to enhance our understanding about the observed experimental behaviour. In fact, one of the fundamental objectives of the current research was to deliver an innovative numerical method to quantitatively simulate the experimental results; both the mechanical and thermal responses of the specimens. It is therefore logical that the final objective of this study is to validate the numerical data and exploit both the experimental and numerical observations to shed light on the vibration fatigue behaviour of composite under elevated ambient temperatures. This analysis will set the ground for in – situ damage growth monitoring, during high frequency vibration testing, exploiting the strengths of the numerical investigation. The outcome of this investigation can also lead to the extraction of other important information such as the establishment of a Paris Law for the material system that is under consideration. Finally yet importantly, the numerical investigation can reveal how the delaminated area will behave during vibration testing and what mechanisms can drive the damage propagation.

1.2. Thesis Outline

In Chapter 2 an extensive review is presented, which aims to introduce the reader on the fatigue of composites. For the purpose of this project, this thesis will bind dynamics, structures and material properties to better understand the fatigue behaviour of composites. Thus, this chapter will begin discussing the fatigue behaviour of composites as well as the damage mechanism and the temperature conditions that influence it. Then, it will conclude with an overview of the experimental and modelling dynamic tools that will be employed to describe the vibration fatigue behaviour at different ambient temperatures.

The overall goal of this project is to fill in the gaps in the literature regarding the vibration testing of composites specimens under different elevated temperatures. For this reason, Chapter 3 describes the way an experimental method was developed which aims to

examine the environmental effects, during resonance testing. It describes the equipment and tools employed as well as the standard experimental procedure followed. It aims to be a guidance for the high frequency vibration fatigue testing, when different environmental conditions need to be considered, since little information is currently available. Furthermore, it highlights the various challenges that can emerge during resonance testing at elevated temperature conditions.

The experimental results acquired are discussed in Chapter 4. This Chapter offers to the literature a novel data set regarding the vibration fatigue behaviour of composites under different environmental conditions. The damage growth is examined, for the first time in the literature, at numerous stages of the fatigue life; employing a fractographical analysis in order to understand what drives the stiffness reduction. Alongside this, the influence of the surrounding temperature levels, in the fatigue life of laminates, is highlighted and examined from a new point of view. In this case, the new knowledge acquired regarding the failure criterion forms the basis for understanding the physics that govern the vibration fatigue. Additionally, this Chapter describes how the in – depth analysis of the experimental results can be employed in order to unveil the relation between the mechanical and thermal responses of laminate specimens. Finally, the knowledge acquired throughout this Chapter will be exploited in order to propose a method for the in – situ suspension of damage propagation.

Chapter 5 presents the numerical techniques used to reproduce the experimental investigation. It is believed that both the mechanical and thermal responses of the system should be simulated in order to capture a better picture of the factors that can influence the fatigue life. For this reason, it is important to develop numerical techniques to simulate both the thermal and mechanical responses of composite specimens that are subjected to vibration fatigue testing at elevated temperatures. This chapter demonstrates the innovative multi – physics numerical techniques that were employed in order to simulate the response of the self – heating of composite specimens, when subjected to the combined effect of ambient thermal and vibration loads. Hence, the FE models employed to simulate the thermal response of specimens are introduced. However, this task is far from trivial since

multiple factors have to be considered, such as the effect of ambient temperatures and frictional heat in the damaged area. For this reason, this Chapter will discuss these factors and their influence to the final numerical results. Many of the techniques exploited, were developed for the first time for the purpose of this research. Additionally, a way to simulate the mechanical response of specimens, at different environmental conditions, is also introduced. Thus, this technique aids the examination of the relation of the fatigue life to different factors. Both the thermal and mechanical model will be exploited in this Chapter to gain important insight into the vibration fatigue behaviour of composites.

The FE data, presented in Chapter 6, compliments the experimental investigation. A progressive damage model is exploited to simulate the fatigue behaviour under different exposure conditions while providing information about the damage propagation and the factors that govern it. The evolution of the internal temperature of a composite specimen subjected to vibration loading, is also simulated with the assistance of an empirical relation which accounts for the energy lost per cycle.

The data from the two techniques are correlated to the experimental result. Furthermore, they are combined in order to numerically link the thermal and mechanical responses of the laminate. The knowledge acquired throughout this Chapter is combined with the experimental investigation to:

1. Simulate the experimental observations and validate the numerical results.
2. Study the accumulation of damage during high frequency vibration testing.
3. Characterise, for the first time, the failure criterion that was employed for the purpose of this experimental investigation.
4. Propose a method for the in – situ monitoring of the damage size during high frequency testing.

Finally, Chapter 7 provides a summary of the achievements presented in this project and draws its conclusions in order to pave the way for future researches.

Chapter 2

LITERATURE REVIEW

This chapter reviews the research produced over the past forty years on the subject of composite materials, highlighting the milestones accomplished on the fatigue testing and environmental conditions. Initial studies draw their knowledge from the work carried for metals but the composites industry quickly developed their own methods and techniques. Starting from a brief history on the subject, this review will discuss the fatigue behaviour of composite structures and their dependency on different ambient temperature conditions. Furthermore, it will discuss the up to date techniques of high frequency dynamic testing alongside the natural phenomena that accompany it. Finally, this section will set the ground for the modelling techniques exploited throughout to investigate the damage mechanisms that govern the vibration fatigue of composite laminates.

2.1. Introduction

A wide range of composites can be encountered when observing nature. From wood to shells and bones, natural composites are formed by combinations of individual components of distinct phases. It can therefore come as no surprise that humans developed composite materials, taking advantage of the fact that their physical properties can be tailored to serve specific needs and being fitted into various applications on the fields of engineering and science.

Composite materials can therefore be separated into at least two constituents: commonly a material that forms the matrix and its reinforcement. A matrix material (e.g. a polymer resin) forms the base of the composite and its main purpose is to protect and hold the reinforcements together while transferring the loads to them. On the other hand, the

main function of the reinforcements is to enhance the composite's performance. One of the most common forms of reinforcements are fibres.

The mass production of Fibre Reinforced Polymer (FRP) composites was first introduced by Owens Corning, in 1935, whose method assisted the manufacturing large quantities of glass fibres [1]. However, the biggest demand for high performance materials came after the Second World War, due to the introduction of composite components into the aerospace sector.

However, the fatigue on metals was identified long before. In fact, through his studies, between 1850 and 1860, Wöhler reported that repetitive application of stress could induce failure to materials while the amplitude of this stress plays a crucial role over the destruction of the material's cohesion [2]. A few years later, he plotted the applied stress against the number of cycles, introducing the first Fatigue Life Curves / SN Curve.

Even though, the research on the fatigue of metallic components had a big influence on the fatigue studies of composites, researchers had to greatly alter and improve the old experimental methods, due to the anisotropic characteristic of composites components. The current study will be focused around the behaviour of FRPs and in particular Carbon Fibre Reinforced Polymers (CFRPs), subjected to high frequency fatigue loading and in conjunction to elevated environmental temperature conditions. In addition, the research work performed for the purpose of this study, aims to investigate the physics that govern the fatigue damage development under vibration and thermal loads; along with the complementary assistance from the implementation of a predictive modelling approach.

2.2. Introduction to Composite Materials

As discussed above, the matrix material plays an important role in the composite system, as it shares many of its physical properties with the composite. Therefore, composites could be classified according to the composition of their matrix material. In that manner, three main categories are formed: The Ceramic Matrix Composites (CMCs), the Metal Matrix Composites (MMCs) and the Polymer Matrix Composites (PMCs). The polymer – based composites are one of the most commonly used categories. Due to their lightweight, they find application in numerous demanding industries such as: the aerospace, the automotive and marine.

Polymers can be classified using multiple ways, however, one common way to describe them is through their behaviour under high thermal loads. In that respect, polymers can be divided into thermosets and thermoplastics. In a nutshell, when heated, thermosets undergo an irreversible chemical process, which is defined as curing. During curing, the molecular chains of polymers cross – link, allowing them to solidify. On the other hand, thermoplastics can also form solids, when heated, but they can be melted and re – shaped under the application of additional heat; since no chemical bond takes place during heating. In general, thermosets are often employed in order to improve the mechanical and thermal properties of the composite system while enhancing their resistance to deformation. Although more expensive, thermoplastics are commonly exploited for their ability to be remoulded without losing their mechanical properties and due to chemical resistance.

This study will be focused on a thermoset composite system, reinforced by continuous fibres. In contrary to other forms of reinforcement (e.g. short fibres, particles), continuous fibres offer a better resistance to deformation. Nevertheless, the failure patterns that emerge due to the exposure of FRPs at cyclic loads, are not fully understood yet. For this reason, multiple studies have been undertaken to investigate their behaviour.

2.2.1. From Metals to Composites

As stressed earlier, the first studies published, regarding the fatigue in composites, had to compare their experimental results against the data acquired from metallic components, since the testing techniques were based on the methods developed for metals. In that sense, the fatigue damage propagation in metals was arranged, by Plumbridge [3], into three categories which are described as: the initiation of crack, the damage propagation and the final failure. In contrary to the common composite behaviour, the three stages of fatigue damage in metals are clearly separated. In particular, the damage onset occurs when the local stresses surpass the yield strength of the coupon. Additionally, the crack propagation can be split into two stages. In the first stage, the high stresses result to the formation of slip bands which supports the extrusion of grains from the surrounding materials. As a result, the atoms in the slip bands are debonding which permits the crack to propagate in a precise manner. Thus, the crack could propagate normal to the direction of the applied stress, under high enough loads. However, the final failure can be mainly attributed to the second stage of propagation which is characterised by the stresses exceeding the ultimate strength of the material.

On the other hand, polymeric materials are consisted of molecular chains which lack the crystalline structure of metals and as such they do not experience similar crack initiation behaviour. As a result, the fatigue damage in polymer – based composites emerge due to the internal flaws on the structure of the material or due to change in the arrangement of the molecular chains. This “re – arrangement” of the polymeric chains could lead to the development of voids on the matrix material and is affected by the ambient temperature conditions as well as the applied stresses.

Following the increasing demand for composite components in the aerospace industry, the research work performed around the subject experienced a rapid advancement during the 1970s, with Griffith’s theory opening the way for the Linear Elastic Fracture Mechanics. He suggested that pre – existing micro – damage in a specimen could be the source of failure. For this reason, he studied glass specimens, through the pre – introduction of damage in the form of notches of different sizes. Then, he concluded that the square root

of the notch's length bares a constant relationship with the fracture stress. Close to the end of the 50s, Irwin [4] took advantage of this relation and modified it in order to express that the sum of the total strain energy can be separated into the elastic strain energy stored and the dissipated energy [5]. This indicated that the stored elastic strain energy is used in order to create a new surface (crack) when it surpasses the Fracture Toughness (G_C) of the material. It is however important to mention that Irwin also introduced a Stress Intensity Factor in order to estimate the impact of the local stresses applied on the crack tip.

A few years after Irwin's discoveries (in 1961), Paris combined the Linear Elastic Fracture Mechanics (LEFM) that was developed for metallic materials and Irwin's work in order to predict the crack growth rate during endurance testing [6]. Thus, introducing his famous equation:

$$\frac{da}{dN} = C K_{\max}^{n} \qquad \textbf{2.1}$$

Where da / dN is the rate at which the crack propagates while K_{max} is the Stress Intensity Factor and C and n are material dependent constants.

2.2.2. Introduction to Fibre Reinforced Polymers

At this point a substantial amount of research work was developed around the behaviour and characteristics of composites. For this reason, D. Dew – Hughes and J. Way decided to gather the information available in the literature, regarding the impact of fatigue loads on Fibre Reinforced Polymers and published a review paper in 1973 [7]. It then became obvious that the failure patterns of fibres can be divided into three phases: nucleation, propagation and final failure. However, these stages did not have a great impact on the fatigue life of testing coupons. On the contrary, it was noticed that the main effect came due to the crack developed in the interface between the matrix material and its reinforcement. In addition to this, it was also revealed that polymer – based matrices experience different behaviour when loaded cyclically. A matrix could be prone to accelerated failure at harsh environmental temperature conditions while they heat up during

fatigue testing which introduced the hysteresis phenomenon. It is therefore evident that a weak interface could lead to rapid accumulation of damage.

Even though fatigue damage was captured, it was yet unclear how to define failure. For this reason, in 1980, Reifsnider attempted to give an in – depth definition of the failure patterns occurring during endurance testing [8]. Hence, he recommended the following series of stages in the fatigue damage propagation.

1. Nucleation of Crack along an off – axis ply
2. Cracks' Accumulation during the "*Characteristic Damage State*"
3. The emergence of damage at the matrix – fibre interface and crack coupling
4. Development of wider damage regions due to this process
5. Formation of through thickness crack due to coupling
6. Final fibres' fracture normal to the load direction

Finally, Reifsnider noticed that after a certain number of cycles in the fatigue life of composites specimens, the accumulation of cracks reaches a point of saturation; concluding that it could be very challenging to predict the fatigue damage patterns and thus, further knowledge in the mechanisms that govern the fatigue failure is necessary (Figure 2.1).

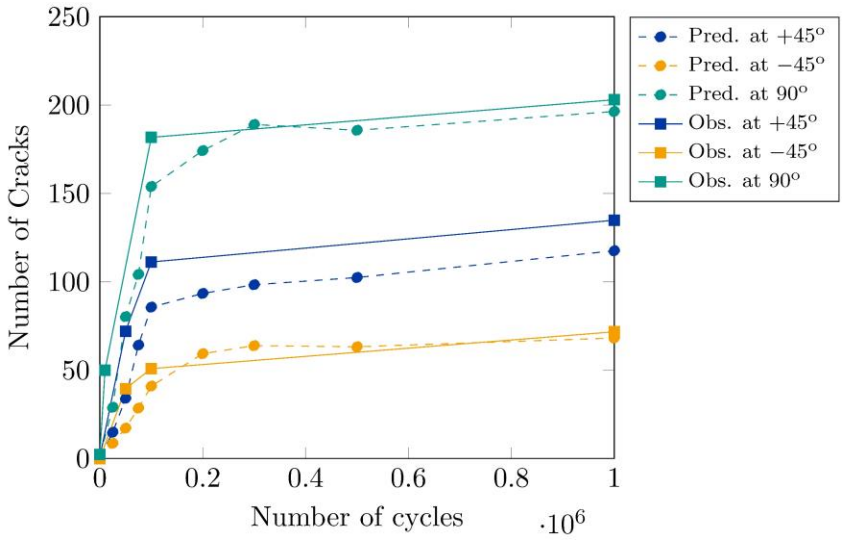

Figure 2.1: Prediction and observation of the amount of cracks in off – axis plies of a $[0, 90, \pm 45]_S$ laminate under fatigue loading at the two thirds of the ultimate tensile strength [8]

Inspired by Wöhler's work, Talreja then used the applied strain level, instead of stress, to develop his Fatigue Life curves (SN Curve) [9]. This way, he managed to incorporate the anisotropy of composites in an SN Curve and thus, eliminate the differences in the elastic modulus between fibres and matrix.

Finally, Hashin paved the way, for characterising the damage mechanisms (Figure 2.2), with his variational approach [10]. Nowadays, following Hashin's work the composites community is investigating the accumulation of microscopic damage [11], while relating the microcracking in the matrix material with the initiation of delamination [12].

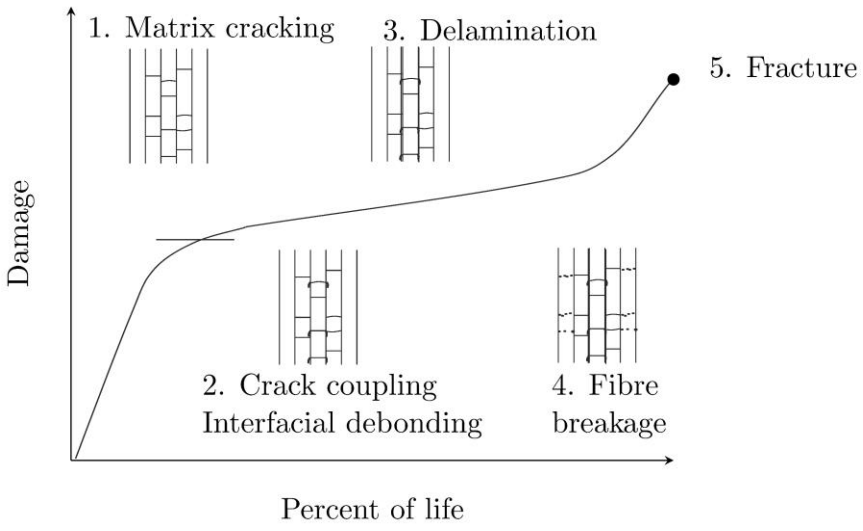

Figure 2.2: Development of damage in composites laminates [13]

2.3. Damage Mechanisms in Composites

The damage occurring on a composite laminate can be classified according to its location; regardless, the load type applied to the component (e.g. cyclic, quasi – static). In that manner, a damage developed within the boundaries of a single ply is referred as intralaminar, while the damage established between the different plies is an interlaminar damage (Figure 2.3).

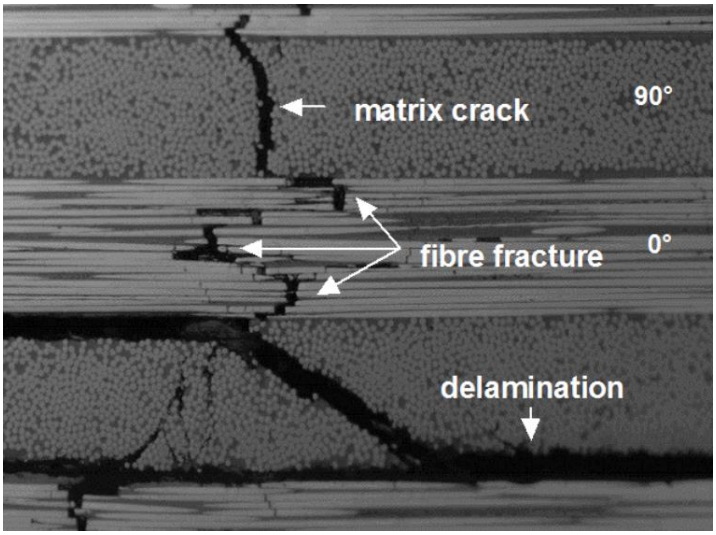

Figure 2.3: Damage Mechanisms in impacted FRP [14]

Despite the location of a crack, the damage will form under the effect one (or more) of the characteristic separation modes. These are the opening mode (mode I), the shearing mode (mode II) and the scissoring shear mode (mode III). In his book, Patron attempted to illustrate the separation modes, using a natural composite material (wood) and practical everyday cases [15]. These illustrations are presented in Figure 2.4.

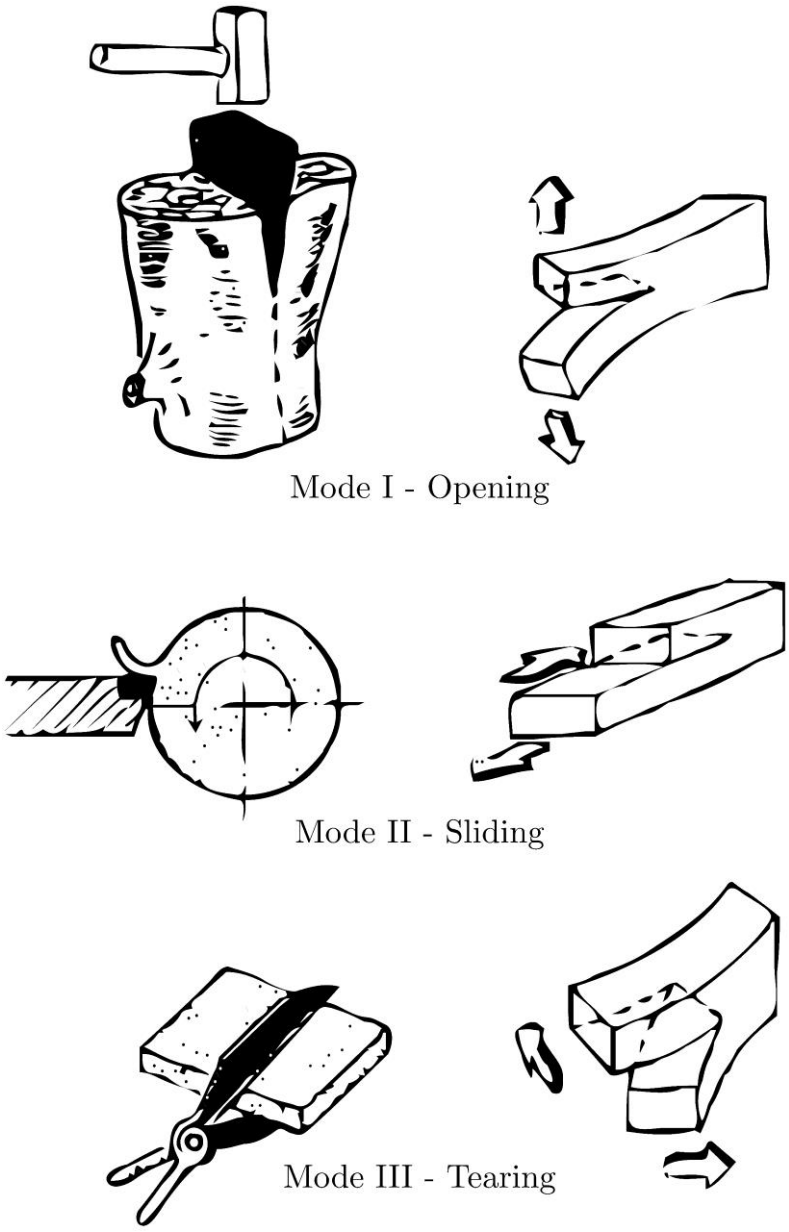

Figure 2.4: Characteristic Modes of Separation [15]

2.3.1. The free – edge effect

Even though, it is very rare to encounter a pure mode regime (either I, II or III) in practical applications, the mode III component could become significant close to the free edges of a laminate. This phenomenon can be associated with the free – edge effect.

A complex stress field should be applied in a composite component, consisted of differently orientated plies, in order to efficiently transfer the load through the thickness. Alternately, the anisotropic elastic moduli configuration could result points of singularities in the stress field, leading to high deformations [16].

In the case of epoxy – based composites, components have to undergo a curing process. During curing, the laminate will be exposed to ambient temperatures, close to (or exceeding) its glass transition temperature, as well as high pressure. At this stage, the resin matrix will therefore be at a stress – free / rubbery state. However, during the cooling process, the matrix material and its reinforcement will usually shrink at different proportions due to their different thermal expansions. It is therefore under this process during which residual stresses could be established at the free edges of a composite component. As a result, crack could initiate at the free edges of a specimen when it is mechanically loaded.

At this point, it is worth noting that Mittelstedt and Becker gathered the information from more than 40 years of research on the subject and published a review in collaboration with the American Society of Mechanical Engineers (ASME) [17].

2.4. Fatigue in Composites

A wide variety of composite material applications is used in the transportation sector, because of the substantial strength and stiffness of FRPs and their low mass. The aerospace industry is a sector where the use of composite material applications is constantly increasing. As a consequence, in the sector expressed an increasing need for a concise characterisation of composites under complex loading conditions, as well as exposure to cyclic loading conditions.

However, before discussing the fatigue behaviour of composites an interesting question is formed: "What is Fatigue?". The American Society for Testing and Materials (ASTM) defines fatigue as [18]:

"The process of progressive localised permanent structural change occurring in a material subjected to conditions that produce fluctuating stresses and strains at some point or points and that may culminate in crack or complete fracture after a sufficient number of fluctuations."

It is obvious that ASTM describes two stages on the fatigue life a testing coupon, regardless its material type (e.g. metal or composite). The first stage is considered as the *"progressive localised permanent structural change"* while the second is defined as the *"crack or complete fracture."* However, it has been proven that the identification of these stages during high frequency endurance testing, could be rather challenging.

2.4.1. Cyclic Loading

The stages on the fatigue life of a composite structure can be classified into three categories: Initiation, Propagation and Final Failure. However, the fatigue life can be heavily dependent on the loading conditions employed. With regards to Figure 2.5, the following parameters can describe the loading conditions during endurance testing.

$$R = \frac{\sigma_{min}}{\sigma_{max}} \tag{2.2}$$

$$f = \frac{1}{T} \tag{2.3}$$

Where R is the stress ratio, f is the frequency of vibration, σ_{max} and σ_{min} is the maximum and minimum stress components while T is the oscillation period. As it will be discussed in the following section, these parameters can play an important role in the fatigue life. In fact, a high excitation frequency could increase the internal temperature of a polymer – based composite, leading to shorter fatigue lives.

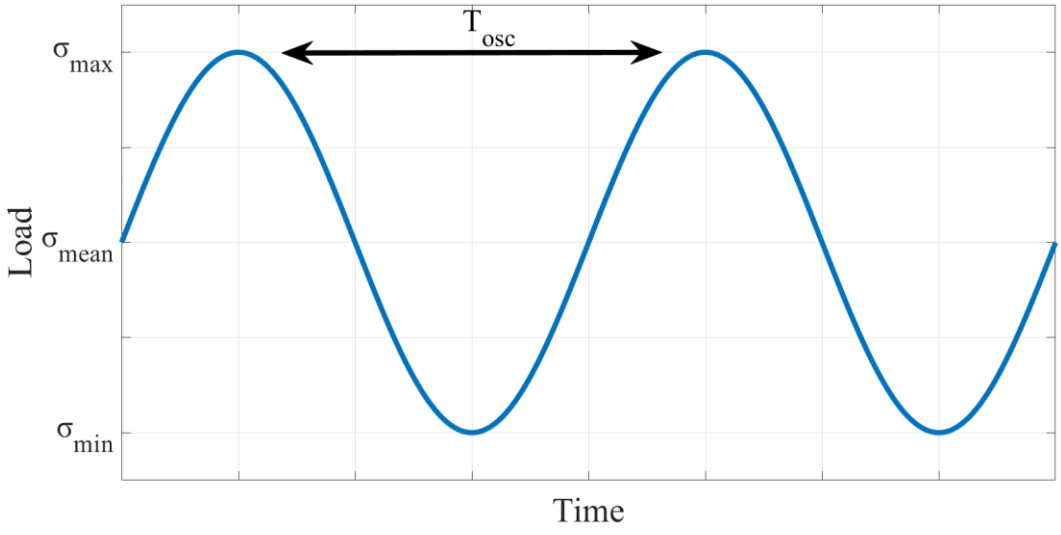

Figure 2.5: Typical sinusoidal loading behaviour over time [19]

On the other hand, the stress ratio *R* can characterise the type of load which is applied. Therefore, a fully reversed load can be represented by an R value of –1, a tension – tension load can get a range of values between 0 and 1, a compression – compression case has an R > 1 while a tension – compression case is less than 0.

2.4.2. The phases of Fatigue Damage development

Following the definition proposed by ASTM, the first stage on the fatigue life of a component can be identified as the damage initiation. Nevertheless, it can be more challenging to identify crack initiation experimentally. Therefore, the onset of damage is usually correlated to a subjective damage length which can vary from micrometres to a few millimetres [20].

It is therefore apparent a lack of a universal criterion for damage initiation exists. For this reason, Reifsnider proposed that the initiation can be related to "*the first nucleation of a transverse cracks along the off – axis plies*" [8]. In contrary, Salkind [21] suggested as the moment of initiation "*the time required to form a crack of detectable size*" while Quaresimin [22] introduced a specific crack value of 0.3 mm that corresponds to the minimum damage size detectable through a microscope. He also argued that cracks of smaller size will not have a great impact on the fatigue life of specimens. In his chapter for "Fatigue in Composites", Sims [23] reviewed the existing fatigue testing technique in composites. He concluded that a failure criterion based on the degradation of stiffness is necessary.

Additionally, May and Hallett studied the fatigue damage initiation, at modes I and II in order to incorporate it in a FE model [24], [25]. For mode I, it was concluded that the initiation coincided to the specimen's separation, since the time elapsed from initiation to final failure was very short. The authors also investigated the ability of two separate testing techniques to capture the onset of damage at mode II. They observed that the Double Notched Shear test is more reliable on identifying damage initiation when compared to the Short Beam Shear test.

As it will also be discussed more detailed in the following sections, the propagation of damage is better understood. At this point it is worth recalling that Irwin correlated the crack growth to the Strain Energy released during the formation of a new area. In fact for a quasi – static case, the damage will propagate when the Strain Energy Release Rate (SERR) is greater than the Fracture Toughness of the material (G_C). Therefore, the SERR (G) can be described by means of crack length a and the Elastic Energy U:

$$G = \frac{\partial U}{\partial \mathrm{a}} \tag{2.4}$$

In a fatigue environment, a SERR greater than the fracture toughness would result to an almost immediate failure. Thus, the Paris' Law can be employed to describe a stable crack growth rate:

$$\frac{d\mathrm{a}}{dN} = C(\Delta G)^n \tag{2.5}$$

With regards to Figure 2.6, the constants C and n are material parameters which are dependent to the environmental temperature and they are usually captured through the log – log Paris' Law plot.

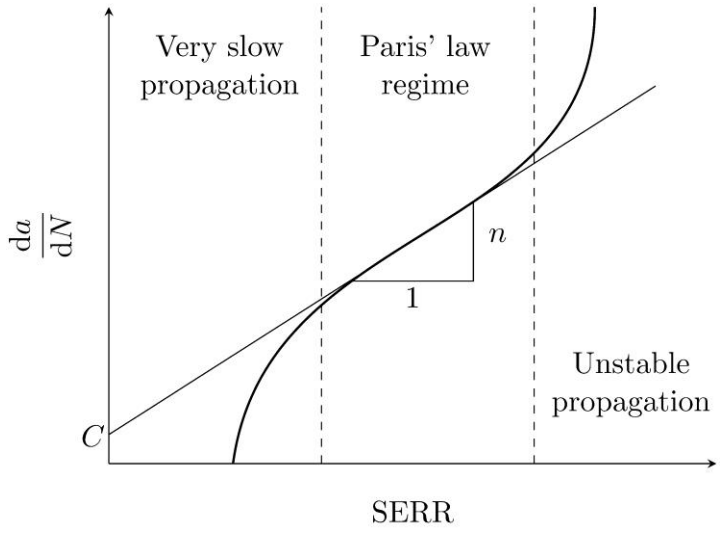

Figure 2.6: Schematic representation of Paris' Law [19]

As for the onset of damage, the final failure can be interpreted through many ways. Due to the nature of anisotropic materials, multiple steps could lie between the initiation and final failure while a small deterioration in the stiffness of a specimen could indicate its failure, even if it is not catastrophic. There are multiple reasons that describe why the failure is usually associated with a particular of stiffness decay. Excessive deflection and the rise of new harmonic during operational conditions could render a composite component inadequate for use. In many cases, coatings are employed to seal the component against the environmental conditions. However, a small crack could bare the component unsuitable for operation. Thus, the definition of failure through a small drop in stiffness may be more suitable. In conclusion, the choice for defining the final failure can strongly lie with the application in question. An expensive and strict damage tolerance could be appropriate for some applications while a more cost – efficient damage policy could be more suitable for others.

2.5. Overview on the Temperature Effects

2.5.1. Fracture Toughness

One of the factors that can influence the fatigue life of composite structural elements is the ambient temperature conditions. It is therefore crucial to incorporate the effects of the operating temperature environment in the fatigue life of components. However, the nature of this influence is strongly dependent on the material system and the characteristic mode, considered.

In 1998, Asp studied the behaviour of Carbon Fibre Reinforced Polymer (CFRP) material system, namely (HTA / 6376C), within a temperature range of –50 °C to 100 °C [26]. In his investigation, he used both dry and wet samples. He reported that in the tests performed in pure mode I and elevated temperature conditions an enhancement of the initiation Interlaminar Fracture Toughness (IFT) can be observed, along with a considerable increase in the values of the propagation IFT. He attributed this behaviour to significant fibre bridging. Nevertheless, the tests conducted in different separation modes, reported diverse results. In particular, the IFT deteriorated with an increasing temperature,

in pure mode II while only minor changes were observed under the combined effect of modes I and II (50 % mode mixity).

Similar to what observed by Asp, Beland et al. [27] also reported that fibre bridging occurs on the experiments conducted under mode I and using CFRP coupons (IM6 /5245C). Hence, he traced a decay in the IFT at elevated temperatures.

Russel proposed that the delamination developing under mode II, is not dominated by the toughness of the matrix. Instead, the strength of the fibre – matrix interface governs the response [28]. Also, he suggested that the thickness of resin rich areas dominate the fracture of the matrix while ambient temperature can influence the interfacial strength. Therefore, it can be concluded that the delamination, in mixed mode conditions, can be defined as a superimposition of the interfacial strength (dominating mode II) and the matrix's toughness (dominated by temperature).

Cowley et al. also studied the IFT at harsher temperature conditions. In this case, they studied Unidirectional (UD) specimens from different material system; a Poly – Ether Sulfone thermoplastic and a carbon – reinforced thermoset. They also reported an increase in the IFT at mode I and they exploited Russel's work in order to understand the difference in the behaviour of delamination at higher temperatures. An extensive deformation of the matrix, followed by a large decrease of the Critical Strain Energy in mode II (G_{IIC}), was apparent at ambient temperature levels close to the glass transition (T_g). On the other hand, the thermoset material experienced interfacial damage in the same mode.

It is therefore apparent that the fibre bridging acts as a restraining mechanism mainly against the propagation of delamination [29]. However, this behaviour can also promote the delamination dependency on the crack length.

On the other hand, Shindo et al. studied the influence of sub – zero temperatures on the delamination of woven Glass Fibre Reinforced Polymers (GFRP). The authors indicated that the increase in the stiffness of the matrix, for the tests conducted at 77K, leads to the increased to the values of propagation IFT [30]. The transition to cryogenic temperatures also affected that crack growth rate, resulting in an unstable propagation.

At even lower environmental temperatures (4K), the fracture toughness is decreased. Nishijima et al. noted that the matrix flow is interrupted, leading also to an unstable growth rate [31]. It was concluded that the deterioration of the fracture is related to a more brittle behaviour of the epoxy resin at this temperature [32]. Additionally, Kasen proposed that the matrix shrinkage is more profound than its reinforcement, which could also be the source of residual stresses [33].

It can therefore be concluded that the mode I Interlaminar Fracture Toughness seems to experience increase under the effect of elevated temperatures while the crack propagation rate does not appear to be significantly affected. Furthermore, the matrix embrittlement appears to dominate the IFT at extremely cold environments. However, the IFT is not characterised solely by the fibre bridging since the interfacial strength will determine whether the bridging will restrain the damage propagation [28]. Moreover, the environmental conditions can promote the deterioration of interfacial strength.

2.5.2. Fatigue Delamination Growth Rate

Nevertheless, only a few studies regarded the impact of the ambient temperature conditions on the damage growth rate under cyclic loading. In a continuation to Asp's work [26], Sjögren et al. attempted to characterise the delamination of a carbon fibre reinforced polymer material system (HTA/6376C) [34]. For the purpose of this study, the authors performed the analysis at pure modes I and II, at a 50% mode mixity and at distinct exposure temperatures (20 ℃, 100 ℃). Their data could be expressed by Paris Law, since they present a linear behaviour on a double logarithmic crack growth rate against Strain Energy Release Rate (SERR) curve (Figure 2.7). Hence, the authors were able to provide information about the Paris Law coefficients, for the respective temperatures. Furthermore, it was concluded that the damage propagation rate will be accelerated at 100 ℃, while the threshold SERR values corresponded only to the 8 % of the respective IFT, at this temperature.

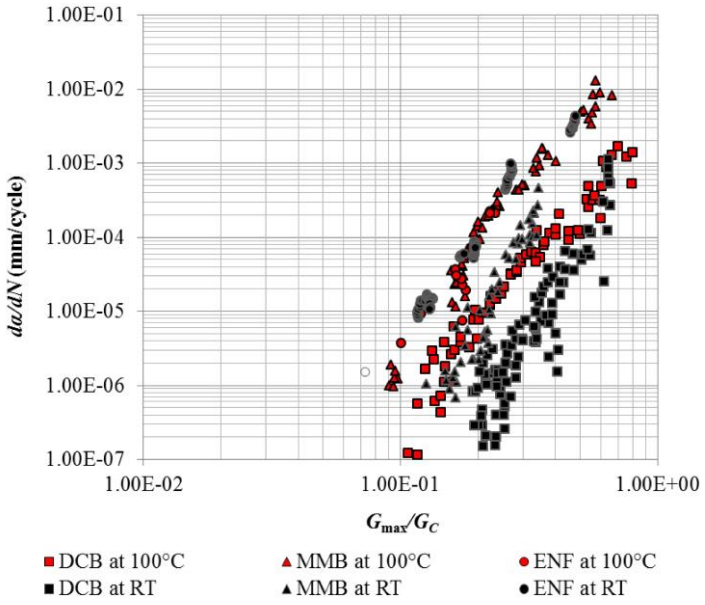

Figure 2.7: Temperature effect on the Damage Growth Rate for a CFRP (HTA/6376C) [34]

Additionally, Gregory and Spearing studied the influence of the exposure temperature on both the quasi – static and the fatigue damage of IM7/977 – 3 [35]. Their tests were conducted at a range of temperatures between 24 ℃ and 149 ℃ and they argued that the resin matrix experienced no dependency to temperature under quasi – static conditions, until the ambient temperature was close to the T_g. Nevertheless, a different behaviour was captured under cyclic loading. The specimens presented a strong dependency to environmental conditions, with a higher propagation rate as well as damage initiating earlier at higher temperatures.

An important research work was presented recently by Charalambous et al. [36]. The authors employed Asymmetric Cut Ply (ACP), made of IM7 /8552 CFRP, along with four point bending to explore the "Temperature Effects on mixed mode delamination under quasi – static and fatigue loading". For the purpose of this study, four ambient temperature levels were investigated: –50 ℃, 20 ℃, 50 ℃ and 100 ℃. The authors reported that the IFT experienced a significant increase at 80 ℃, at quasi – static conditions. However, the IFT values didnot present a significant change, for the temperature range between –50 ℃ and 50 ℃. Moreover, the authors presented multiple interesting findings for the fatigue

behaviour of specimens, too. It was described that the fatigue growth rate slows down, regardless the testing temperature. This behaviour was attributed to the increase in compliance of the coupons due to the damage accumulation.

In the same study, the authors were able to correlate the crack growth rate with the Energy Release Rate (Figure 2.8). It is apparent that the curves present a dependency to ambient temperature. Moreover, it is noticed that the energy required to further extend the delamination is higher, at lower exposure temperatures; thus, resulting to a lower propagation rate. The authors followed the results expressed in [35] and concluded that the deterioration of the yield strength of the matrix will assist the development of new cracks as well as the delamination propagation. Finally, fractographic analysis indicated that the higher damage rates occur due to superimposition of different damage mechanisms at elevated temperatures which lead to decrease in the strength of the interfacial bond.

In conclusion, the fatigue delamination growth rate can be strongly affected by the environmental conditions. This is a strong indication that the resistance of CFRP to fatigue damage deteriorates at harsher ambient conditions.

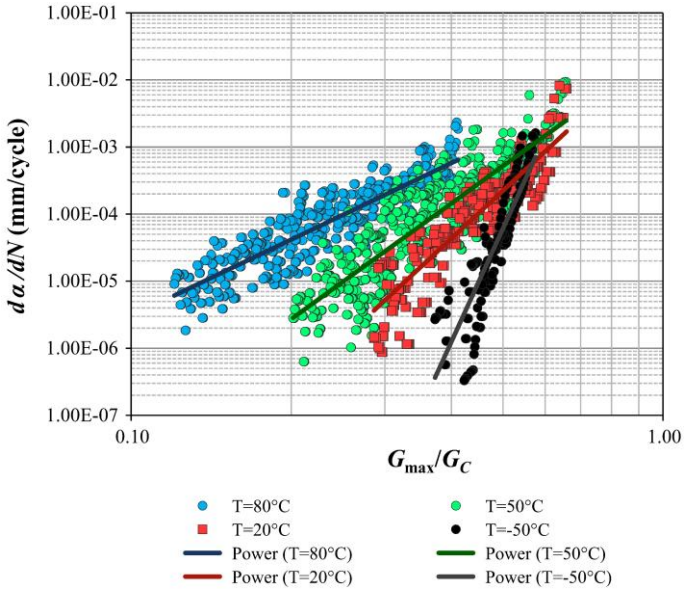

Figure 2.8: Temperature effect on the Damage Growth Rate for a CFRP (IM7 /8552) [37]

2.6. Overview on Vibration Fatigue

2.6.1. Introduction to Dynamics

The previous sections discussed the fatigue behaviour without considering the loading type. However, this study exploits the fatigue behaviour under the effect of a specific type: the dynamic loading. It would therefore be worth focusing our attention on the characteristics of vibration fatigue.

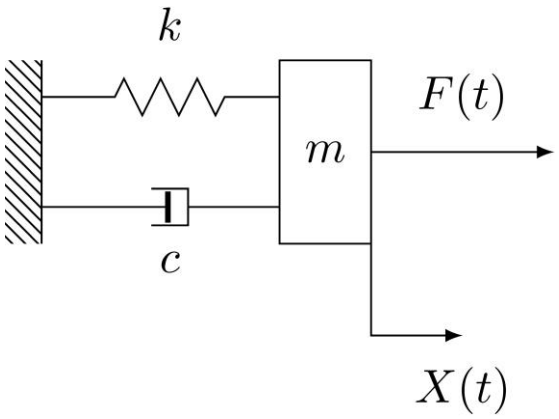

Figure 2.9: Schematic representation of Mass – Spring – Damper System [19]

The concept of vibration endurance testing is not entirely new [38]–[42], since exciting a component at resonance can provide useful information about its structural characteristics. In its simplest form, a structure excited under a dynamic load can be expressed by a mass – spring – damper system and it is called a Single Degree of Freedom system (SDOF) (Figure 2.9). It is defined by the equation of motion:

$$m\ddot{X} + c\dot{X} + kX = F(t) \tag{2.6}$$

Where c is the damping coefficient, k is the spring's stiffness, F is the time dependent excitation force and X is the displacement of the system. However, in a real – life situation, this equation is not able to completely describe the motion of a component which is excited by a dynamic exciter.

Throughout the current study, a dynamic exciter was to explore the fatigue behaviour of CFRP components. Even though, a contactless excitation system could also be employed for this purpose, the most common choice is the use of an Electromagnetic Shaker (Figure 2.10). Hence, the composite specimen is attached to the table of the shaker which is vibrated through the application of a coil and an alternating magnetic field. The response phase (φ) and Transmissibility function (T) of this base excitation system can therefore be expressed, by means of the excitation frequency, as follows:

$$\varphi(\omega) = tan^{-1}\frac{mc\omega^3}{k(k-\omega^2 m)+(\omega c)^2} \tag{2.7}$$

$$|T(\omega)| = \frac{|X|}{|X_b|} = \frac{\sqrt{k^2+(\omega c)^2}}{\sqrt{(k-\omega^2 m)+(\omega c)^2}} \tag{2.8}$$

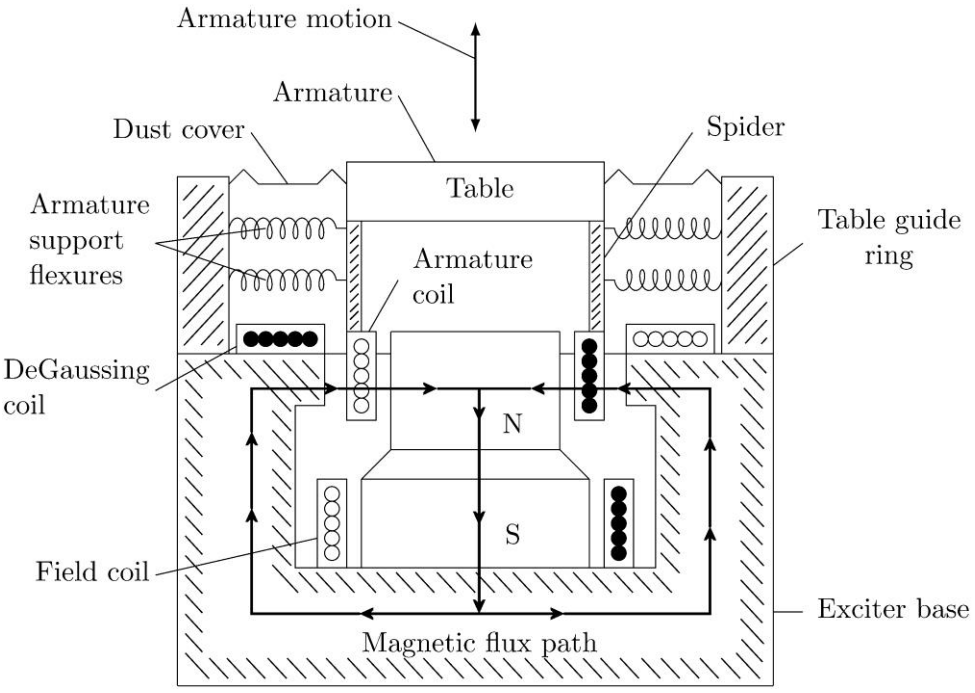

Figure 2.10: Schematic representation of Electromagnetic Shaker [43]

2.6.2. Fatigue by vibration loading

Even though, the theoretical knowledge around the fatigue behaviour of composites experiences a continuous evolution, the experimental techniques seem to undergo a period of slower progress. The fatigue methods that are mostly adopted dictate that tests have to be performed at frequencies below 10 Hz, in order to avoid excessive increase in specimen's temperature and overcome the limitations that are set by the hydraulic machines. However, recent studies exploited the three and four point bending testing and provided data regarding the High Cycle Fatigue (HCF) [44], [45].

The study of fatigue under dynamic resonant conditions is dated back to the 50s and Lazan who studied metallic components [46]. On the other hand, the investigation of resonance fatigue of FRPs is more recent. In 2009, Just – Agosto introduced a resonance three – point bending technique and he studied a foam core material system [47]. The method was then employed by Gu et al. in order to analyse the stiffness of glass fibre specimens [48]. In 2012, Pickard reported structural changes on composite components and he focused more on the non – linear dynamics. Additionally, he introduced a modelling method to capture the location of fatigue damage [49].

Furthermore, Di Maio introduced a method for studying the fatigue behaviour of composite components, at resonance, and he applied it using both contact and contactless techniques [38]. In a later study, Magi exploited the advantages of this experimental technique to the explore the fatigue behaviour of tapered CFRP composite components [50]. He excited the coupons at the 1^{st} bending mode, close to their resonance frequency and at constant vibration amplitude. Even though, most dynamic tests trace the changes in the resonance frequency by maintaining a constant response phase, Magi implemented a Frequency Lock Loop for his experimental investigation. In fact, he maintained a constant excitation frequency throughout the endurance test while monitoring the dynamic parameters (e.g. the response phase) of the laminates. He reported that by fixing the excitation frequency one can observe how the dynamics of the specimen evolved due to the change of its internal stiffness distribution. Finally, he defined the fatigue failure as a

Critical Event during which an abrupt change in the dynamic parameters of the system, was captured (Figure 2.11).

The current study will follow Magi's steps, in combination with Di Maio's contact excitation method, in order to investigate the fatigue behaviour of CFRP specimens under different elevated temperature conditions.

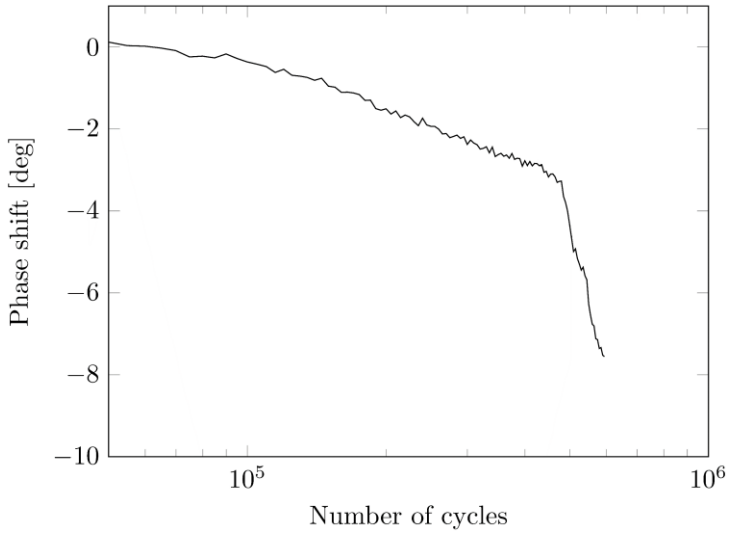

Figure 2.11: Typical Phase evolution during vibration fatigue testing [50]

2.7. The Self – Heating Effect

As it was previously discussed, an effort was made in order to omit the use of accelerated testing, for the analysis of fatigue in polymer – based composites, due to their viscoelastic nature. When tested at high frequencies, out of phase oscillations between the applied stress and strain are observed. This hysteretic loop is the result of the viscoelastic nature of the polymer matrix. Moreover, a common feature of polymers is their poor thermal conductivity which leads to the dissipation of the mechanical energy in the form of heat. The increase in the endogenous (Self – Heating) temperature of FRPs laminates during fatigue testing, corresponds to the localise increase in stress, especially at stress raiser points [51]. Unfortunately, low frequency tests were proved to be a very time – consuming task which implies that the Self – Heating effect cannot be neglected anymore.

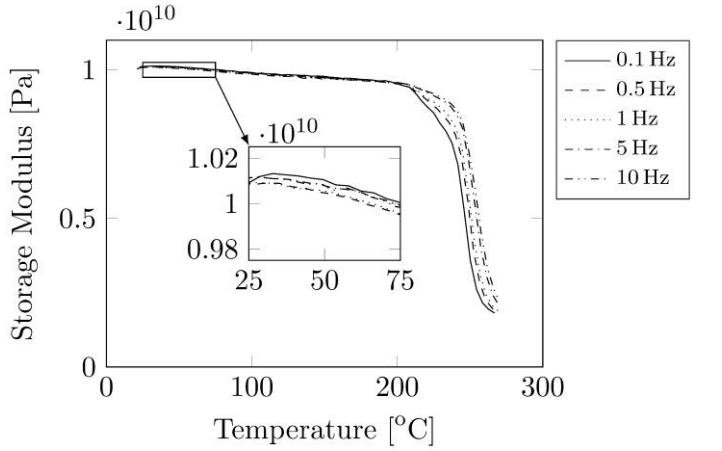

(a)

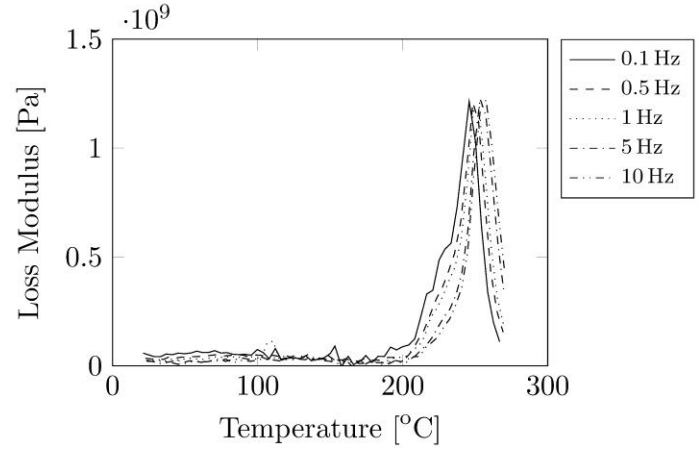

(b)

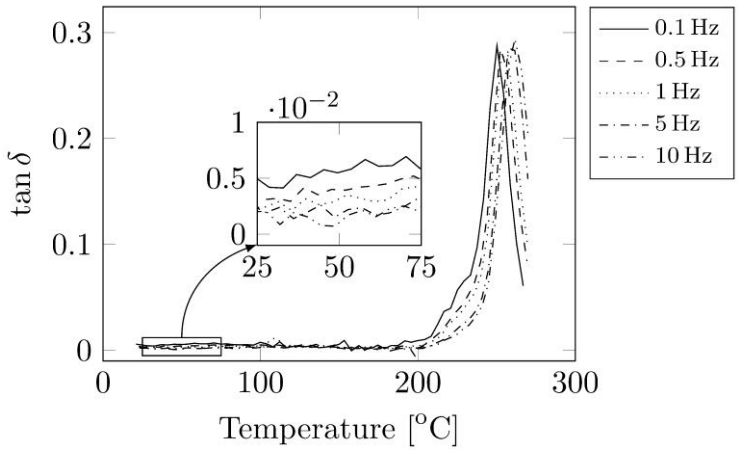

(c)

Figure 2.12: Three – point bending DMA data for unidirectional IM7 / 8552. Storage Modulus a) and Loss Factor B) are zoomed – in around the testing temperatures [19]

Therefore, the Dynamical Mechanical Analysis can be implemented to study the material system dependency to the both the ambient temperature and time. During a DMA test, the specimen is excited under variable frequencies while exposed to different thermal loads. Thus, the relative stress can be measured which permits the calculation of the complex modulus. Magi utilised this technique in order to prove that CFRP (Hexcel IM7 / 8552) coupons are not affected greatly by the change of ambient temperature level, up to 75 °C [19]. In fact, he reported that the storage modulus will vary only up to 2 %, for all frequencies, while the loss factor will change more than 0.005, in the same frequency range (Figure 2.12).

An extensive research on the self – heating effect, associated to the fatigue life of FRPs, was conducted by Katunin [52] – [61]. In his initial steps, Katunin formulated an expression which describes the internal heat, emerging under cyclic loading. For this reason, he started using the Boltzmann – Volterra equation [61]:

$$\varepsilon(t) = \frac{1}{E}\left(\sigma(t) + \int_0^t \prod (t-\tau)d\tau\right) \tag{2.9}$$

Where $\varepsilon(t)$ and $\sigma(t)$ are the deformation and stress at the moment of measurement t, τ is the time elapsed until this moment and E is the Young's Modulus. It is possible to solve the heat transfer equation, for 1D, while considering the time / temperature dependency. Hence, the heat (Q_{sh}) due to hysteresis can be expressed as follows:

$$Q_{sh}(t) = \frac{2\pi}{\omega}\int_0^t \sigma_{ij}\dot{\varepsilon}_{ij}dt \tag{2.10}$$

Katunin then used this expression to simulate the self – heating behaviour. Additionally, he studied the effect at both high and low excitation frequencies. In his later research, he employed multi – harmonics excitation, while also exploiting the self – heating effect, to identify the damage in laminate specimens [54]. Most specifically, he was able to detect the presence of damage due to the local increase in the self – heating temperature, when exciting a composite component under multiple harmonics for a few seconds.

2.7.1. The Time – Temperature Superposition Principle

It is therefore apparent that multiple factors can influence the fatigue life of FRP components. The time – temperature superposition principle was developed in an effort to describe the effects from both the excitation frequency and the exposure temperature.

In 1995, Miyano introduced the superposition theory in order to predict the fatigue strength in laminates [62]. A few years later, he proposed four conditions that should be met in order to predict the fatigue limit of the material [63]:

1. Identical failure mechanisms for static, creep and fatigue tests
2. Identical time – temperature superposition principles for different strengths
3. Monotone loading is characterised by a linear cumulative damage law
4. Linear relationship between fatigue strength and stress ratio

With regards to Figure 2.13, Miyano defined as a master curve: the graph that occurs when plotting the experimental data of multiple temperatures and frequencies, on a "pseudotime" axis in order to produce a smooth envelope. A shift factor can therefore be traced through the amount of time a graph requires to be shifted in order to lay on the envelope.

Then, Miyano took advantage of the theory in order to compare experimental results capture at different excitation frequencies and temperatures. He concluded that when the specimens are excited at the same frequency but at higher environmental temperatures, the resulting SN curves will be shifted downward.

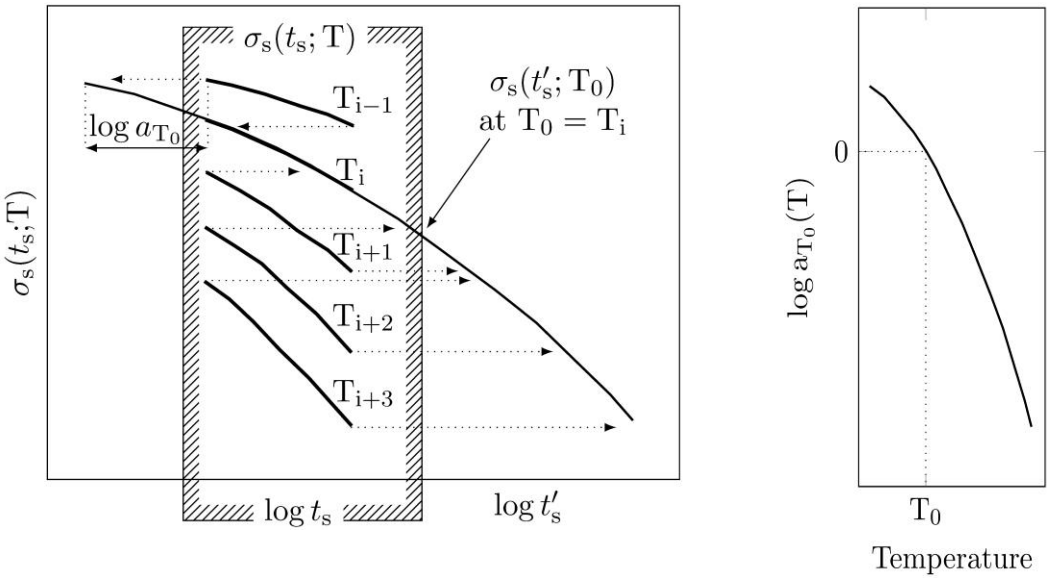

Figure 2.13: a) Master curve for a temperature level Ti, b) Time – Temperature Shift Factor [63]

2.8. Fatigue Damage Modelling

2.8.1. Introduction in the Fatigue Damage Modelling

Capturing the fatigue behaviour of composites is only the first stage towards the prediction of the total life under cyclic loading. In his book, Vassilopoulos describes the phenomenological models that are commonly implemented to simulate the fatigue behaviour as well as the improvement on the predicting methods [64].

Empirical methods, such as the SN curves and the Goodman diagrams, are commonly employed for the prediction of the fatigue life. Usually, they do not consider the damage mechanisms, since they are constructed from the experimental data acquired after the completion of the endurance test.

On the other hand, progressive damage models follow a different approach. The basis of this type of models is the simulation of the damage mechanisms, resulting to fatigue failure. Techniques such as the J – Integral Method [65] and the Virtual Crack Closure

Technique (VCCT) [66] follow a pre – imposed crack and use an estimate of the SERR to propagate the damage.

Cohesive Zone Modelling takes the next logical step in the simulation of the fatigue behaviour. In contrary to the most common progressive damage techniques, Cohesive Zone Models (CZMs) are able to predict both the initiation and propagation of damage. CZMs incorporate a cohesive elements zone at the damaged region which promotes the estimation of fatigue damage grows when a strain (or stress) dependent stiffness degradation law is applied.

In the past, it become clear that CMZs can be employed to predict accurately the initiation and propagation of quasi – static fatigue damage [24], [25]. Unfortunately, the inherently non – linear nature of cohesive elements does not permit their use in linear dynamic analyses. For this reason, the current study will take advantage of the VCCT to explore the fatigue damage growth at various temperature conditions.

2.8.2. The Virtual Crack Closure Technique

As it was discussed, the VCCT will need to calculate the SERR at the crack tip in order for the damage to propagate. The idea is that the energy required for a crack to grow is proportional to the work needed to be done by the forces at the tip of the crack in order to close it. Additionally, following Irwin's work [5], the crack will open when the energy at the crack tip surpasses the Fracture Toughness (G_C) of the material.

With reference to Figure 2.14, the work at the crack tip can be calculated by:

$$\Delta E = \frac{1}{2}\left(X_{1l}\Delta u_{2l} + Z_{1l}\Delta w_{2l}\right) \qquad 2.11$$

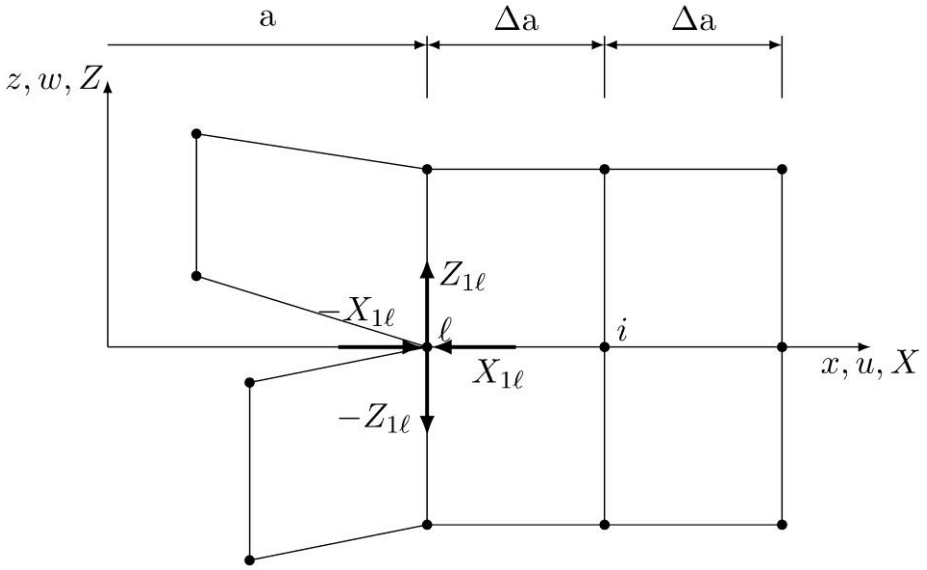

(a)

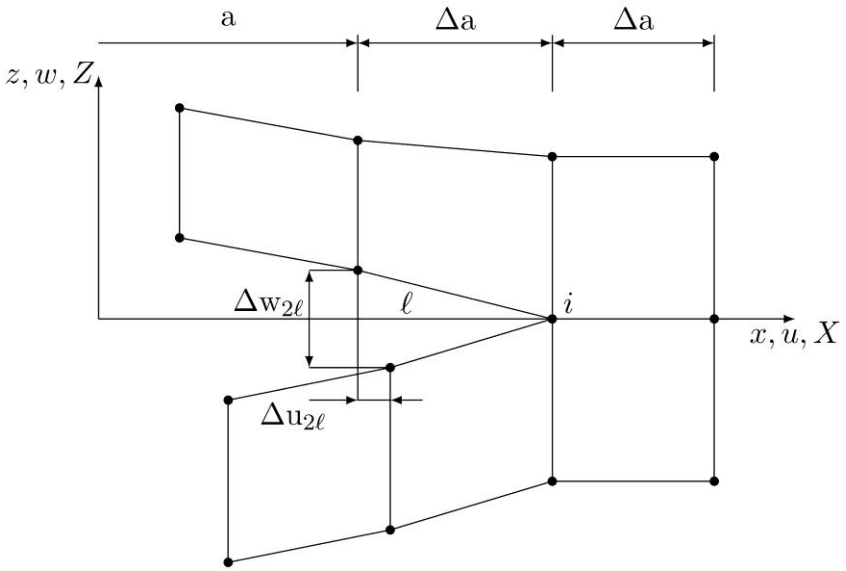

(b)

Figure 2.14: Two steps VCCT – a) The forces exerted at the node close the crack, b) crack is opened **[**67**]**

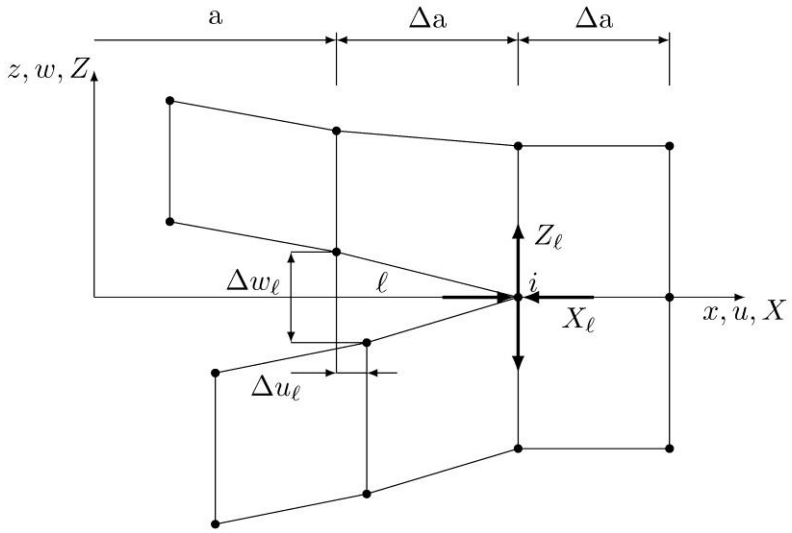

Figure 2.15: Single Step VCCT [67]

Where X_{1l} are the horizontal forces and Z_{1l} are the vertical forces at the node l when the crack is closed while Δu_{2l} and Δw_{2l} are the respective displacements when the crack is open. Furthermore, with reference to the Figure 2.15, the VCCT dictates that the SERR will be computed from the individual contributions of the work done by the forces at modes I and II. Using the crack propagation Δa for a single step, these are defined as:

$$G_I = \frac{1}{2\Delta \mathrm{a}} Z_i(\Delta w_l) \tag{2.12}$$

$$G_{II} = \frac{1}{2\Delta \mathrm{a}} X_i(\Delta w_l) \tag{2.13}$$

2.8.3. The Paris' Law in Fatigue Damage Modelling

It is worth noting that the application of VCCT does not appear usually alongside the vibration fatigue modelling. It seems that Pickard introduced the idea, which consisted of an automated MatLab routine that was able to interact with ABAQUS in order to extend the damage when necessary [49]. In his Finite Elements (FE) model, he employed a set of massless springs to represent the damaged interface which also permitted the extraction of the nodal forces. A spring was removed to simulate propagation of delamination.

The assistance of the Paris Law theorem is necessary to reproduce the damage growth at a dynamic environment, since the VCCT was formed to simulate the damage mechanisms occurring during quasi – static fatigue. However, the implementation of a Paris Law based numerical model, requires the material parameters C and n (Eq. 2.1) which are dependent to the mode mixity G_{II} / (G_I + G_{II}), the stress ratio R and the ambient temperature.

In his latest work, Magi followed Pickard's footsteps and introduced a FE model which was able to simulate the mechanical response during the vibration fatigue testing of tapered CFRP specimens [68]. He reported that the actual mode mixity during endurance testing can be calculated from the contributions of the pure modes I and II while the only R ratio that is suitable for this case is –1 since the contact in the interface is not actually simulated.

Finally, for the purpose of the current study Magi's method will be adopted and improved in order to simulate the mechanical response of CFRP specimens at elevated temperatures.

2.9. Conclusion

This brief literature review on the fatigue life of composites has illustrated that various damage mechanisms can affect their behaviour under cyclic loading. Environmental temperature conditions can also govern the fatigue response of laminates while their viscoelastic nature should not be neglected. Various studies seem to disregard the effects from the viscoelastic temperature of composites materials systems by avoiding accelerated testing and setting limits to the loading rate. Unfortunately, these approaches also confine the wide range of possibilities that accompany resonance vibrational testing.

Furthermore, another lack in the review of fatigue testing methods can be tracked down to the shortage of vibration testing techniques. This study will be mainly focus on understanding the physics that govern the fatigue life of CFRP laminates while taking into consideration the ambient temperature conditions as well as the effects that arise from the viscoelastic nature of the specimens. To achieve it, a vibration testing method will be exploited and enhanced it in order to incorporate the effect of the different thermal loads.

Finally, the experimental results will be blend with the numerical analysis to deliver an in – depth insight in the fatigue life composites. Different FE techniques (e.g. the VCCT) will be employed for simulating both the mechanical and thermal responses of laminates during endurance testing.

Chapter 3

A New Approach for Vibration Testing at Elevated Temperatures

The development of an experimental method, for investigating the fatigue behaviour of composite components subjected to vibration loads and elevated ambient temperature conditions, is described. The new testing method is based on an established testing technique which indicated that fatigue failure can be determined by monitoring the dynamic parameters of specimens during endurance testing. Thus, this failure criterion should also emerge under different environmental conditions. Consequently, the testing procedure ought to be extended in order to support the new experimental requirements.

3.1. Background

As it was discussed in Chapter 2, the resonance testing is not commonly employed in order to investigate the fatigue failure of composites. This mindset can be attributed due to the inherent characteristics of high frequency testing which lead to excessive self – heating as well as various other challenges, associated to the experimental set – up and the extraction of useful information during testing (e.g. in situ damage growth monitoring). In an effort to avoid these complications, the more conventional ways of testing (low frequency) are generally more accepted for the examination of the fatigue life in composite components.

This project has its roots in the work carried out by Dr. Di Maio at the University of Bristol. In his work, Di Maio introduced a method for contactless endurance testing [69]. The research of High Cycle Frequency (HCF) Testing continued at the University of Bristol with the work carried out by Dr. Magi [38]. Following a natural evolution and due to the challenges of the contactless method, Magi improved the method and developed a contact excitation technology for testing at dynamic resonance conditions. He then applied his experimental technique to investigate the fatigue life of Carbon Fibre Reinforced Polymers specimens (Figure 3.1, Figure 3.2) . Finally, he proposed that the stiffness degradation of testing component can be measured by the change in their dynamic parameters (e.g. response phase / acceleration) during cyclic loading [50].

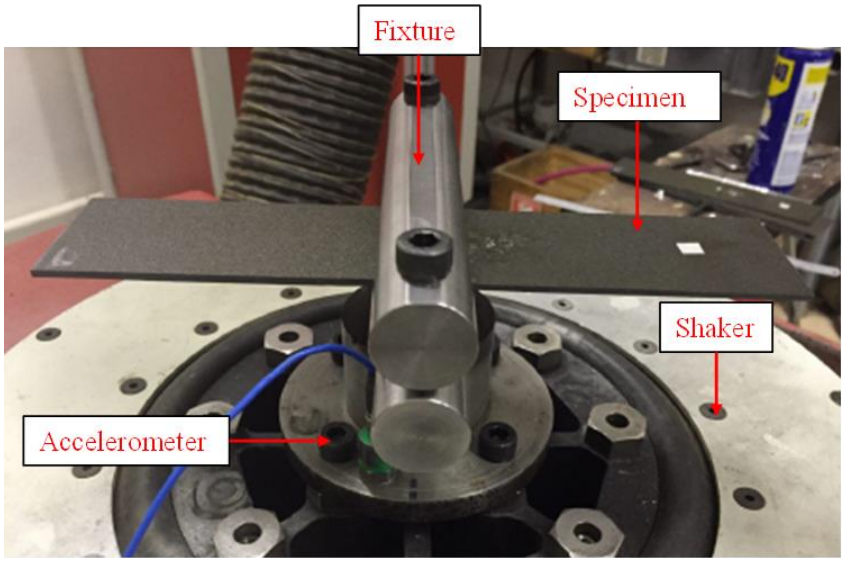

Figure 3.1: Specimen clamped for testing

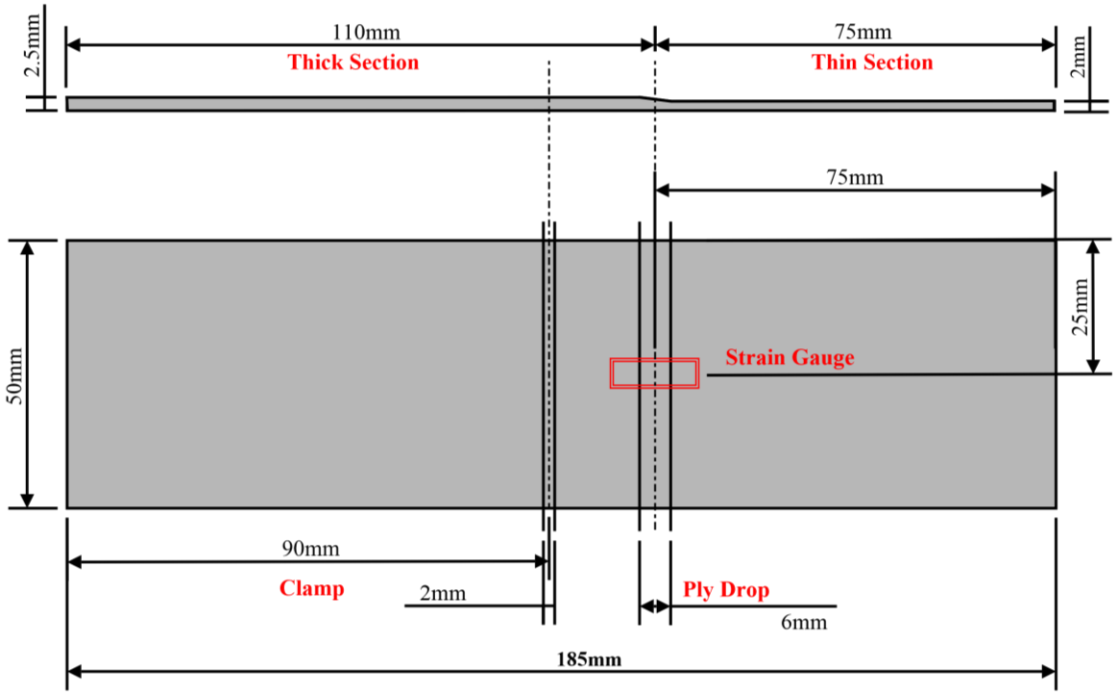

Figure 3.2: Side & Top View of specimen with regions of interest

During the initial stages of his project, Magi examined rectangular composite components that were characterised by their large size. He also employed additional metallic weights in order to produce an even mode shape along the length of his specimens, during vibration testing. His experimental analysis was conducted close to resonance of the composite specimens, at 133 Hz. However, he quickly abandoned this approach in favour of a smaller component where no additional weights are required. In this case, the specimens were excited close to 266 Hz.

Following this path, the current experimental study exploited and improved the resonance testing technique proposed by Magi in order to investigate the fatigue life of smaller CFRP specimens, excited at 395 Hz and under the effect of various thermal loads. Figure 3.3a compares the fatigue life curves captured, utilising the same experimental procedure, between Magi's work and the current project.

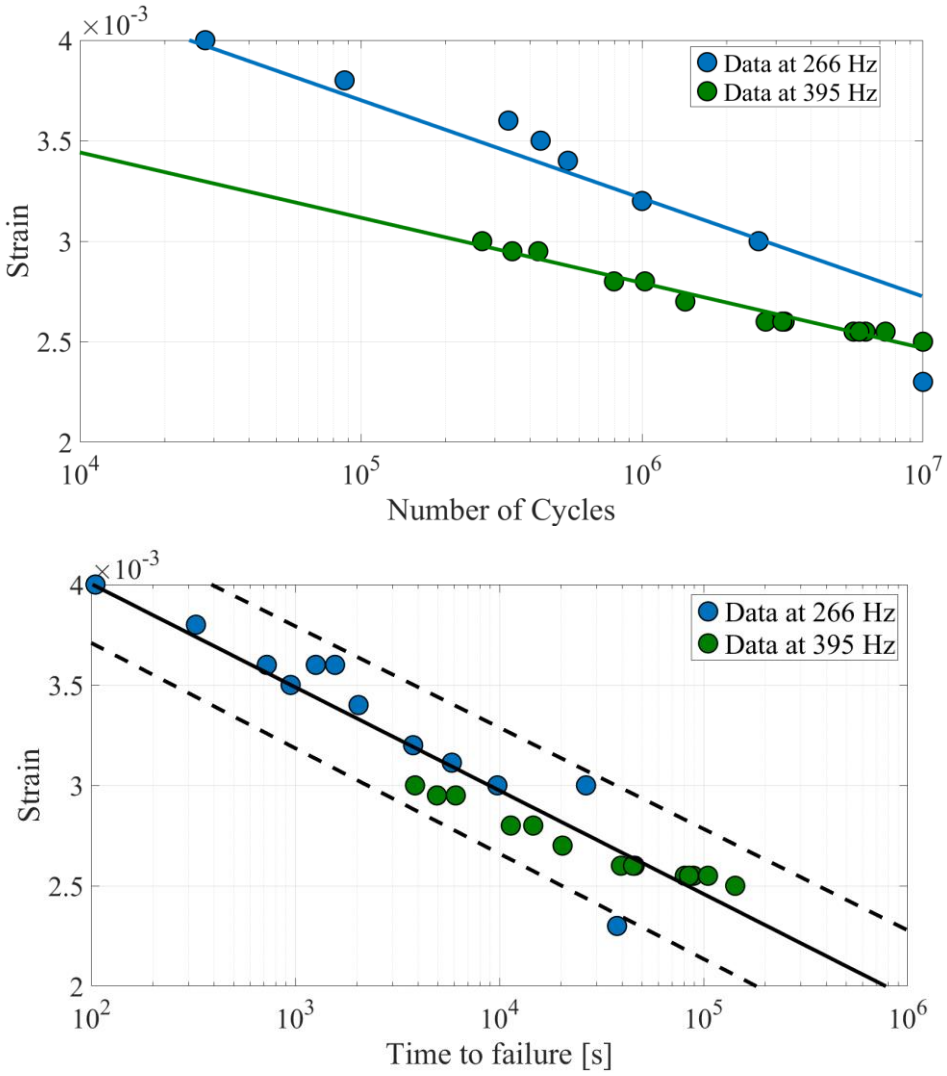

Figure 3.3: A comparison between the Fatigue Life Curves by means of Cycles to Failure (Top), Time to Failure (Bottom)

As it is illustrated in Figure 3.3 (Top), the data suggest dependency upon the excitation frequency. In fact, under sinusoidal excitation and the same number of cycles, the time spent at high strain is less with at higher excitation frequencies. Therefore, in order to take into account, the time spent at a given severity, the fatigue curves can be plotted against the time of failure. The data are presented in Figure 3.3 (Bottom), in a unique master curve.

In conclusion, the current project follows in the footsteps of the aforementioned experimental techniques in order to understand the vibration fatigue behaviour of CFRP laminates under different thermal loadings. The following sections will account for the adjustment to the existing experimental set up in order to meet these critical requirements.

3.2. Apparatus and Experimental Set Up

The previous studies, performed by Magi, succeeded on developing delamination on laminates within 10^6 cycles and thus being able to analyse their fatigue life [70]. The knowledge generated from this research work can contribute towards the establishment and improvement of an experimental technique that accommodates the new objectives of ambient temperature testing. Therefore, the next step for the purpose of this study is to introduce a controlled way to maintain the Exposure Temperature Levels during vibration fatigue testing.

With reference to Figure 3.4 and Figure 3.8, the complete rig – set up is presented. A metallic cubicle was assembled around the electromagnetic shaker. An Infrared Thermal Camera (IRC) was used to capture thermal images from the composite's surface, with a sensitivity < 0.05 ℃, while a Scanning Laser Vibrometer (SLDV) was employed to measure the peak displacement of a specimen subjected to vibration loading. The base acceleration was captured by an accelerometer attached to the base of the fixture. It is therefore possible to extract other dynamic parameters of the system, such as the vibration velocity, acceleration and the response phase. The camera and the SLDV were supported by the cubicle.

The Environmental Chamber is an essential part of the test set up, since it permits the accurate control of the ambient temperature. The openings, on the Environmental Chamber, were insulated with glass wool and insulation rubber; apart from a small hole on the top to allow the IRC and the SLDV to acquire the necessary data. The constant heat lost due to the small gap on the insulation can be neutralised by choosing the appropriate heat input value from the chamber. A fixture was manufactured to fit into the chamber and hold the testing samples into position during the test. Each piece of the aforementioned lab

apparatus was not moved or changed during the full duration of the test campaign, in an effort to ensure the repeatability of the tests. Strain gauges were installed on the top surface of a composite sample to measure the strain level (Figure 3.2). In order to ensure the repeatability of the experimental measurements, the gauges were installed always at the same location; 67 mm from the front edge (of the thin section) of the specimen and 25 mm from the side edge. More specifically, the centre of the strain gauge is aligned with the centre of the ply drop (along the length of a specimen) while it is also placed along the centre of a specimen (along its width).

Additionally, an air pipe was introduced, from the lower end of the chamber, which acted as a cooling source during a smaller test campaign where the effect of cooled air was investigated. Finally, the experimental equipment was controlled by an in house made software: Monteverdi.

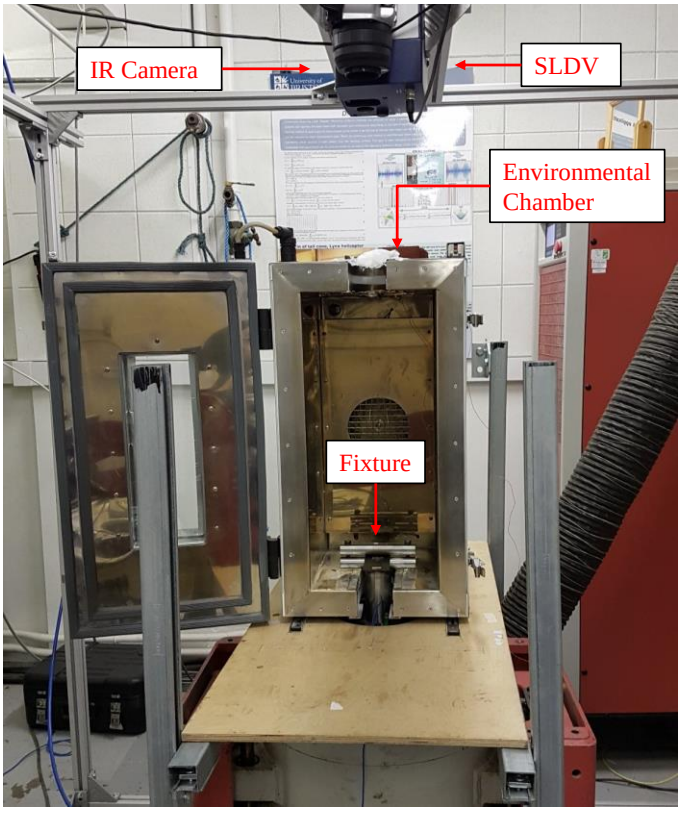

Figure 3.4: Test Set Up

One can understand that the assurance of the repeatable and stable fatigue tests is of great importance. The main factors that may interfere with the experimental results in this test campaign will be discussed in the following sections and they can be identified as:

- Excessive specimen's rotation under the clamp during testing.
- Incorrect tightened load applied on the clamp.
- Improper clamping position of specimen, resulting in eccentric movement.
- Large temperature variation during the time span of an endurance test.
- Inconsistent exposure temperature levels for different tests.
- Interference in the safe operation of the testing apparatus due to environmental conditions.
- Temperature dependency on the Strain Gauges readings.

3.2.1. Acquisition Systems

The operation conditions of an acquisition system (e.g. SLDV, IRC) are critical for ensuring quality results since they could give rise to false reading, alternated results or generally intervene with the smooth execution of an experiment. The SLDV and the IRC were positioned over the chamber in order to exploit a hole in the insulation and acquire the necessary readings. They were attached from a metallic cubicle and at a safe distance from the chamber where heat loss, due to the opening in the insulation, could not influence their operation. Furthermore, both the cubicle and the acquisition systems were not physically connected to the shaker, thus, ambient vibration could have no effect on their operation.

Nevertheless, the room temperature and humidity, in close proximity to the acquisition systems, were measured and verified on multiple occasions, by means of air humidity meter, thermocouples and infrared thermometer. Due to the lab's underground location, it was observed that it maintained a constant room temperature and humidity of 19 °C and 20 %, respectively. Hence, the IRC's properties were adjusted accordingly since its readings can be temperature and humidity dependent. In addition to these, the IRC's distance from

the specimen was greater than the minimum focus distance which permits capturing clear thermal images.

3.2.2. The Fixture

An important update on the pre – existing experimental set up came with the new fixture. The fixture was redesigned to take into account the requirements of this project and thus being able to fit inside the environmental chamber. The fixture (Figure 3.6) consisted of three pieces and it was manufactured from silver steel that can transfer the vibration loads without adding greatly to the damping of the system. The base that enables the fixture's connection to the electromagnetic shaker. The new fixture has a longer cylindrical neck that gives the extra distance required between the shaker and the component. This way the specimen can be positioned inside the environmental oven during fatigue testing. The neck could fit through the elliptical opening located on the bottom side of the chamber. The two clamping rods are located on the top part of the fixture. It was essential that the fixture could survive under a large amount of fatigue cycles; thus, it was crucial to avoid wear and corrosion on the clamping rods. The bottom rod was welded perpendicularly to the cylindrical neck (Figure 3.6) while verifying that was welded parallel to the armature head of the electromagnetic shaker. More specifically, the armature provides the excitation which implies that the response is parallel the excitation.

The rotation of specimens under the clamp, along its vertical axes (yaw), is another experimental challenge that is commonly related to the fixture morphology. A composite specimen was considered failed, if it had experienced visible rotation during an endurance test; even if it lasted for just a few cycles. In the majority of the cases, the rotation was so extensive that it forced the testing to a halt minutes after the test was commenced since the SLDV was not able to track the vibration amplitude, anymore (Figure 3.5).

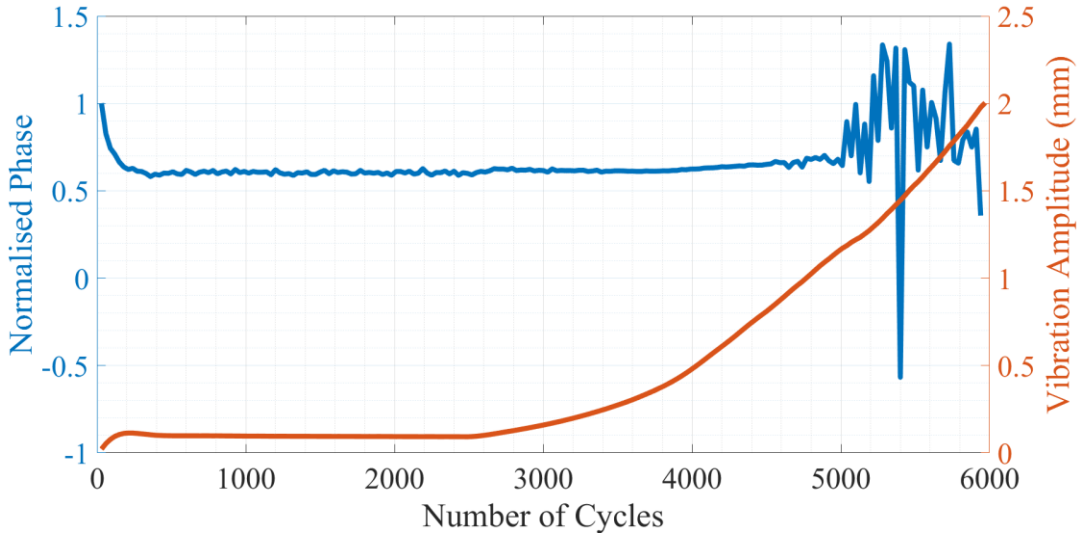

Figure 3.5: Response Phase and Vibration Amplitude (0 to peak) Evolution for a test experiencing rotation

For this reason, different rod widths were assessed during the initial fixture designs. In fact, it was initially believed that a lower overall mass will lead to a requirement for smaller excitation loads; thus, multiple tests were carried out with rods of 100 mm width. However, this fixture promoted the uneven clamping of specimens due to the small rod to specimen width (50 mm) ratio. For this reason, almost all the trials ended with an excessive rotation (Figure 3.5). A behaviour that was not present with the 150 mm rods. For this reason, 150 mm rods were employed for the current experimental investigation.

Another factor that contributed on the rotation of a specimen during testing, is associated with the holes that were bored on the two edges of a rod. The holes were threaded and M8 bolts were employed to connect the top and bottom rod together. Therefore, a close tolerance, in the threaded holes, was essential since loose bolts could lead to an unbalance compression load being applied along the width of a specimen. Additionally, a loose tolerance can also lead to misalignment between the top and bottom rod which could also have the same effects.

In conclusion, empirical observation revealed that all these factors could force a specimen to rotate under the severe loading required for fatigue testing; thus, rendering the

specimen inappropriate for further testing. As a result, the final fixture design was manufactured taking into account the information gathered by the aforementioned study.

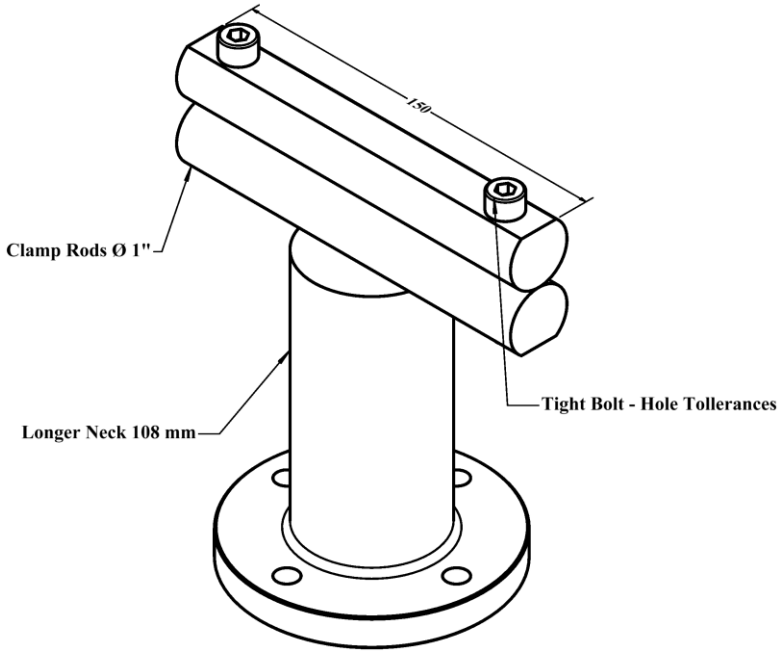

Figure 3.6: New Fixture used to clamp the components inside the environmental chamber

3.2.3. Environmental Chamber

The Environmental Chamber is a critical piece of equipment for this experimental study. The chamber can control and maintain the ambient temperature surrounding the specimen. Although, specialised coolants (e.g. CO_2) were required for producing temperature levels below 25 ^{O}C, the chamber had the ability to maintain temperatures greater than 25 ^{O}C. Due to the underground location of the lab, the use of coolant was considered extremely dangerous, therefore, this study only focuses around the elevated temperature conditions ($\geq$ 25 ^{O}C).

From the early stages of this study, it became apparent that certain equipment (e.g. IRC, strain gauges) can give temperature dependent results. The strain gauges readings are principally affected from the environmental temperature since it can influence the gauges' resistance which is also exploited in order to evaluate the strain level. It was therefore

observed that great variations in the strain reading could be the consequence of slight differences in the exposure temperatures due to the change in strain gauges' resistance. In that account, it is crucial to share consistent heat transfer rates between a specimen and its environment for experiments performed at the same ambient temperature. For this reason, a sensitivity study was performed. Composite laminate was positioned inside the environmental oven and different thermal loads were applied to them without the application of vibration loads. The chamber's heat input value was controlled, for each temperature level, resulting to higher or lower heat transfer rates. It is worth noting that the heat input value is associated with the time required by the chamber to reach the desired temperature. Thus, the chamber can reach the desired temperature at a smaller amount of time when the heat input value is higher.

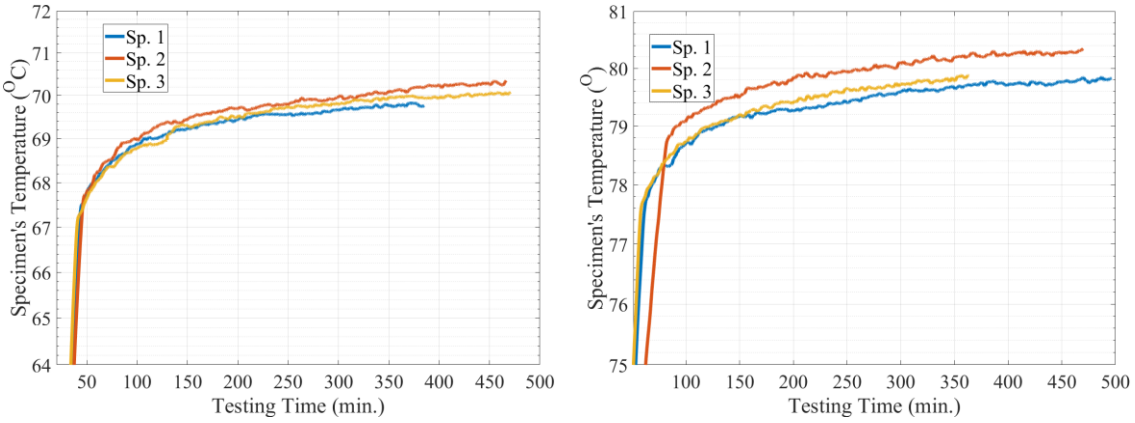

Figure 3.7: Surface Temperature of specimens exposed to 65 ℃ (left) and 75 ℃ (right) – no vibration load

Figure 3.7 presents the results captured by the IR Camera, for different specimens but at the same heat input rate; for 65 ℃and 75℃. The first thing, one could observe is the fact that the data from different specimens are characterised with considerable consistency (less than 0.5 ℃) while they follow similar behaviour. Even though, consistent data are harder to achieve with increasing ambient temperature (Figure 3.7), in both cases, the surface temperature seems to increase quickly up to about 100 min. Beyond this point, the temperature will not rise more than 1 ℃ for the duration of the remaining 450 min. In the light of these observation, a settling period of 100 minutes was permitted. This value was

chosen for practicality reasons since increasing the transient period further could lead to extensive testing time while having just a small impact to the actual settling temperature.

Another interested finding is illustrated in Figure 3.7. The settling temperature (at 100 min. on the graph) varies from the temperature that was set on the chamber by ≈ 5 ℃. This implies that when the surface settling temperature is 70 ℃, the chamber's temperature is set on 65 ℃ (or 80 ℃ when the chamber is set at 75 ℃). However, it is worth noting that this behaviour was mainly observed for the current temperature range of interest (25 ℃ to 75 ℃).

3.2.4. The Specimen

Another development in the pre – existing design specifications come in the form of the redesigned specimen. The rectangular coupons consisted of cross directional plies, made of IM7 / 8552 which is an aerospace grade Carbon Fibre Reinforced Polymer (CFRP); provided by Hexcel. Composite plates were prepared from pre – preg sheets and cured according to Hexcel's regulations [71]. As it is presented at Figure 3.8, the stacking sequence was $[0, 0_{cut}, 90_{cut}, (0, 90)_3, 0]_S$. A Ply – Drop was a key feature of the testing coupons. Ply – Drop is a common feature for numerous composite components, with tapered geometries, such as the fan blade roots. However, for the purpose of this experimental procedure, they are used as stress intensifiers.

Furthermore, it was decided that one 0^O plies should be positioned above the ply – drop since, in the presented experimental study, the specimens are flexed in the 1^{st} bending mode, along their length. As a result, 0^O plies can bear the bending loads. Alternatively, if the terminated plies were located in the outer face, the delamination could have initiated almost immediately.

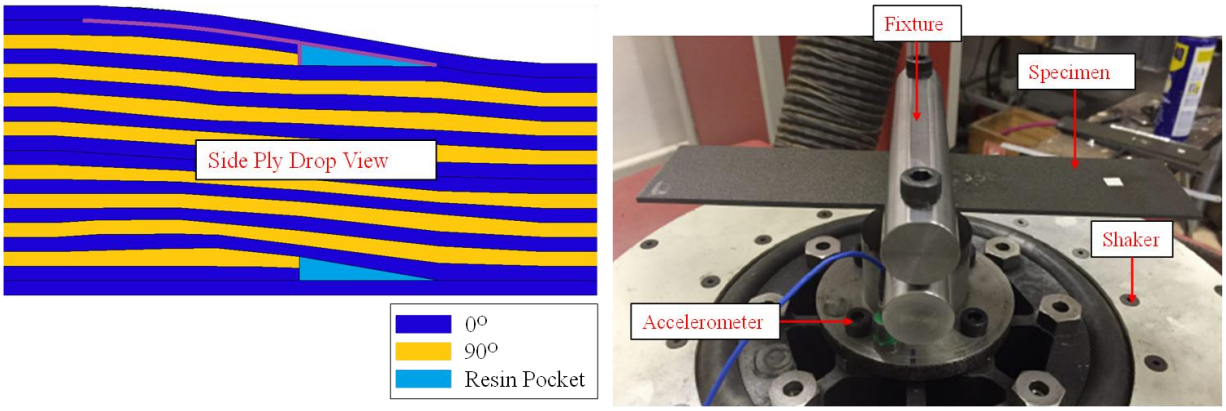

Figure 3.8: Specimen's Lay Up (left) / Specimen clamped for testing

In the past, CFRP samples were excited at the 1st bending mode while equal vibration amplitude was achieved in the two sides of a specimen by means of added weights [50]. However, this experimental approach was abandoned quickly and a different method was adopted. For the purpose of the current study, equal peak displacement at both sides was achieved by fabricating a smaller specimen (Figure 3.1, Figure 3.2) that was clamped along the centre of its mass, during endurance testing. However, the centre of its mass does not coincide to the half – length point, due to variations in the specimen's thickness (ply – drop). Following this method, the coupons were 185 mm × 50 mm × 2.5 mm to 2 mm; leading to a resonance frequency of ≈ 395 Hz.

It was discovered that inaccurate manufacturing of specimens, could introduce unwanted rotation of the testing samples. Poor processing can lead to the development of uneven stiffness distribution which in turn will affect the mode shape. Many of the initial experiments suffered from this phenomenon until an improved manufacturing process was adopted. Smaller rectangular CFRP samples were cut and trimmed from larger laminate plates. After that the composites were inspected and measured for the orthogonality of their edges. By trial and error, it was decided that coupons with orthogonal deviation greater than $\pm 1^{O}$, will lead to extensive rotation and thus they were not tested. Nevertheless, the

coupons were then polished into the desired dimensions (± 1 mm) to ensure the repeatability of the tests and secure that the experimental data can be compared.

Operating Deflection Shape (ODS) scans were conducted, both experimentally and numerically in order to inspect the final mode shape (Figure 3.9) of the new testing sample. Figure 3.9 presents the data for a single mode of vibration while both investigations were performed at the same excitation frequency. It can be observed that the numerical and experimental results experience only a slight deviation. This deviation is the result of the difference between the simulated and the experimental strain distribution which emerges due to certain simplifications on the FE model (2D geometry, not fully representing the fixture etc); these assumptions will be discussed in the following chapters. Despite that, it can be noticed that both sides of the new specimen vibrate at the same maximum displacement which implies that odd deflection shapes were avoided. Finally, the small drop (starting at 0.07 m) in the experimental data is the result of the difference in fixture's amplitude.

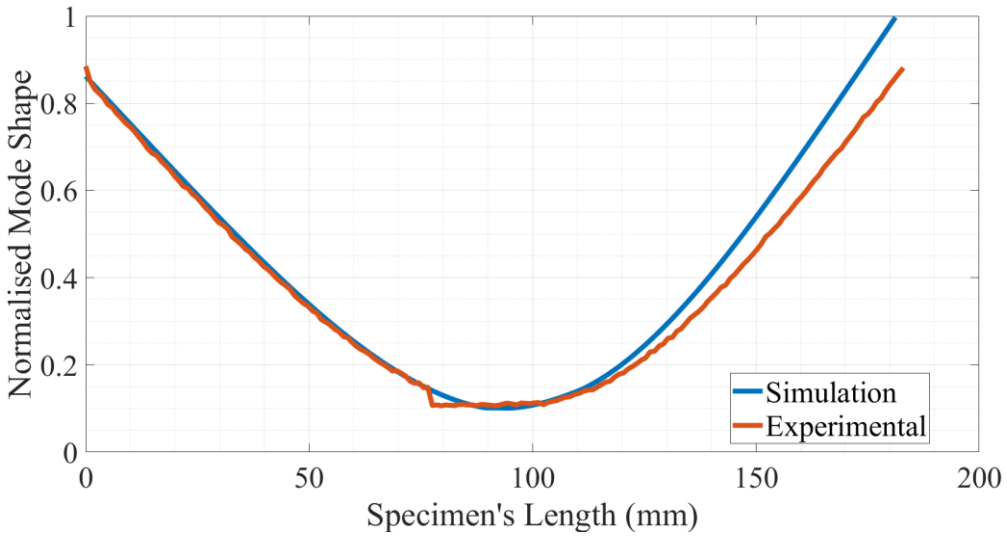

Figure 3.9: Simulated and Experimental ODS

3.3. Vibration Testing Method

A novel testing procedure for vibration testing of composite components, was developed by Di Maio and Magi [38]; which is defined by its ability to capture fatigue damage of small size with great accuracy, through tracing small variations in the stiffness.

As it was discussed throughout the literature review, their initial tests were not able to capture the stiffness degradation due to fatigue damage by any other means, albeit a hot spot did appear the thermal images. During these tests, the commonly used Phase Lock Loop (PLL) was in operation to maintain the response phase close to the resonance frequency for the entire duration of each test. A turning point in the method was reached when the decision was made to abandon the PLL for the less common Frequency Lock Loop (FLL). The FLL enables the tracing of the Response Phase rather than the Resonance Frequency.

The new experimental procedure dictated that the CFRP composites were excited at the 1st bending mode, close the resonance frequency and at constant 0 to peak displacement and frequency. By fixing the excitation frequency one can observe how the dynamics of the specimen evolves due to the change of its internal stiffness distribution. In fact, for a Single Degree of Freedom mass – spring system, with constant mass (m) and damping (c), Magi [50] expanded the Taylor series of the Transmissibility function. He concluded that small stiffness (k) variations can be related to the response phase (φ) with:

$$\varphi(\omega) = tan^{-1}\frac{m\omega}{c} + \frac{m^2\omega(k - m\omega^2)}{c^3 + cm^2\omega^2} + \mathcal{O}((k - m\omega^2)^2) \qquad 3.1$$

Where ω is the resonance frequency. Figure 3.10 depicts the experimental results of vibration test performed at constant 25 °C inside the environmental chamber. On contrary to the previous experimental work that conducted at room temperature (between 18 °C to 25 °C) [50]. It can be observed that the phase of a specimen when subjected to vibration fatigue testing, traces a constant slope decay up to a sudden change which is defined as the "Critical Event" which is the opening of the delamination (fatigue failure) [50]. On the

other hand, the acceleration of the specimen follows a mirrored behaviour. Nevertheless, for practical reasons, throughout the presented study, the response phase was preferred over the acceleration for analysing the experimental result. In fact, it was noticed that the phase could capture the fatigue life in a more consistent way compared to the acceleration since the initial phase value was always kept the same throughout the different experiments (within a range of ± 5°); regardless the ambient temperature and the applied strain. The behaviour of the response phase will be discussed in depth in the upcoming chapters.

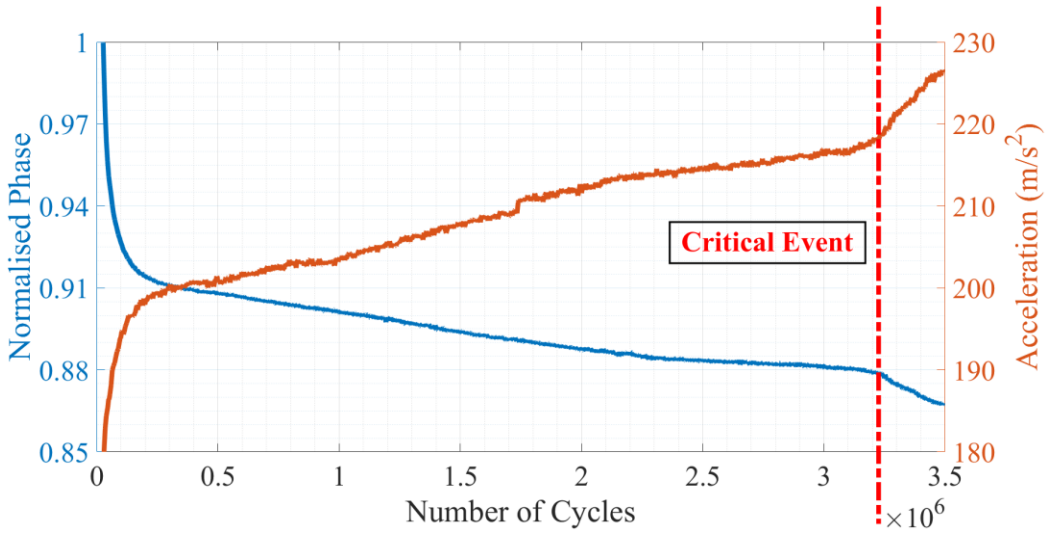

Figure 3.10: Typical evolution of dynamic parameters of specimen (test at 25 °C)

It is therefore possible to develop SN Curves (Fatigue Life Graphs) for various ambient Temperature levels based on the appearance of Critical Events. In particular, a fatigue life test was terminated if either the Critical Event or 10^7 cycles were reached. Thus, the number of cycles at the moment of the Critical Event can be plotted against the applied strain of the respective test. Alternatively, if the test had reached 10^7 cycles, the specimen was considered pristine. It is worth stressing here that the SN Curves were not developed to characterise the material but rather to aid the current scientific investigation.

3.3.1. Experimental Procedure

Throughout the entire duration of the current project, multiple tests were performed exploiting various set – ups and arrangements. Eventually, a detailed testing method was developed from the knowledge that was accumulated.

It was found that it is essential to follow a detailed test procedure in order to ensure the consistency of the experimental results. It is apparent that small variation in the testing procedure could lead to variations in the experimental results. For example, a difference between the strain measurement points of two specimens, results in variation in the final readings. Hence, only when the specimens' dimensions were verified, the strain gauges were applied to each specimen. The sensors were positioned on top of the most stressed area (ply drop). While the actual strain field of the tested coupons may not be influenced, the strain reading could be affected by slight misalignment or rotation of the gauge. For this reason, the position was carefully measured prior to each application.

On the next stage, the composites were fixed under the clamp. It was observed that inadequate or uneven tightening of the bolts on the clamping rods, could give rise to unwanted rotation of the CFRP laminated during endurance. It was decided through empirical observations that 8 N/m is a good value of torque to overcome these challenges. Despite the fact that the torque was carefully applied; the distance between the two clamping rods had to be measured by means of thickness gauges (clearance Figure 3.10). This way the uniform compression load was ensured through the adjustment of the applied torque when necessary.

When the sample were secured inside the chamber and thermal equilibrium was achieved between the two, the vibration fatigue testing was initiated. In particular thermal equilibrium was ensured utilising a combinations fromthe readings acquired by the IRC, the thermocouples placed inside the environmental chamber and the knowledge gained form the aforementioned analysis (Figure 3.7).

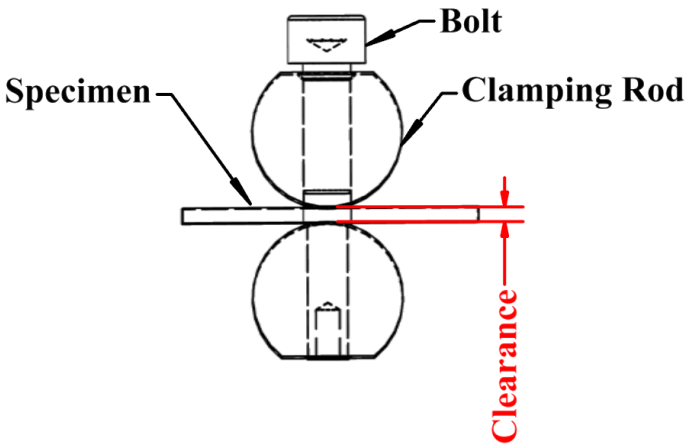

Figure 3.11: Schematic representation of specimen adapted to the clamp

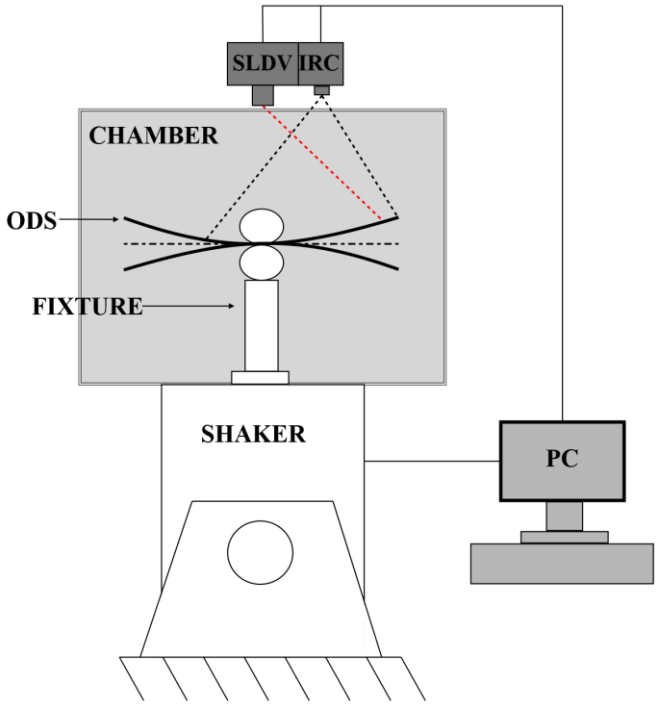

Figure 3.12: Schematic representation of the experimental set – up

Monteverdi was the software suite, coded in LabView, in charge of monitoring and controlling the experiment (Figure 3.12). MONTEVERDI is an acronym for the full name "MOdal eNdurance Testing for the EValuation of compositE stRuctures Dynamic propertIes". The software is used for acquiring data from the fatigue tests while controlling the test equipment.

Figure 3.14 depicts the experimental procedure. During the first stage Monteverdi utilised the acquired data from the SLDV and the base accelerometer to compute the Frequency Response Function (FRF). Thus, a bandwidth around the resonance frequency was chosen. This bandwidth is then used as an input for the Sine Step Test.

Even though during the first stage, Monteverdi excited the sample of interest using a pseudo – random waveform, at this stage it was loaded with a sine step at different vibration amplitudes [72]; similarly to the final endurance test. As a result, the transmissibility can be calculated from the excitation amplitude and the acceleration.

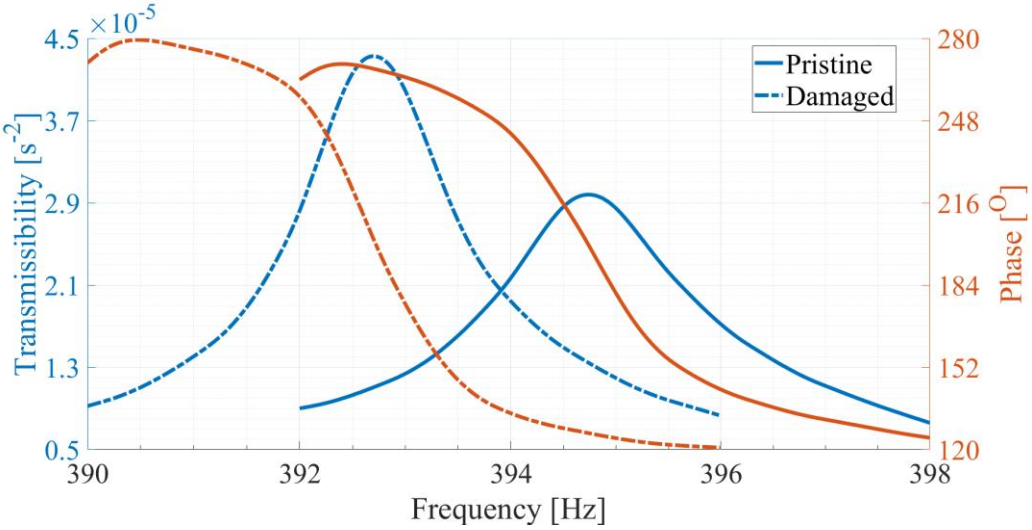

Figure 3.13: Transmissibility and Phase Response Functions before and after endurance

For a stable amplitude control, the response phase and its correspondent excitation frequency were chosen to be on the right – hand side of the transmissibility response and close to the resonance frequency (Figure 3.13, ≈185°). At this point, it is worth noting that the acceleration was exploited in order to evaluate the response phase, instead of the excitation force which is most commonly used. For this reason, the resonance phase is close to 185° instead of 90° since there is a 180° difference between the vibration displacement and acceleration. This way, for a constant peak displacement, while the stiffness of composite deteriorates, the transmissibility shifts to lower frequencies; resulting in a decrease in the phase and increase in the acceleration (Figure 3.13). On a different scenario, the acceleration traces an initial increase followed by a decrease. Instead, it is important that the starting phase of each test is kept constant for each test in order to produce repeatable and comparable data.

During the sine step, the strain level was also measured and correlated to the respected vibration amplitude. It was essential that the resistance of the gauge was calibrated prior the sine step excitation, by adjusting their voltage, in order to compensate for the effects of the surrounding temperature. However, the strain gauge was removed after the sine step and Monteverdi was able to maintain a constant displacement during the fatigue tests. This assumption is based on the fact that the damage size is so small that the excitation amplitude remains unchanged during the fatigue test. As a result, it can be assumed that the strain level remains constant up to the occurrence of the Critical Event. Finally, the endurance test sequence consisted of the following steps:

1. Initiate IRC recording
2. Initiate auto amplitude control & PLL for a brief period until the resonant conditions are reached
3. Conduct Vibration Fatigue Test
4. Complete the endurance test, when either of the termination criteria are met (Critical Event / 10^7 cycles)
5. Evaluate the modal parameters after the test (sine step analysis)

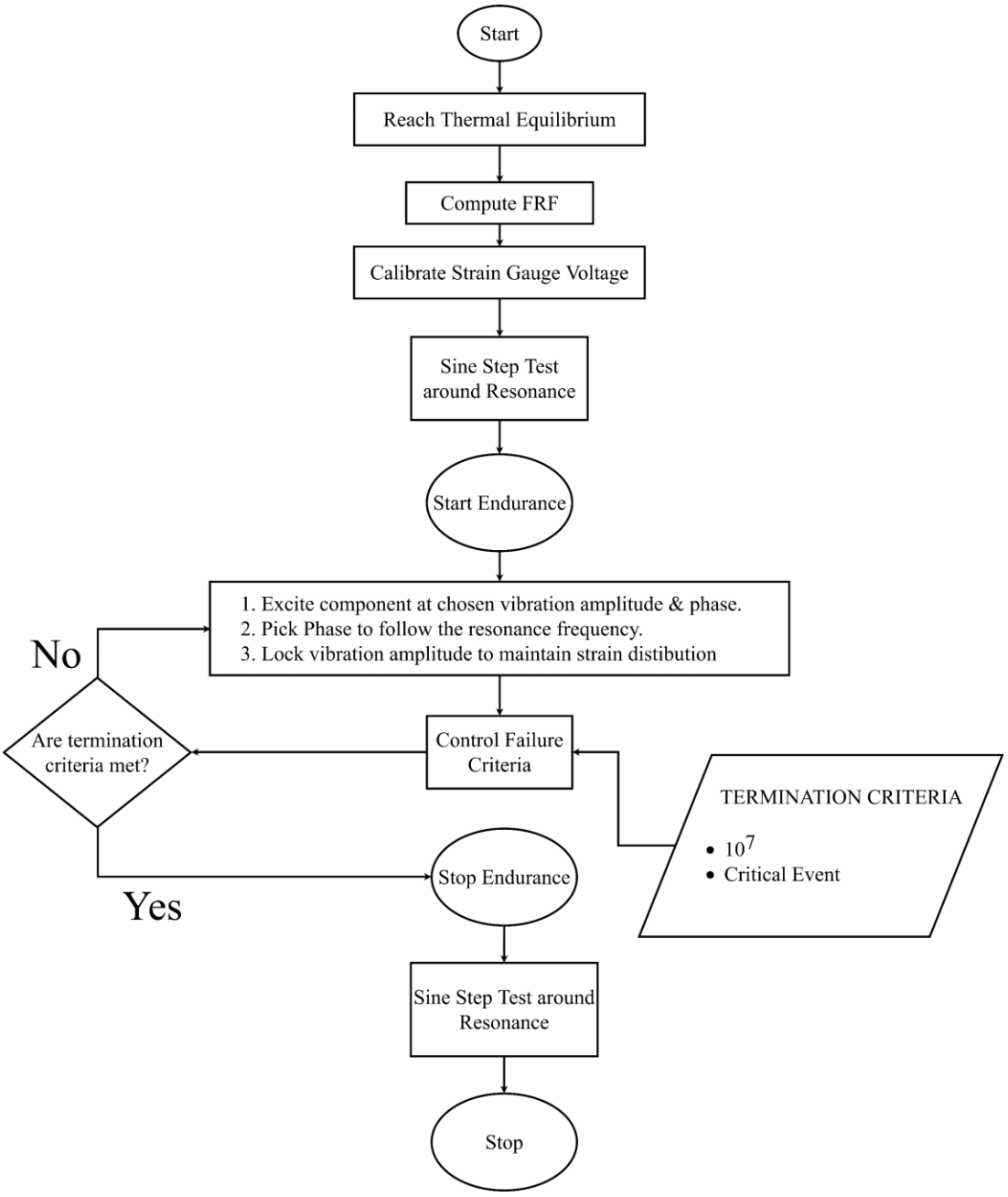

Figure 3.14: Monterverdi Process Flow Chart

3.3.2. Modal Analysis

It is widely known that the viscoelastic properties of composites are inherently temperature dependent while the structural damping is tightly linked to the viscoelastic behaviour of the laminate. It is therefore interesting to study the effects of temperature on the dynamic properties of a specimen.

The resonance frequency was evaluated at four different temperature levels. Figure 3.15 indicates the variation in the resonance frequency for the testing samples used during the experimental research of this project. One could notice that the experimental data fall within the range of 390 to 400 Hz (2% error); which implies that there is a small scatter on the excitation frequencies regardless the various thermal loads. Nonetheless, it seems that the deviation of measurements, within the same temperature level, is broadened as the ambient temperature is increased.

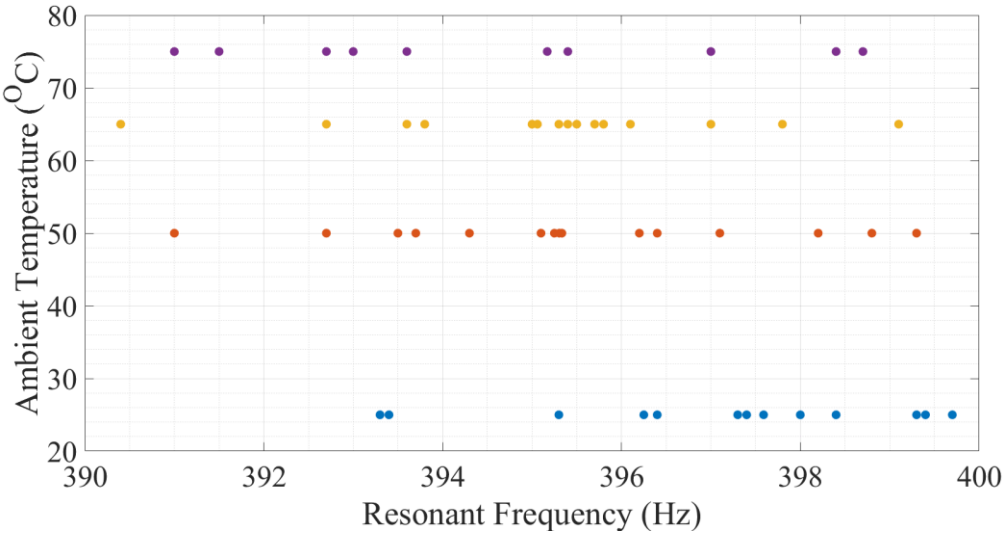

Figure 3.15: Resonance Frequencies of specimens at different exposure temperatures

The effects of the environmental temperature conditions over the structural damping, are also of great importance. The resonant conditions (frequency and phase) are necessary for acquiring the damping factor of a composite laminate. The experimental results, for the resonance phase and frequency, are presented in Figure 3.15 and Figure 3.16. Similarly to

the resonance frequency, the exposure temperatures' influence over the structural damping of the components does not appear to be great. The experimental data fall within the range of 3.4×10^{-3} to 3.9×10^{-3} (15% variation). It appears that the standard deviation is smaller at 75 ℃; when compared to the data acquired at lower temperature levels. However, one should also consider that the number of experimental measurements that acquired at 75 ℃ is smaller than in the rest of the temperatures. Thus, it can be assumed that this outcome does not conceal any other behaviours. Moreover, it can be observed that the experimental data follow a mean damping value of ≈ 0.0035.

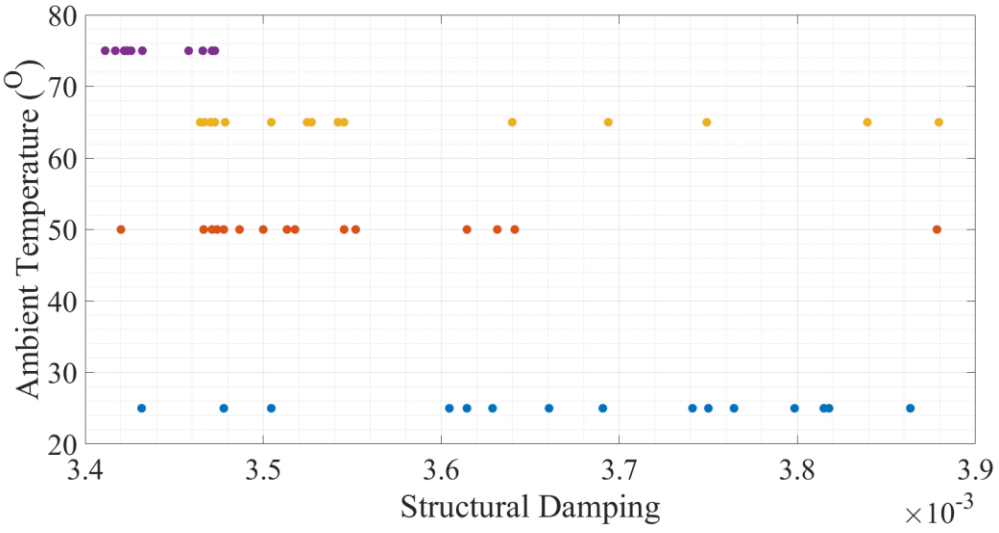

Figure 3.16: Structural Damping of specimens at different exposure temperatures

3.3.3. Strain and Vibration Amplitude

Amplitude control is an essential part of the experimental method. The strain level had to be kept constant during the endurance test, until the occurrence of the Critical Event, in order to analyse and compare the behaviour of CFRP at multiple levels; since the peak displacement proved to be a less reliable severity. The maximum vibration amplitude of an undamaged specimen was corelated to a specific strain level prior the initiation of the endurance test. Thus, during the endurance test, a constant strain level was achieved by maintaining a fixed vibration amplitude. Due to the assumption that the system is not

altered during testing, it can be assumed that the correlation between the two remains unaffected while the stiffness of the specimen is unaffected. In fact, the following will extensively discuss the point, on the fatigue life of a specimen, during which the damage size is considered sever and thus changes the stiffness of a specimen, considerably.

Furthermore, it is worth discussing the effects of ambient temperatures on the measurement of strains. The rate of change of the strain / displacement curves are reported in Figure 3.17, for all the specimens tested during the entirety of this test campaign. It is noticed that the evaluation of the experimental data can be proven challenging at higher temperatures since the scatter is increased. This behaviour could be attributed to the operation temperature capabilities of the strain gauges which, in this case, was below 80 ℃. In the light of these observations, it was decided that the ambient temperature levels, that will be investigated throughout this study, will fall between 25 ℃ and 75 ℃.

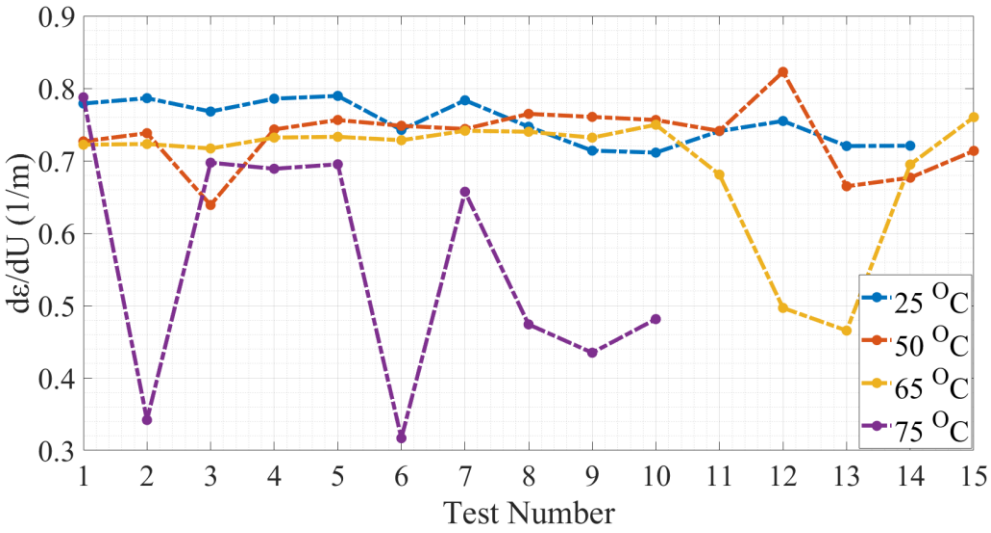

Figure 3.17: Variation in the rate of change of corelation curves due to ambient temperature

Besides these, the selection of the laser measurement point is another crucial factor of the experimental procedure. With a maximum measurable velocity of 20 ms^{-1}, the SLDV, that was used in this study, is able to capture a maximum displacement of only about 4 cm at 395 Hz. Accordingly, the measuring point cannot coincide with the point of maximum

deflection due to the signal limitations. Thus, it was decided that the measurement point will be located 12 mm away from the front edge (of the thin side) and in the middle with respect to the width (25 mm). This way the point will be closer to the node, capturing a smaller deflection while not being affected by torsional harmonics.

3.4. Remarks

A vibration testing technique was adopted for investigating the high cycle fatigue life of composites laminate. The method indicated the use of amplitude control along with constant excitation frequency in order to monitor the stiffness degradation of the composite components by means of abrupt change in the response phase. Many trials had to be performed in order to renovate the existing procedure to accommodate the requirement for researching the effects of elevated temperature levels while establishing a stable testing procedure. In respect to this demand, multiple features were re – evaluated and improved.

On top of that, modal analysis was carried out under different exposure temperature levels, illustrated that the resonant parameters of CFRP are not heavily affected by the thermal conditions that were investigated. In fact, it was found that the structural damping and the resonance frequency experience minor changes between 25 ℃ and 75 ℃. An observation that will be important in the coming chapters.

On the other hand, special care should be demonstrated towards certain equipment. Therefore, recognising the fact that strain gauges fail to operate under harsh temperature and specialised sensors are required.

In conclusion, a testing method was developed for studying the fatigue behaviour of CFRP laminates subjected to dynamic and thermal loads. Furthermore, the ground was set for the examination of structural degradation using resonance fatigue testing; even when the composites are exposed to elevated temperature conditions.

Chapter 4

EXPERIMENTAL INVESTIGATION OF FATIGUE LIFE

The fatigue behaviour of composite components, subject to vibration load and elevated temperature conditions, is investigated exploiting the advantages of the experimental method, described in Chapter 3. The dynamic and thermal properties were captured and utilised in order to better understand the physics that govern the fatigue damage development. In addition to this, a CT scan analysis was employed alongside the experimental examination to provide further insight in the structural degradation of composite components under cyclic loading. Finally, the relation between the mechanical and thermal responses is discussed.

4.1. Introduction

In the previous chapter, a vibration testing procedure for investigating the fatigue life of composites was presented. The method suggested that failure is determined by the appearance of a "Critical Event" which can be defined as an abrupt change in vibration parameters (e.g. response phase, base acceleration) of the CFRP components. It was then reported that the proposed method could capture the stiffness degradation on specimens subjected to both dynamic and thermal loads. Although, it is apparent to assume that delaminations and microcracks should be present before the Critical Event, no information is available for this stage of the test. As a result, the state of the specimens could be analysed through X – Ray Scans (CT Scans) and then compare them against the established failure criteria.

Despite the fact that the viscoelasticity of the resin forms a strong relation between the thermal and the mechanical properties of composite laminate their specific connection under vibration loading has not been defined. Instead, it is possible to introduce a relationship between the two, utilising the experimental techniques introduced in Chapter 3. Additionally, it is widely accepted that the fatigue damage can be confirmed during endurance through thermography [73]–[77]. This chapter will discuss the relationship between the evolution in specimens surface temperature and the suggested failure criterion.

In conclusion, this chapter discusses the experimental investigation for the fatigue behaviour of carbon reinforced polymer laminate under different thermal loads and resonance testing. It also attempts to offer some analytical insight and establish a relation between the mechanical and thermal responses of a laminate. Finally, it will exploit the knowledge developed in order to alter the fatigue growth rate during endurance.

4.2. Mechanical and Thermal Responses during endurance

The response phase and the self – generated – temperature of a composite component, are two factors that can provide insight about the fatigue life of specimens. The response phase of composites is linked to their mechanical properties and it can be directly proportional to the stiffness of the testing coupon [50]. On the other hand, the endogenous heating temperature of the specimen is closely linked to its thermal properties and it is enhanced under fatigue loading due to the viscoelasticity of the polymer matrix. A measure of the self – heating temperature could be captured during endurance when tracing the surface temperature of a composite.

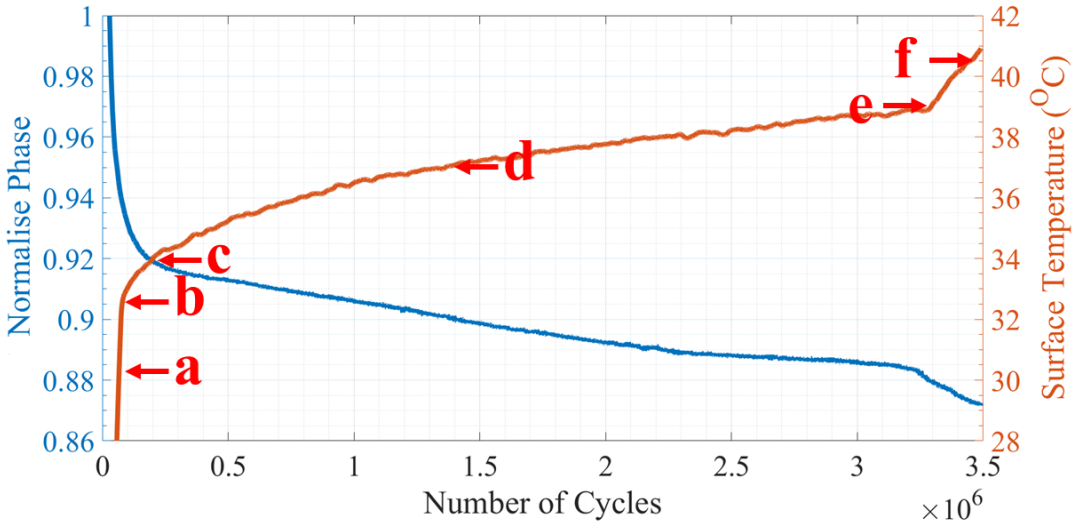

Figure 4.1: Typical Response Phase and Self – Heating Temperature evolutions during fatigue testing

From the early stages of the test campaign, it became apparent that the response phase and the self – heating temperature of the specimens follow an almost mirrored behaviour. Figure 4.1 presents the typical self – heating temperature and phase behaviours of composite specimens during resonance testing. It was noticed that vibration phase follows a constant slope decay until the Critical Event where a sudden change occurs. Figure 4.1 also illustrates the progression of the maximum surface temperature as it was captured from the region of the ply – drop (highest strain area). One can observe that a sudden increase in the specimen's temperature coincides with the Critical Event. This phenomenon arises due to the delamination propagation. As it will be discussed in the following sections, the mechanical and thermal responses of specimens are tracing similar behaviour under different elevated temperatures.

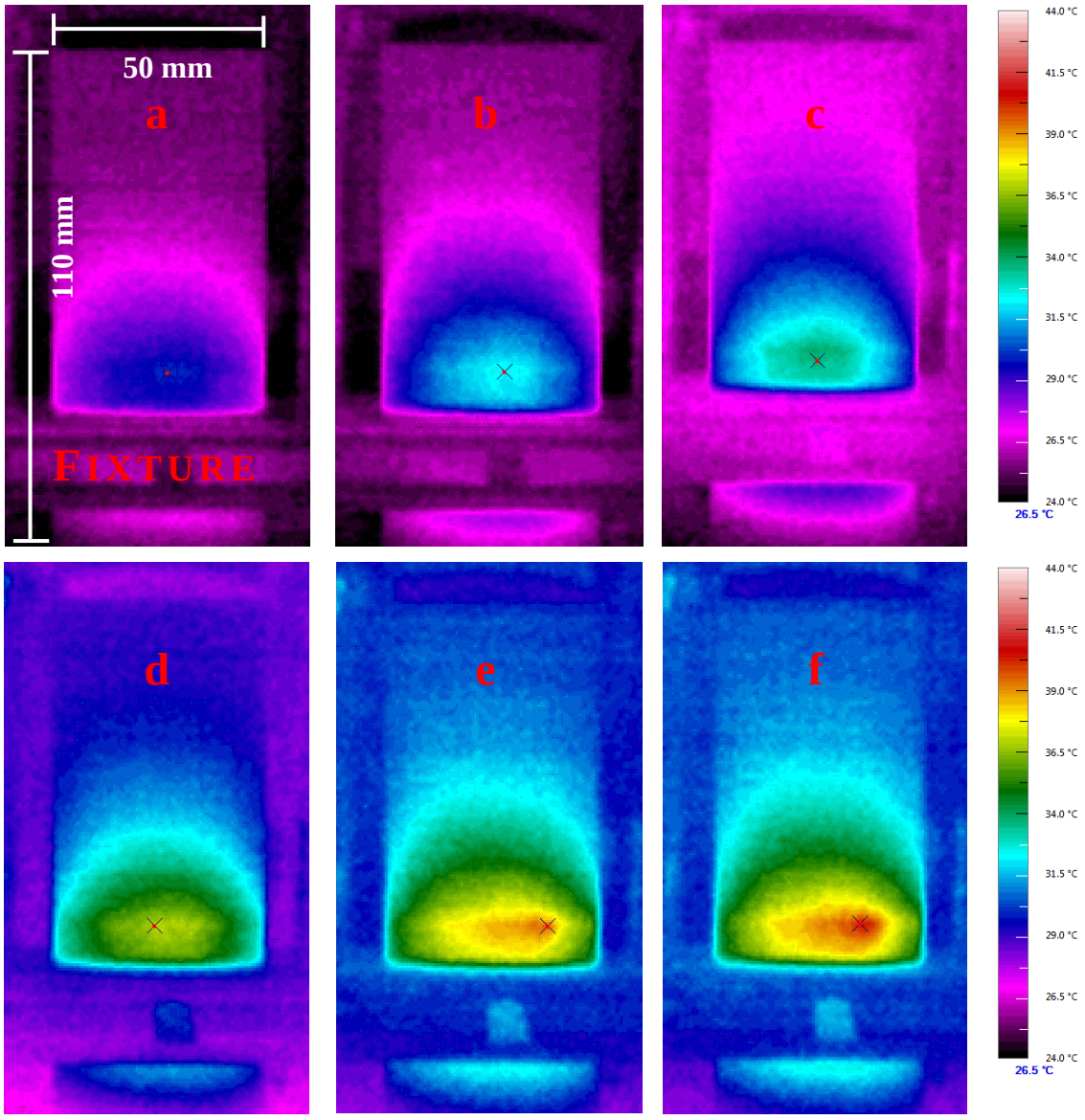

Figure 4.2: Thermal Images of a specimen during fatigue testing (Top View) correspond to Figure 4.1 / Typical evolution of the temperature distribution

Additionally, Figure 4.2 illustrates the progression of the temperature distribution along specimen, at different times during an experiment. The thermal images correspond to the experimental data that were introduced with Figure 4.1; which took place at 25 ℃.

Figure 4.2 captures the top side of the specimen and the top clamping rod of the fixture is also visible. The ply drop is characterised by an approximately straight line of higher temperature along the width of the specimen and it is marked by an x. Unfortunately, the thermal camera's field of vision is limited by the small opening at the top surface of the environmental chamber and only the ply – drop region was captured.

An oval temperature distribution shape appears along the specimen which is developed due to the combination the strain distribution and air flow around the specimen. The shape appears unaffected by the viscoelastic temperature increase; from Figure 4.2a until Figure 4.2d. Furthermore, Figure 4.2e was captured at the critical event. A hot – spot is visible in this figure. This area of higher temperature overlaps the normal oval shape of the temperature distribution and it is developed due to the delamination in the ply drop region. Finally, Figure 4.2f illustrates the typical thermal behaviour of a testing coupon after the critical event. The shape of the hot – spot has increased which reflect to the increase in the size of the delamination and the local temperature has risen.

4.3. Fatigue Damage Evolution

The acquisition of a wide variety of data, for both thermal and mechanical properties of the test samples, has been fundamental both for understanding the damage growth and expanding the knowledge for the elevated surrounding temperature levels. Thermal and mechanical responses were found to follow and inverse behaviour. Nevertheless, a closer look to the experimental data reveals interesting information. With reference to Figure 4.3, one can observe that both the self – generated temperature and the response phase can be separated into 3 distinct regions. In fact, one can observe the fatigue life can be divided into 3 quasi – linear trends.

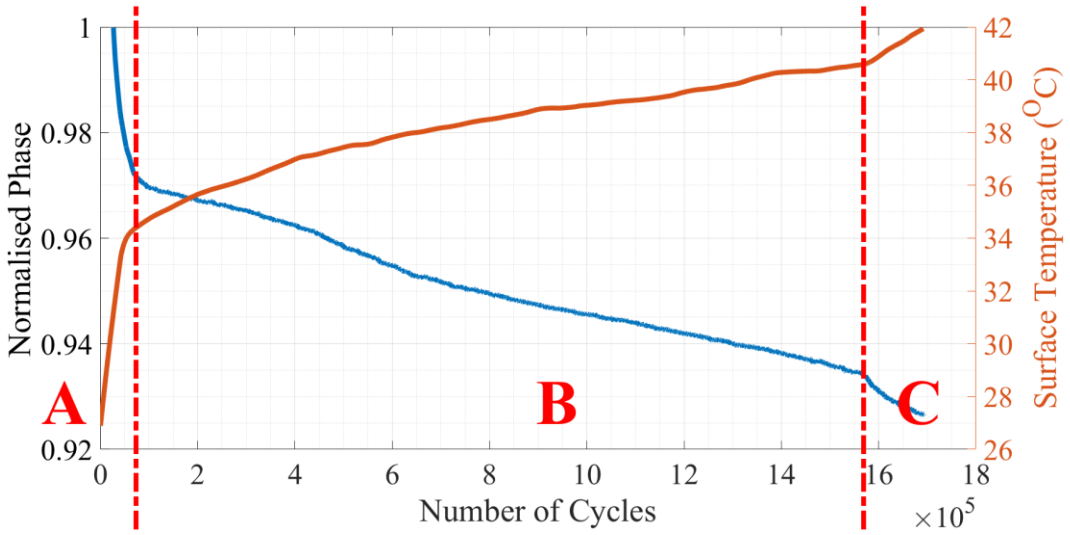

Figure 4.3: The three distinct regions of the phase and self – heating temperature evolutions

For this reason, it was decided that interrupted tests will be conducted in an effort to analyse the fatigue damage development during endurance testing (Figure 4.4) as well as to understand the difference between the 3 stages. The experiments were interrupted at about every 2.5×10^5 cycles (about 1 ℃ increase of the self – heating temperature). At this point it is worth noting that even though the tests were conducted using identical specimens, the applied strain and ambient temperatures were closely monitored to ensure the repeatability of the results. Hence, it can be assumed that the behaviour of the response phase of the components traced the same patterns although different specimens were considered for each test.

Thermal Images indicated that fatigue damage will develop only in the ply drop region, during endurance (Figure 4.2). For this reason, the tested coupons were trimmed down to smaller than the size of the ply drop (48 mm × 6 mm × 2.5 mm). The trimmed specimens were then analysed by means of X – Ray scans (CT Scan). The small size of the coupons was necessary to allow the dye to penetrate successfully though their thickness of the sample since the only available entry point was the edges. The outcome of these tests will

be discussed in the following sections while reflecting over the different stages of the viscoelastic temperature and phase evolution.

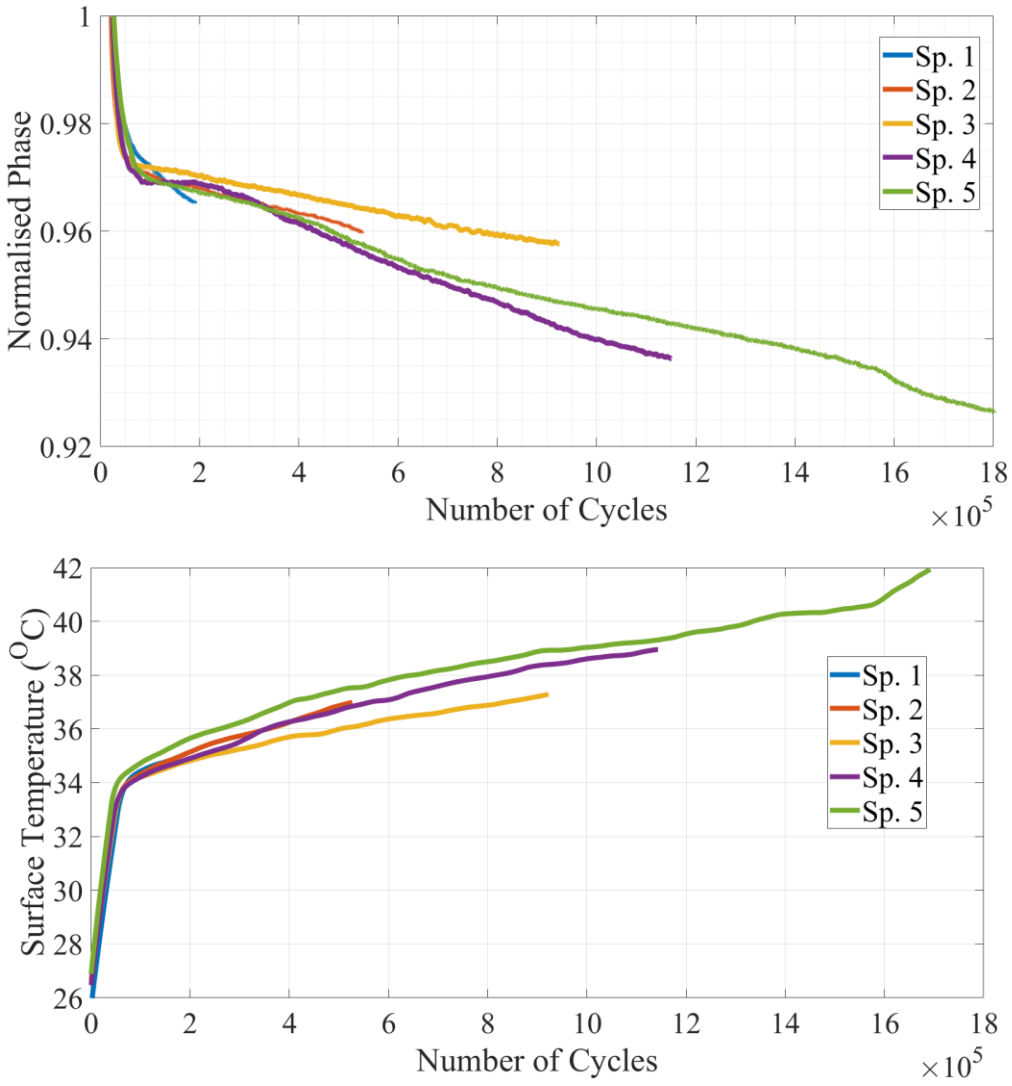

Figure 4.4: Response Phase and Self – Heating Temperature evolutions of the interrupted tests

4.3.1. The initial stage of Fatigue Testing

In **Figure 4.5** the first stage is identified. An experiment has just started at Region A and thermal equilibrium between the specimen and the ambient temperature has already been achieved. It can be noticed that during this stage the phase experiences a substantial decrease which is followed by a rise in the endogenous temperature of the component; until an equilibrium is reached (Figure 4.5 – point A). This stage corresponds to the transient state of an experiment where the sudden load input forces the thermal and mechanical responses to change, rapidly. As it will be discussed in the next section the equilibrium temperature is only affected by the surrounding temperature level. Furthermore, this stage only just lasts for few minutes which is arguably a very short period of time compare to the entirety of a fatigue life test (up to 9 hours) and no hot spot appears in the thermal images. For these reasons, no further analysis was considered necessary for this part of the experiment.

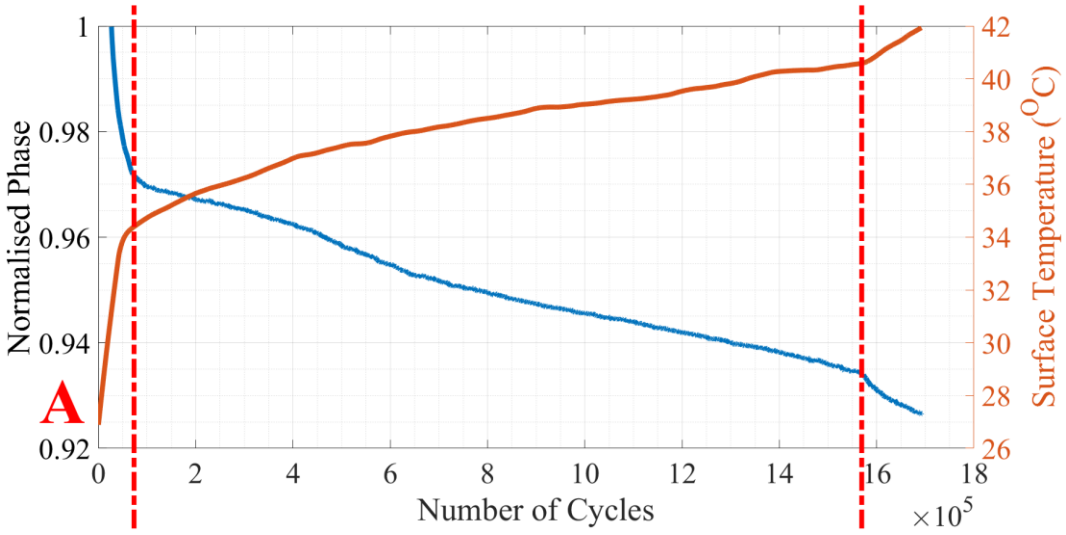

Figure 4.5: Transient State of the Thermal and Dynamic Responses / Equilibrium Point A

4.3.2. Development of Fatigue Damage

While, Region B (Figure 4.6) is the main stage of an experiment and it extends through the most testing time, no information is available regarding the fatigue damage development on this stage. As a result, several measurements are required.

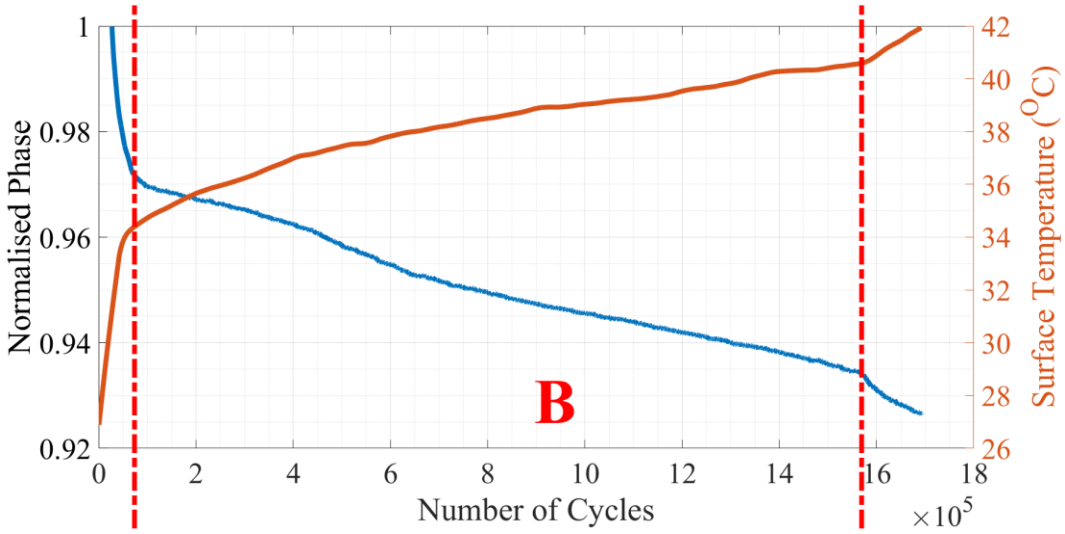

Figure 4.6: Steady State of the Thermal and Dynamic Responses

The interrupted test with the shortest life – span was arrested during the initial moments of this region. Figure 4.7 presents the isolated self – heating and phase progression of Sp. 1 (Figure 4.4) during testing as well as its corresponding CT scan images. The first 50 seconds of response phase data have been removed, since it is the time required for the FLL to reach the specified phase which leads to a transient behaviour. Nevertheless, it shows that this test was arrested extremely close to the equilibrium point A (Figure 4.5).

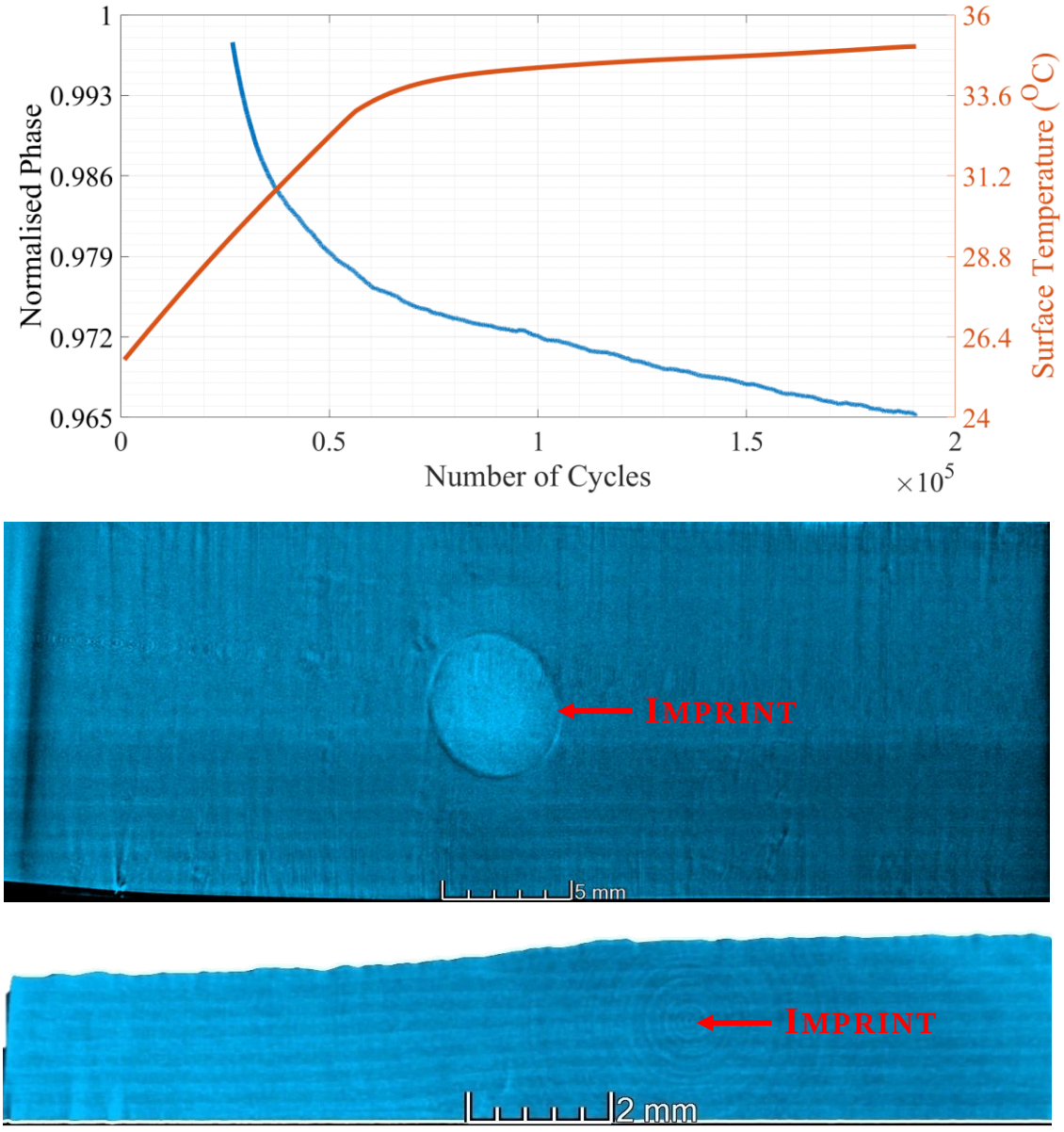

Figure 4.7: Top – Thermal and Dynamic Responses of the 1st interrupted test (at 1.9 x10^5 cycles) / Middle – Top View of the respective CT Scan / Bottom – Side View of the respective CT Scan

Additionally, Figure 4.7 presents the top and side ply – drop views of the CT Scan sample. It is apparent than no damage has been developed at this stage. This observation also agrees with the assumption that no damage has been developed during the transient state (Region A) of the experiment. It is worth noticing that the circular imprint that appears on these images is due to the small plastic leg used to stabilise the sample during the scan. Furthermore, the 0^O and 90^O plies appear as lighter and darker lines, respectively. In some cases, the cut plies and the resin pocket can also be seen in the side view.

The next interrupted test is displayed in Figure 4.8. This experiment was extended by additional 2.5×10^5 cycles compared with the first test (Sp. 2 Figure 4.8) and fatigue damage was captured on the CT scan results. Two types of damage can be distinguished easily from the top view. One quick examination through the width of the sample can reveal the identity of these types. The long white line corresponds to a transverse crack between the resin pocket of the ply drop and the two cut plies (Figure 3.6). This region is characterized by weak interphase bonds and it was safe to assume that the damage will initiate at this area. Moreover, the second type of damage, which is apparent on this test, forms a circular shape and it is associated with the opening of the delamination towards the thick side of the ply drop. Unfortunately, excessive dye penetrant in the outer surfaces of the sample could induce false reading. Instead, they could be identified by corelating the data from the top and the side views and due to their high dye concentration.

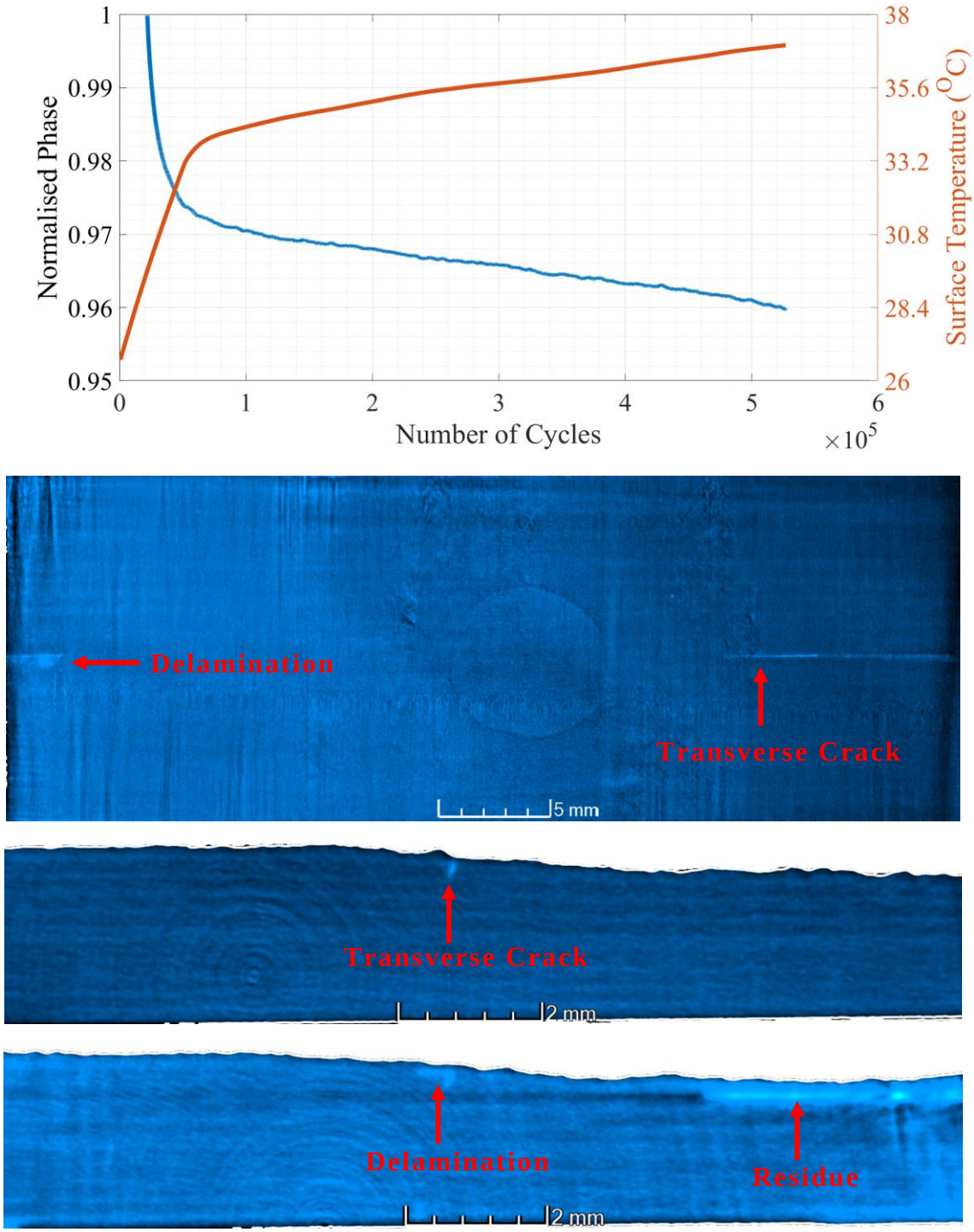

Figure 4.8: Top – Thermal and Dynamic Responses of the 2nd interrupted test (at 5.6 x10^5 cycles) / Middle – Top View of the respective CT Scan / Bottom – Side View of the respective CT Scan

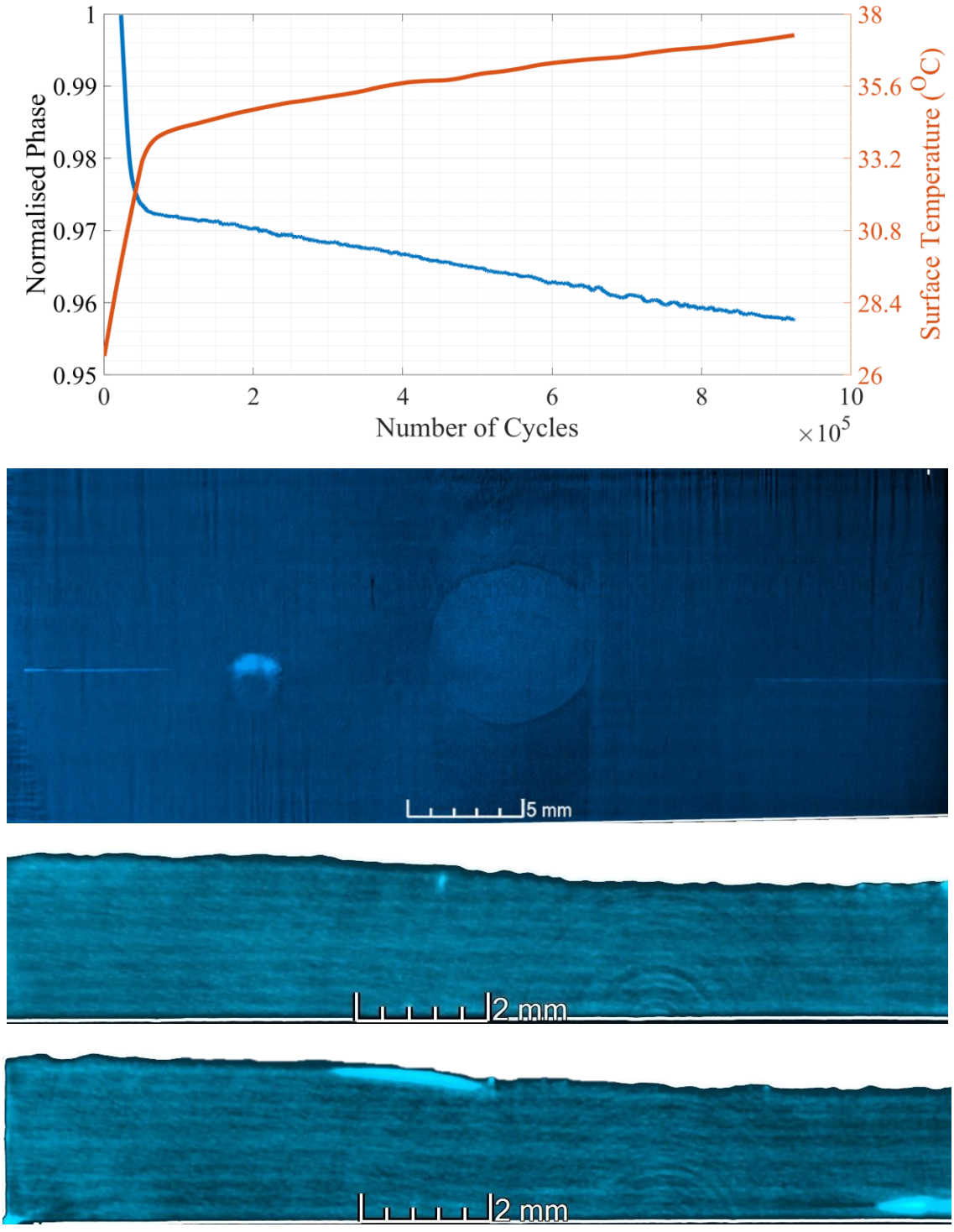

Figure 4.9: Top – Thermal and Dynamic Responses of the 3rd interrupted test (at 9 x10^5 cycles) / Middle – Top View of the respective CT Scan / Bottom – Side View of the respective CT Scan

The following analysis took place again, within Region B (Figure 4.6) and it is featured in Figure 4.9. Even though, this experiment terminated at 9×10^5 cycles, the transverse crack did not extend far from the previous test. On the other hand, it is clear that the delamination has now propagated both towards the thick and the thin side of the specimen.

Figure 4.10 demonstrates the final investigation that was conducted within Region B and it was terminated close to the Critical Event. The damage detected is now covering the whole width of the sample. Delamination has propagated towards both sides and this image shows a clear T shape between the vertical and the transverse crack. Finally, the delamination size, at this stage, is 2 mm × 1mm; where the transverse crack is two plies deep.

In conclusion, the CT scan investigation revealed that fatigue damage is being developed during Region B (Figure 4.6). It is therefore safe to assume that the linear decline in the response phase, observed at this stage, is the result of stiffness degradation on the composite laminate. Additionally, the self – heating temperature experiences a steady increase at this stage until the Critical Event is reached. It is therefore possible that the temperature rise is also connected to the appearance of damage as well as due to the effect of cyclic loading

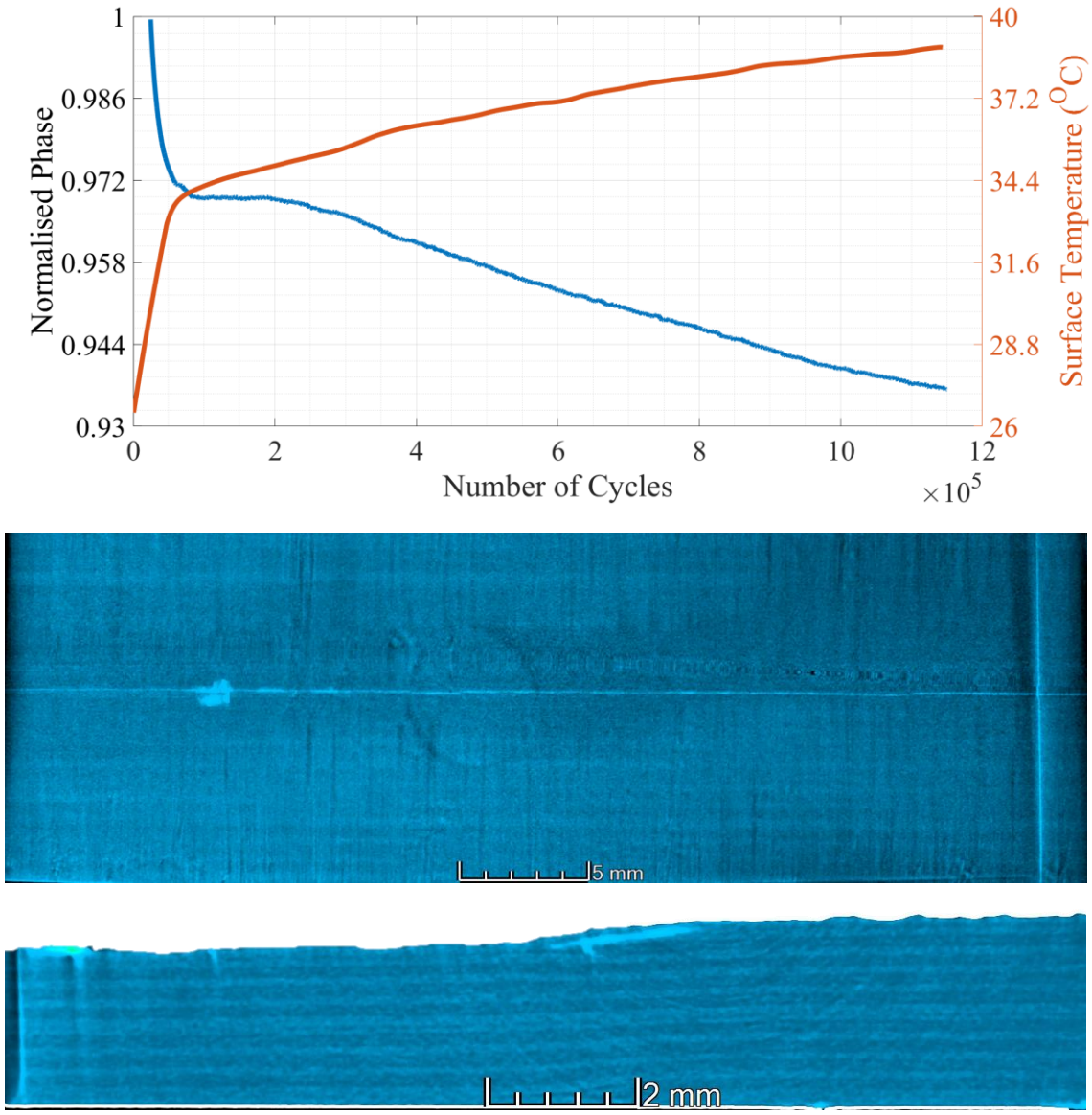

Figure 4.10: Top – Thermal and Dynamic Responses of the 4th interrupted test (at 1.15 x10^6 cycles) / Middle – Top View of the respective CT Scan / Bottom – Side View of the respective CT Scan

4.3.3. A Final Stage of Fatigue Testing

In the previous section, it became apparent that damage is present long before the Critical Event. Be that as it may, the Critical Event occurs at Point C (Figure 4.11). CT scan results revealed that delamination is greater; in both the thick and the thin side. In this case, damage can also be captured from the rapid increase in the surface temperature (Figure 4.12) which indicates an increasing damage size. Moreover, the rapid increase in the acceleration of the system (Figure 3.10) implies the application of an increasing excitation force in order for the system to maintain a constant vibration amplitude. Therefore, the rapid increase in the self – heating temperature alongside the abrupt change in the response phase, suggest that the plasticity of the component is increasing which is the result of a high stiffness deterioration.

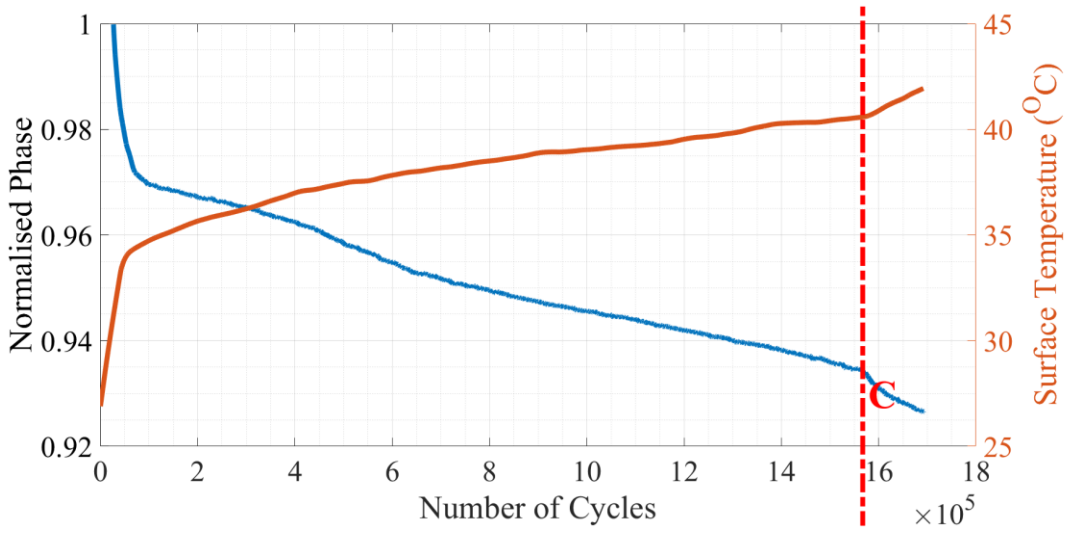

Figure 4.11: Critical Event State of the Thermal and Dynamic Responses / Critical Event Point C

It is therefore safe to assume that the Critical Event defines a Critical Damage Size beyond which the fatigue loading is capable to drive the crack propagation at higher rates. In comparison to Region B, where the crack growth rate is lower. It is worth noting that in the past [50] thermography was the only method employed to capture the fatigue damage while previous studies depended on Finite Element modelling to predict the damage

development [68]. Thermal images revealed that damage was present only during Region C and thus microdamage on Region B was omitted.

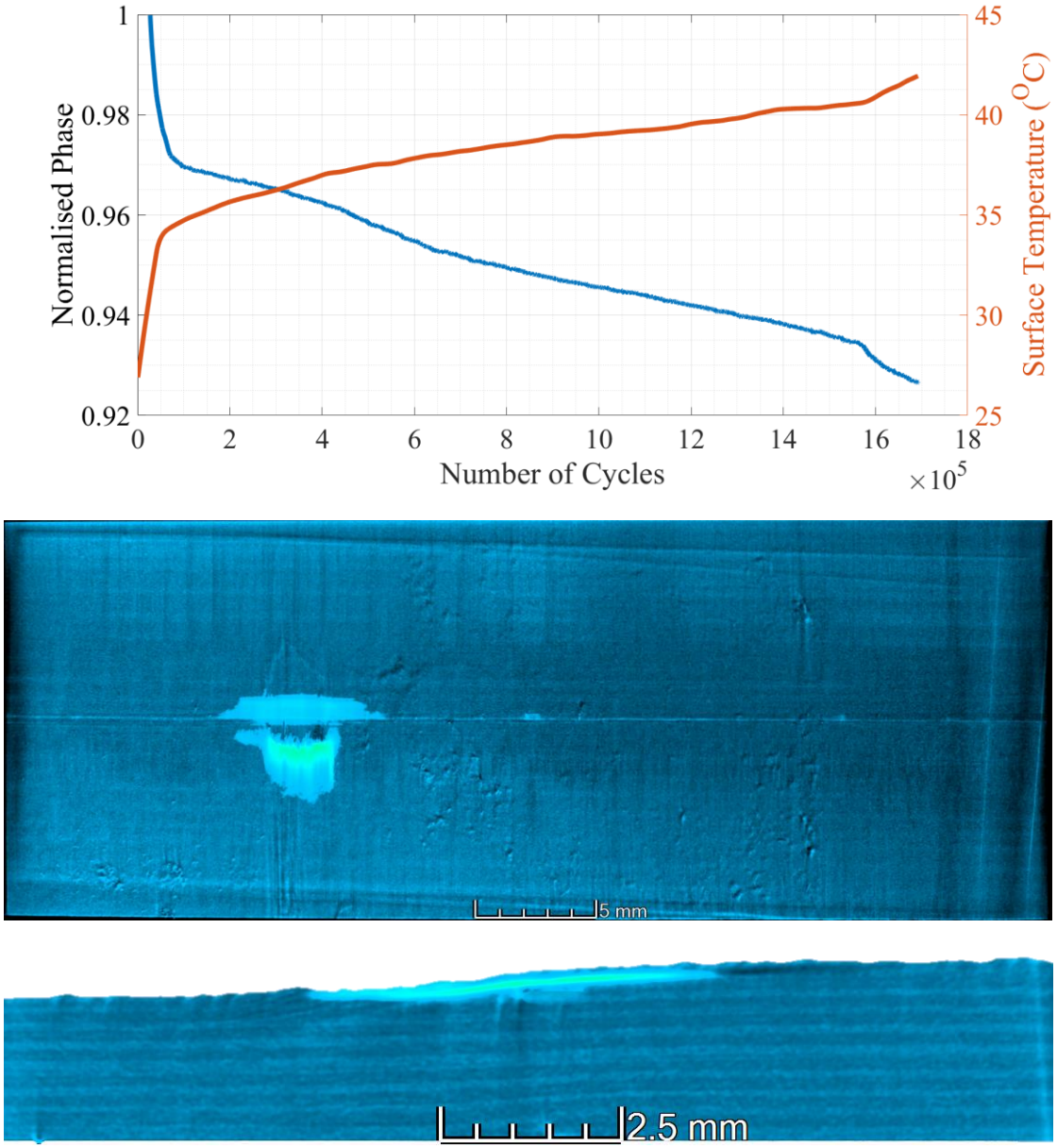

Figure 4.12: Top – Thermal and Dynamic Responses of the 5th interrupted test (at 1.7 x10^6 cycles) / Middle – Top View of the respective CT Scan / Bottom – Side View of the respective CT Scan

4.4. Fatigue Life at Elevated Temperatures

4.4.1. Self – Heating Temperatures

The knowledge that emerged from the interrupted tests can form a new base for analysing the delamination growth under various ambient temperatures. A series of elevated ambient temperature tests were carried out for the characterisation of the Critical Event. Experiments were conducted at four ambient temperature levels; 25 ℃, 50 ℃, 65 ℃ and 75 ℃. Unfortunately, the experimental investigation at 75 ℃ becomes challenging and tests at higher temperature levels could not be considered reliable. The results of the test campaign are presented in Figure 4.13.

The first thing that can be observed is that the equilibrium temperature of the specimen (e.g. Point A – Figure 4.5) is about 2 ℃ higher than the surrounding temperature. This event is attributed to the combined effect of the environmental temperature and air flow around the testing sample. The phenomenon will be investigated further with the assistance of a FE model in the next chapter.

Another aspect that was captured investigating throughout these graphs is the influence of the severity level over the equilibrium and Critical Event Temperatures (e.g. Points A, C – **Figure 4.5**). A closer look at the experimental data of Figure 4.13 revealed that the temperature levels at points A and C are not affected by a higher strain level which is better described in Figure 4.14. It is of course obvious that higher environmental temperature leads to a higher surface temperature. However, in order to examine the influence of the applied strain regardless of the ambient temperature, and also for practical reasons; it was necessary that the data were normalised using the same temperature value. Therefore, for each ambient temperature level, the same temperature normalisation value (e.g. Equilibrium or Critical Event Temperatures) was employed but the normalisation value was different across various temperature levels.

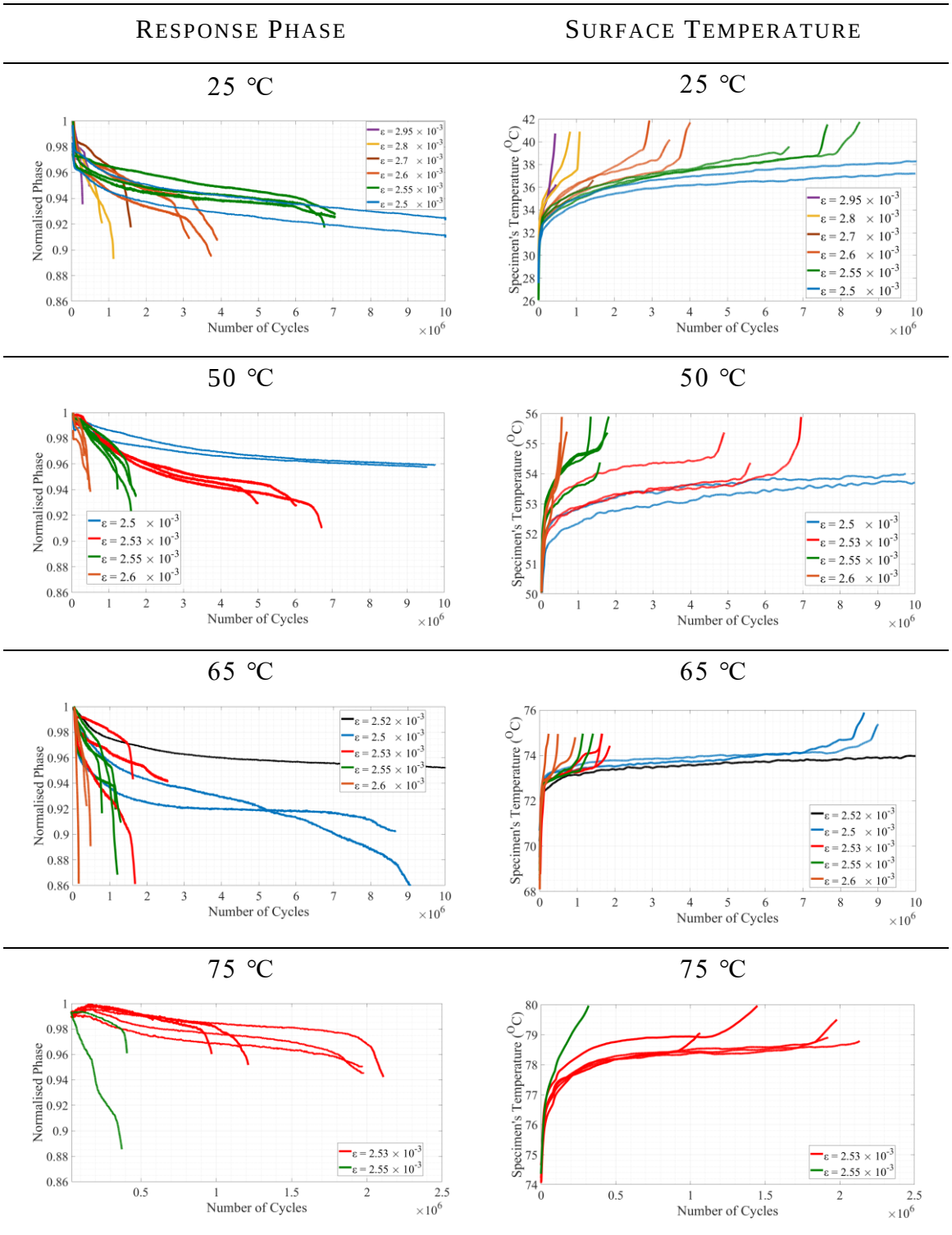

Figure 4.13: Thermal and Dynamic Responses of the test campaign at different ambient temperatures/ Data are colour coded according to their strain level

Figure 4.14 shows that the strain does not have a significant influence over the temperatures of point A and C. With reference to Figure 4.13, this implies that the equilibrium and Critical Event temperature levels do not vary more that ± 1 ℃ across experiments that were conducted at higher strain levels, regardless the ambient temperature. Obviously, one could argue that this might not be the case for extremely high severity levels. Unfortunately, this scenario was not investigated since the current experimental apparatus was unable to support it. Nevertheless, Figure 4.13 suggests that identifying the different regions within an experiment, would be very challenging, due to the short testing time.

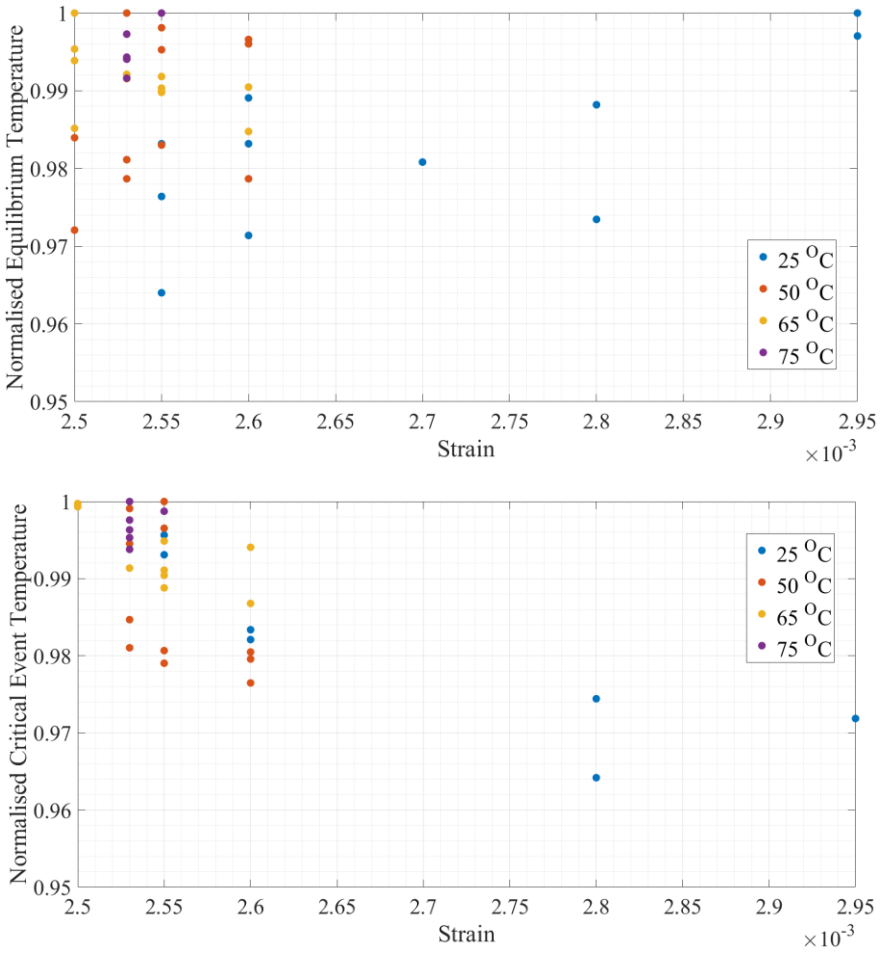

Figure 4.14: Top – Equilibrium Temperatures (Point A) over strain level / Bottom – Critical Event Temperatures (Point C) over strain level / The data correspond to the entirety of the test campaign and they are colour coded according to their ambient temperature

4.4.2. S – N Curve

By defining the failure criterion as the appearance of a Critical Event, the fatigue life of composite laminate can be characterised. So far, it was discussed that a sequence of microcracking and delamination is followed by the Critical Event which is the indication of a critical delamination size and corresponds to a sudden change in both mechanical and thermal responses.

The series of experiments conducted at elevated environmental temperatures reported a similar behaviour in the responses, too. Figure 4.15 traces the response phase of fatigue tests performed between 25 °C and 75 °C but at the same strain levels. The Critical Event develops earlier at higher surrounding temperatures compared to the room temperature which in turn necessitates the establishment of microdamage and delamination initiation at a much earlier stage; as it was described by the CT scan results.

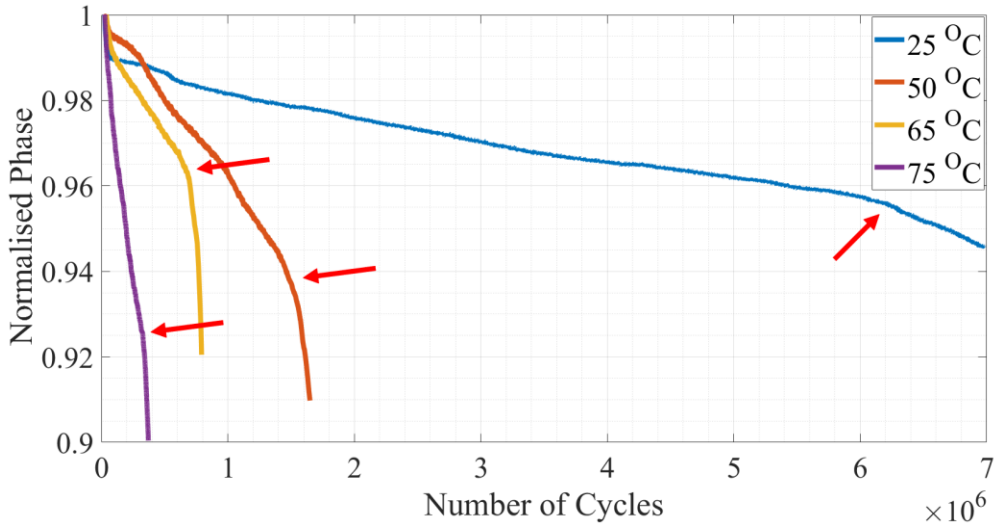

Figure 4.15: The occurrence of Critical Event at different ambient temperatures but at the same strain level

At this point, it worth noting that the data presented on Figure 4.13 are colour coded according to their severity level. One can observe that the coupons tested at the same strain and ambient temperature levels are forming separate groups. More specifically, they experience the same rate of change during Regions B and C while their Critical Events

appear at the same time; taking into consideration a small scatter. Another interesting outcome arises from the specimens exposed to low strain levels. These responses are illustrated as straight lines where no Critical Event is present (Figure 4.13). Moreover, their endogenous temperature was close or lower to their respective Critical Event temperature. Yet, the strain levels that fail to initiate a Critical Event at lower temperatures (25 ℃ or 50 ℃) were capable to develop a Critical Event on coupons tested at 65 ℃ or 75 ℃.

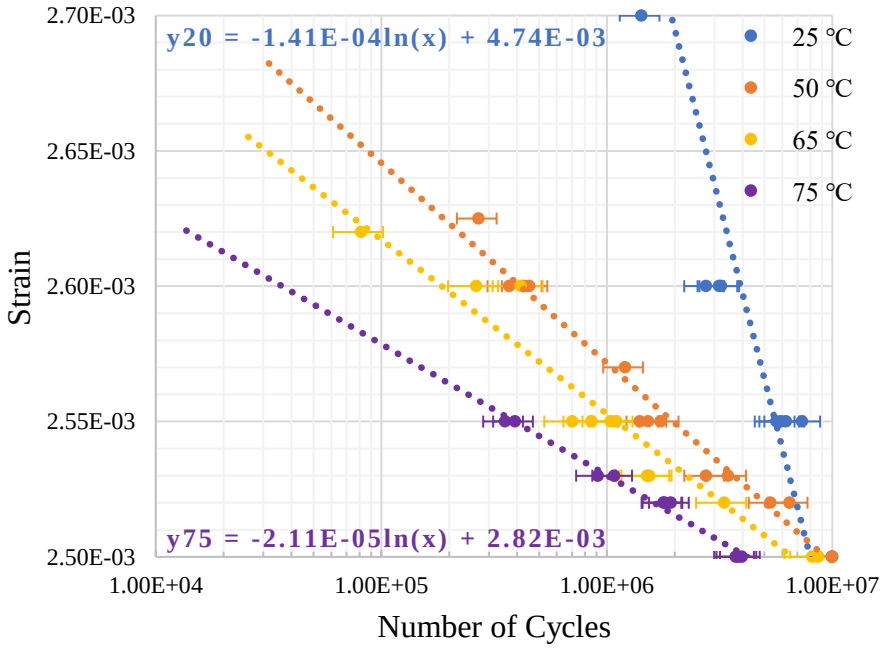

Figure 4.16: Fatigue Life curves at different ambient temperatures

The fatigue life curve for different ambient temperatures and strain levels is presented in Figure 4.16. As it was expected both the environmental conditions and the imposed strain contributes to the degradation of composite samples, subject to high frequency vibration testing. Strain levels above 2.6×10^{-3} were investigated for 25 ℃, leading to short testing times (< 20 m). For this reason, it was decided that the behaviour at elevated temperatures will be examined between 2.5×10^{-3} and 2.6×10^{-3}.

4.4.3. Response Phase and Damage Propagation

In Section 4.3, it was discussed that the response phase evolution is able to describe the occurrence and early propagation of fatigue. Moreover, it was shown that the two quasi – linear regions B and C (Figure 4.3) identified during the phase progression, coincide with different damage stages. It is therefore logical to exploit these quasi – linear trends in order to acquire further insight about the fatigue damage development at elevated temperature conditions.

In that sense, the rate of change of the response phase for regions B and C and for the entirety of the test campaign, were extrapolated using a linear method (Figure 4.17). The top graph shows the relation between the exposure temperatures and the rate of change before the Critical Event. In accordance with the observations made by the CT scan analysis, this figure illustrates the acceleration in stiffness degradation due to the development of microdamage during fatigue testing; in relation to both ambient temperature and strain level. The experimental data suggest that microdamage, in the form captured by the CT images, develops at an increasing rate under higher strain. However, the influence of the environmental temperature conditions is more significant.

On the other hand, the rate of change of phase after the Critical Event is presented in the bottom Figure 4.17. It is apparent that the harsh temperature conditions impose a rapid change in the phase. Phase decreases faster at 75 °C than at room temperature which coincides with the increased loss of stiffness. Hence, it is safe to assumed that the rate of damage opening is greater under severe temperatures.

In conclusion, the experimental investigation revealed that the effects of temperature are similar in both cases and it hinted towards a connection between the testing temperature and the fatigue resistance of composite specimens.

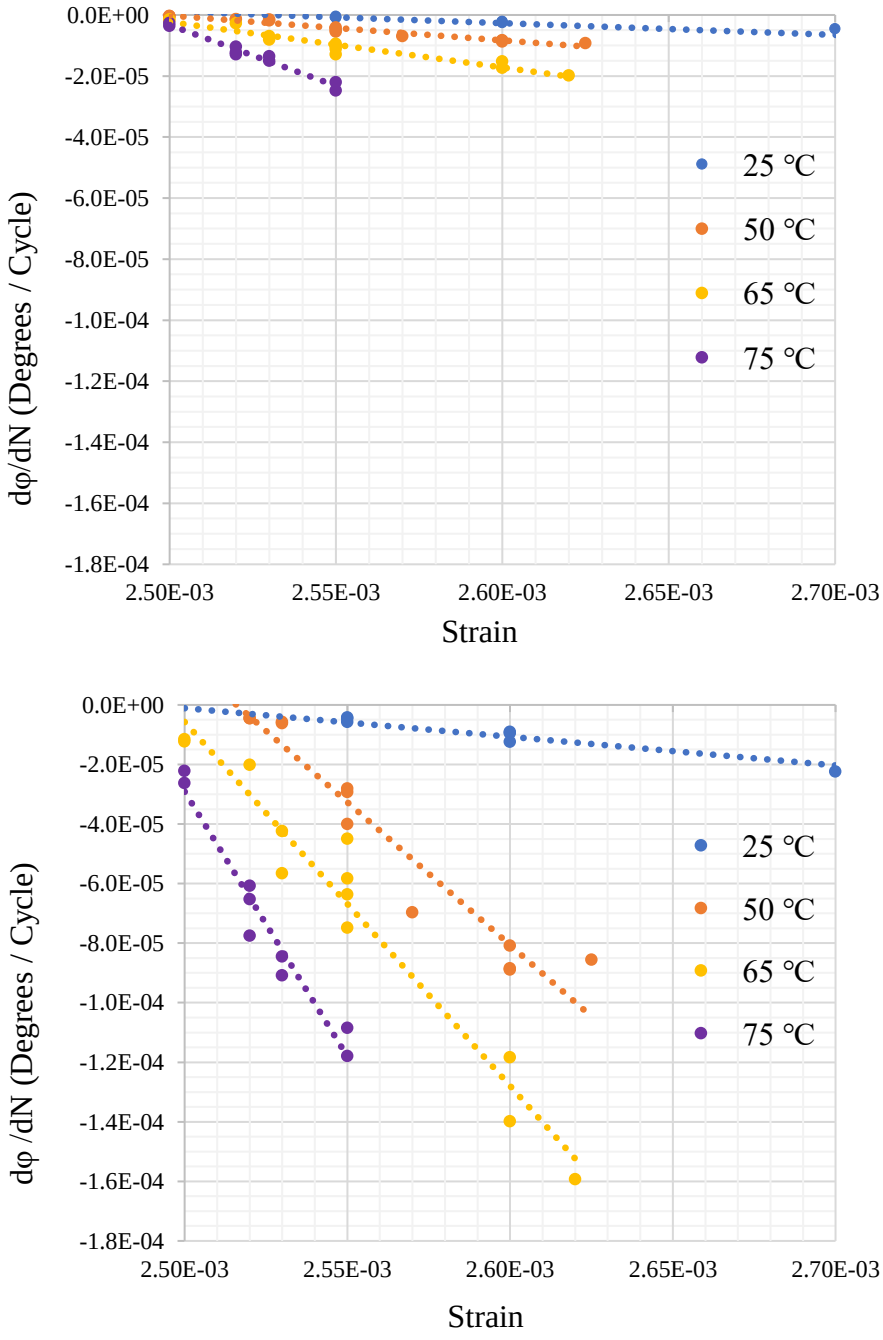

Figure 4.17: Rate of Change of Phase at different ambient temperatures / Top – Before the Critical Event (Region B) / Bottom: After the Critical Event (Region C)

4.5. The relationship between the Thermal and Mechanical Responses

Let us consider a single degree of freedom (SDOF) mass – spring – damper system subjected to a dynamic base excitation. This scenario is similar to that of a specimen being excited by an electromagnetic shaker under base excitation. In a base excitation, the response phase (φ) and the transmissibility (T) are given by [78]:

$$\varphi(\omega) = tan^{-1}\frac{mc\omega^3}{k(k-\omega^2 m)+(\omega c)^2} \quad \textbf{4.1}$$

$$|T(\omega)| = \frac{|X|}{|X_b|} = \frac{\sqrt{k^2+(\omega c)^2}}{\sqrt{(k-\omega^2 m)^2+(\omega c)^2}} \quad \textbf{4.2}$$

Where φ is the response phase, ω is the excitation frequency, m is the mass, c is the damping factor, k is the stiffness of the system, T is the transmissibility X is the response in terms of displacement and X_b is the displacement of the base. Furthermore, Eq. 4.1 can be approximated as follows:

$$\varphi(\omega) = \tan^{-1}\frac{m\omega}{c} + \frac{m^2\omega(k-m\omega^2)}{c^3+cm^2\omega^2} + \mathcal{O}((k-m\omega^2)^2) \quad 4.3$$

employing a first order Taylor expansion, when the specimen is excited close to resonance. Eq. 4.3 implies that the stiffness of the system is proportional to the phase since the structural damping and mass of the system can be considered constant and the excitation frequency is fixed.

Viscoelastic materials are commonly defined by their characteristic phase lag between the applied stress and strain response. Under cycle loading, this Hysteretic behaviour can be exploited for characterising the fatigue life of composite laminate. Figure 4.18 illustrates the typical stress – strain loop for one cycle of oscillation, schematically.

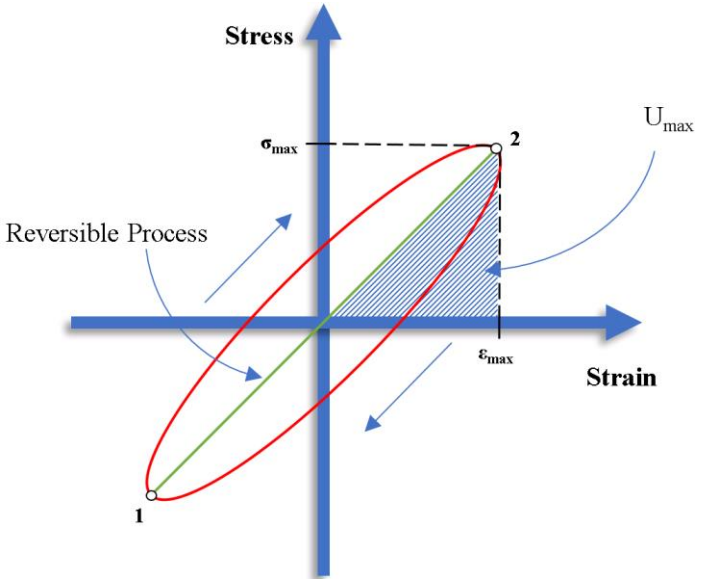

Figure 4.18: Typical Hysteresis Loop

This non – Reversible Process leads to unbalance between the energy introduced during each loading cycle and the energy returned during each unloading. Thus, the load strain energy is not equal to the unload strain energy resulting in energy loss in the form of heat transfer during each cycle. Hence, the direct effect of the generation of heat on viscoelastic materials, is the rise on the specimen's temperature (self – heating temperature). Therefore, the energy loss, on a composite component subject to cyclic loading, is related to the reversible strain energy ($U_{\max}$) with a loss (damping) factor:

$$c = \frac{\Delta U}{U_{\max}} \qquad 4.4$$

Where ΔU is the energy loss and U_{max} is the maximum strain energy that can be stored per unit volume which can then be approximated as follows [79], [80]:

$$U = \frac{\sigma_2^2 - \sigma_1^2}{2E} \quad \textbf{4.5}$$

Where σ_2, σ_1 are the maximum and the minimum tension, respectively. In order to capture the heat transfer within the system the heat convection equation can be utilised where heat is related to Temperature (T) by the following equation:

$$Q = h \cdot \Delta T \quad \textbf{4.6}$$

Where Q is the heat loss while h is the convection coefficient. Moreover, ΔT is the difference between the ambient temperature (T_a) and the object's (T_s) temperature. Therefore, Eq. 4.5 and Eq. 4.6 can be combined to form a relationship which describes the connection between strain energy and Temperature, as it was presented by Lahuerta [81]:

$$T_S = \left[\omega \cdot c \cdot \frac{\sigma_2^2 - \sigma_1^2}{E} \cdot \left(\frac{t^2}{4k_T} + \frac{t}{2h}\right)\right] + T_a \quad \textbf{4.7}$$

Where E is Young's Modulus, k_T is the thermal conductivity and t is thickness of the laminate. In addition to this, it was also reported that the SDOF system can be described, alternatively, as a composite beam of length L and section S [50]. This implies that the axial stiffness of the beam can be described as $k = E \cdot S / L$ which can be used to associate the composite to its stiffness.

Therefore, for a composite beam subject to vibrations of fixed frequency and constant vibration amplitude, Eq. 4.3 and Eq. 4.7 can be respectively formulated as:

$$\varphi = A \times E + B \tag{4.8}$$

$$T_S = \frac{C}{k} + D \tag{4.9}$$

Where A, B, C, D are constants that correspond to:

$$A = \frac{S \cdot (m^2\omega)}{L(c^3 + cm^2\omega^2)} \tag{4.10}$$

$$B = tan^{-1}\left(\frac{m\omega}{c}\right) - \frac{m^3\omega^3}{c^3 + cm^2\omega^2} \tag{4.11}$$

$$C = \omega \cdot \mathrm{c} \cdot \mathrm{S} \cdot (\sigma_2^2 - \sigma_1^2) \cdot \left(\frac{t^2}{4k_T} + \frac{t}{2h}\right) \tag{4.12}$$

$$D = T_a \tag{4.13}$$

Although, certain assumptions are definitively required; it can be concluded that Eq. 4.8 and Eq. 4.9 suggest a linearly proportional relationship between the stiffness and the response phase of the composite component and reverse proportional to the self – heating temperature, during the fatigue testing. In other words, while the stiffness of a specimen deteriorates its temperature rises but the response phase decreases; following what it was observed from the experimental analysis. One could therefore come to the conclusion that the phase is reverse proportional to the self – heating temperature.

It is therefore possible to explore the aforementioned assumption by plotting the self – heating temperature, captured during an endurance test, against the relevant phase lag. Thus, Figure 4.19 contains the results acquired for regions B and C (before and after the Critical Event) and for the entirety of the test campaign. Region A, however, was not

investigated since as it was discussed earlier, it corresponds to a transient state of the test during which no damage has been developed. The results are also colour coded following the approach used for Figure 4.13.

The experimental results seem to follow an analogous behaviour, regardless the strain level. In fact, the data acquired within same environmental temperature, trace an almost linear trend which remains unaffected from the applied strain level; considering a small scatter of 5%. On top of that, the rate of change of these linear trends becomes more severe with each increasing testing temperature.

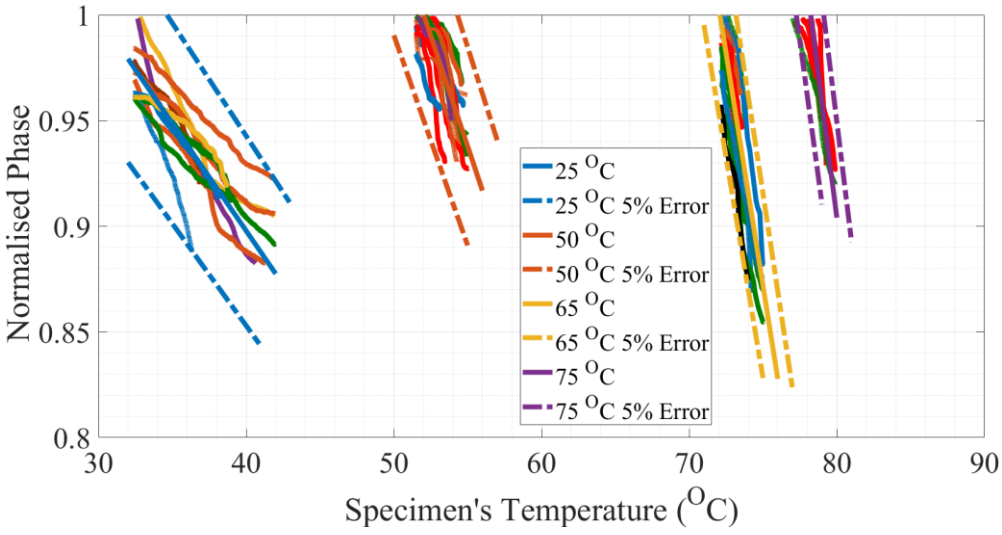

Figure 4.19: The Mechanical Response over the Thermal Response at different ambient temperatures for the entirety of the test campaign

The outcome of this analysis can be partially explained, using the knowledge established from the aforementioned experimental investigations. Hence, it can be presumed that the damage evolution supports the self – heating temperature increases at the same rate at which it prompts the phase decline. Furthermore, the ambient temperature seems to affect the crack growth rate, resulting to a rapid change in response phase. Following on from what was discussed in Chapter 2, it can be assumed that the energy required to open is higher with lower ambient temperature.

In conclusion, the linear trends highlighted in Figure 4.18, indicate that the mechanical and thermal responses of the system bear a linearly proportional relation; in line with what was also described by the numerical analysis.

4.6. Suspension of Fatigue Damage

So far, it was discussed the crack opening accelerates due to the harsher ambient temperature conditions and as a result the fatigue life of composite laminate. It can therefore be anticipated that the opposite could occur through the application of different thermal loads during endurance testing. Thus, the crack propagation should be slowed when heat dissipation between the component and the surrounding environment is accelerated.

In order to investigate this hypothesis, the experimental set up was slightly altered. A small air pipe was introduced inside the environmental chamber through its lower part (Figure 4.20). As a result, it was possible to lower the local temperature of the most stressed region (ply – drop) during endurance testing. The air flow had to be kept as low as 0.5 bar and it was controlled with the use of a pressure regulator gauge. Furthermore, the tests were conducted at the same strain and ambient temperature levels. The air was released when the specimens reached the same self – heating temperature and it was extended for 10^6 cycles. It was believed that the surface temperature of the components could provide a more accurate indication of the damage size prior to the Critical Event; following to what was reported by the CT scan analysis.

The experimental investigation is shown in Figure 4.21. The graphs present the two “cooled” tests in comparison to a test where no additional thermal load was applied. The extensive drop in the self – heating temperature is the result of the accelerated heat convection and corresponds to the release of air. It is apparent the fatigue life of the specimens was extended when exposed to cooled air. In fact, the difference between original and the cooled experiments reaches the 35 % while the accepted error for the aforementioned test campaign (Figure 4.13) was just 20 %.

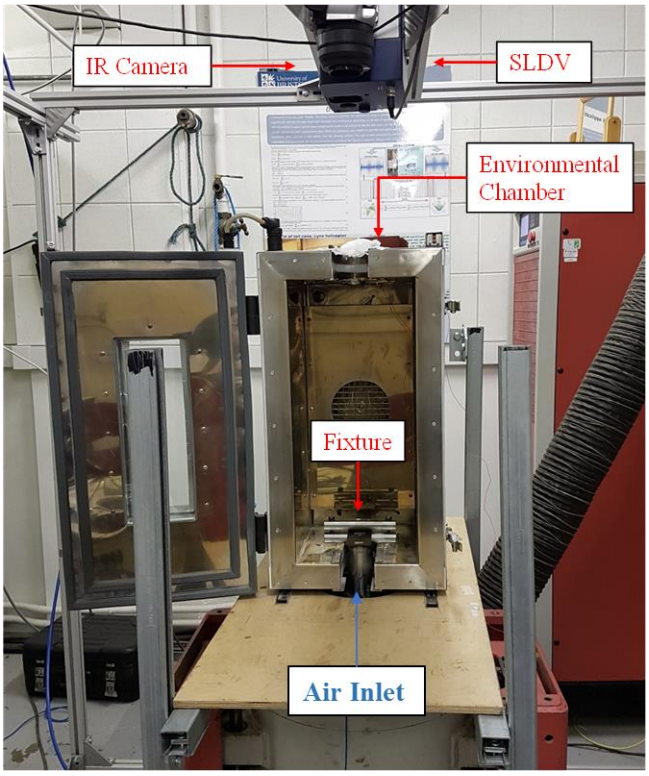

Figure 4.20: Updated Experimental Set Up for the Fatigue Damage Suspension Tests

Apart from that, the graphs also captured another interesting piece of information. It can be observed that the rate of change of the vibration phase is less pronounced when the specimen is being cooled but it returns to its initial state, afterwards. Moreover, the rate of change in the two cooled test is similar in the respective regions; prior, during and after the cooling. With reference to Eq. 4.3, this behaviour could imply a lower rate of stiffness degradation during this period which can justify the extended fatigue life. The appearance of this phenomenon seems to emerge from a deterioration in the localised fracture toughness, at the crack tip, due to the increase in the self – heating temperature.

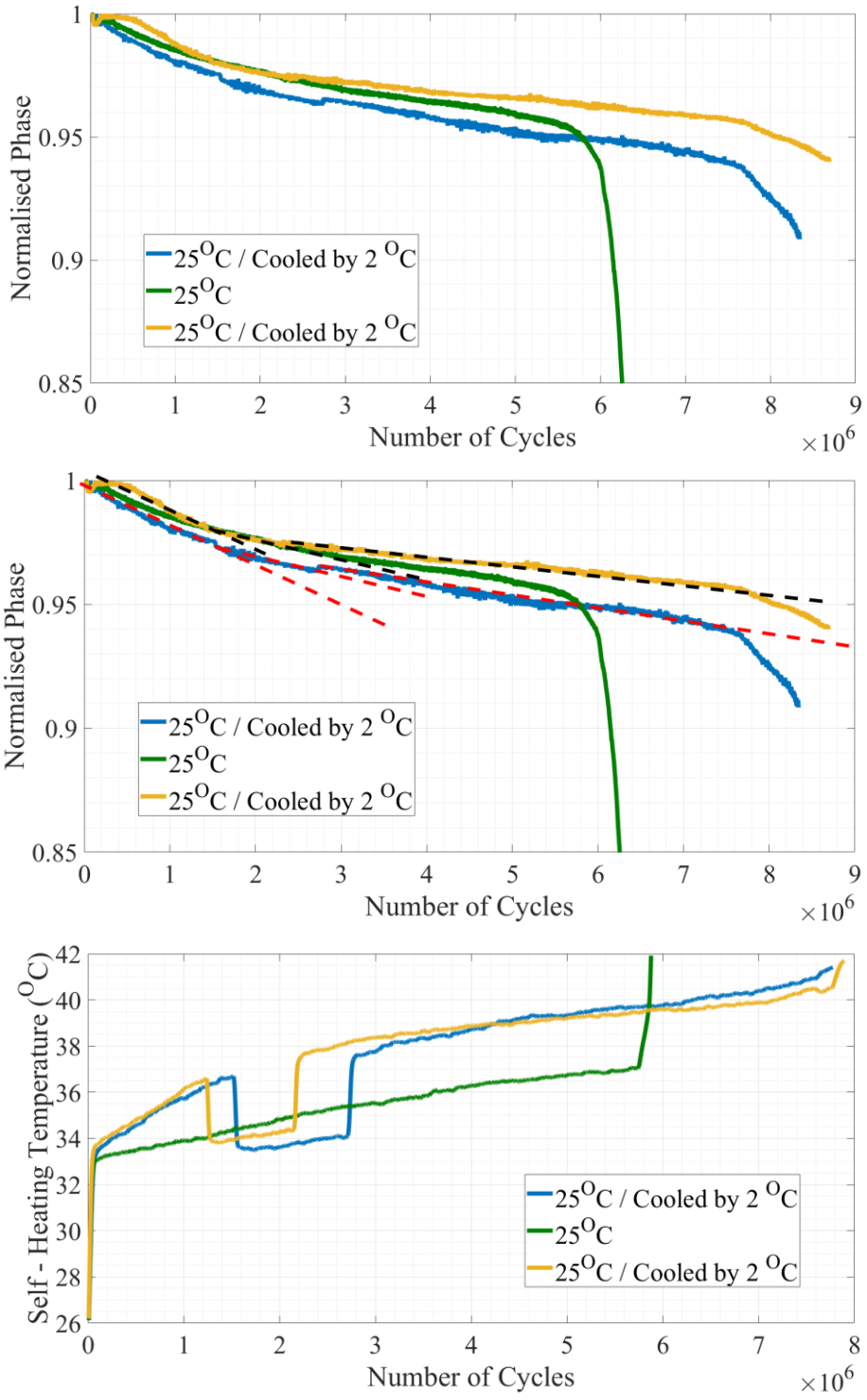

Figure 4.21: Fatigue Damage Suspension Tests at the same ambient temperature and strain levels / Top – Response Phase evolution of Cooled Tests / Middle – Response Phase evolution of the Cooled Tests compared to the original / Bottom – Self – Heating Temperature evolution of the Damage Suspension Tests

4.7. Remarks

The vibration testing method established in Chapter 3, was employed in order to provide further insight on the physics that govern the fatigue damage development of carbon reinforced composites subject to elevated temperature conditions. For this reason, endurance tests were carried out in a dynamic environment exploring the effects of different mechanical and thermal loads.

It became quickly apparent that the mechanical and thermal responses of the testing components, in the form of vibration phase and self – heating temperature, trace an almost inverse behaviour; What's more, they can be isolated into three quasi – linear stages, regardless the applied strain and environmental conditions. As a consequence, the appearance of these regions was exploited in order to support the in – depth analysis of the fatigue life.

Additionally, X – Ray scanning was implemented to accommodate the characterisation of the linear regions as well as to investigate the fatigue damage development. It was revealed that micro – damage, in the form of a transverse crack, is developed from the early stages of an endurance test. The crack is then transformed into a small delamination which propagates first towards the thick side of the ply drop. The crack will then continue to expand towards both the thin and thick side, in an unpredicted manner, until eventually a critical damage size is reached. This damage size corresponds to the Critical Event, which is followed by and extensive opening of the delamination until the end of the experiment.

The examination of the different phases in the self – heating temperature evolution reported that the initial equilibrium temperature as well as the Critical Event temperature are affected mainly by the ambient temperature; implying that the damage size at the respective stages is always the same regardless the severity level. On contrary to this, the rate at which both the response phase and the endogenous temperature will progress from the state of equilibrium (Point A) to the Critical Event (Point C) is affected by the severity level, too. As it is expected, this behaviour indicates that both the mechanical and thermal

loads can impact the crack propagation rate which leads to shorter fatigue lives at elevated ambient temperature environments.

Unfortunately, the crack propagation rate monitoring during vibration testing can be a particularly challenging task; especially prior to the Critical Event where the damage cannot give rise to a clear hot – spot. However, for the purpose of this study, an alternative approach was attempted. A method was introduced which captures the opening of the delamination through the in – depth analysis of the response phase decay. The resulting data revealed a close connection between the environmental temperature and the damage growth. Furthermore, it was described that the self – heating temperature and the response phase follow an almost linear relation between which is only affected by the surrounding temperature.

Additionally, these observations could be exploited in order to extend the fatigue life of a carbon reinforced composite component at a specific ambient temperature level. In fact, the final trial attempted to show that by increasing the heat dissipation the dependence between the stiffness degradation and the environmental temperature is diminished allowing longer fatigue lives.

Chapter 5

SIMULATING THE VIBRATION FATIGUE TESTING

This chapter describes the development of FE models that intend to support the experimental investigation. Hence, they are aiming to assist the study of the physics that govern the high cycle fatigue behaviour of composite components while always taking into account the ambient temperature conditions. The first method utilises the existing knowledge around the VCCT in order to simulate the mechanical response of the system. The main purpose of this method is to quantitatively simulate the fatigue life of CFRP under different ambient temperature conditions, since the temperature – dependent fatigue exponents and pre – factors of the investigated material system are not currently available. Additionally, the second method will employ multi – physics models in order to reproduce the thermal life of the component. Both cases ought to follow closely the experimental requirements. For this reason, various parameters, that could affect the final results, are discussed.

5.1. Introduction

In Chapter 3, it was shown that a vibration testing technique can be implemented in order to investigate the fatigue life of composite components; subjected to elevated ambient temperature conditions. As a result, it was discussed that the experimental campaign was able to explore the fatigue behaviour of carbon reinforced specimens. However, it has yet to answer the question of "Why the Critical Event occurs?".

The basis of another crucial question was formed in [82]. Ruzek et al. investigated the effects of loading frequency (0.5 Hz to 15 Hz) on the fatigue behaviour, failure mechanisms

and self – heating temperature of tapered CFRP specimens. They were able to observe a rapid increase in the surface temperature of the specimens due to the increased damage size. However, they reported no relation between the self – heating temperature and the fatigue life, prior to this phenomenon. In other words, the authors pondered about the relation between the mechanical and thermal responses of composite components under cyclic loading.

The first objective of this study is to investigate the effects of the environmental temperature conditions over the Critical Event. For the purpose of this study, a 2D Finite Element (FE) Virtual Crack Closure Technique (VCCT) model was employed. It can be assumed that a 3D VCCT model will produce scaled but quantitatively similar results to a 2D model. In fact, Magi reported that the 2D analysis can be more conservative, with respect to both the 3D model and the actual experimental data [68], when exploiting VCCT in order to study the vibration fatigue behaviour. In order to address these objectives, a steady state dynamic analysis was employed in ABAQUS alongside the evaluation of the Strain Energy Release Rate (SERR) in order to estimate the propagation of delamination.

On the other hand, the analysis of the aforementioned experimental approach would not be complete without considering the influence of the internal thermal loading due to the self – heating. For this reason, a 3D multi – physics FE model was necessary. Its objective was to form the basis towards the establishment of a relation between the thermal and mechanical responses of the system.

In conclusion, this chapter will introduce the FE models exploited in order to explore the fatigue behaviour of composite laminates, subject to different dynamic and thermal loads.

5.2. Modelling the Dynamic Environment

The first step, towards simulating the fatigue life behaviour into a FE environment, is to reproduce the dynamic testing environment. As it was discussed in Chapter 3, the testing coupons are restrained by a steel fixture which is then attached to an electromagnetic shaker. Hence, the armature of the exciter exerts a sinusoidal base excitation to the components. The armature is much stiffer than the first bending mode of the specimens. For this reason, it was not deemed necessary to include it on the FE model. However, both the fixture and the armature are simulated with a non – structural mass, located within the contact region of the two rods of the fixture (Figure 5.1). Thus, a non – structural mass of 15 kg was added in the location of the fixture.

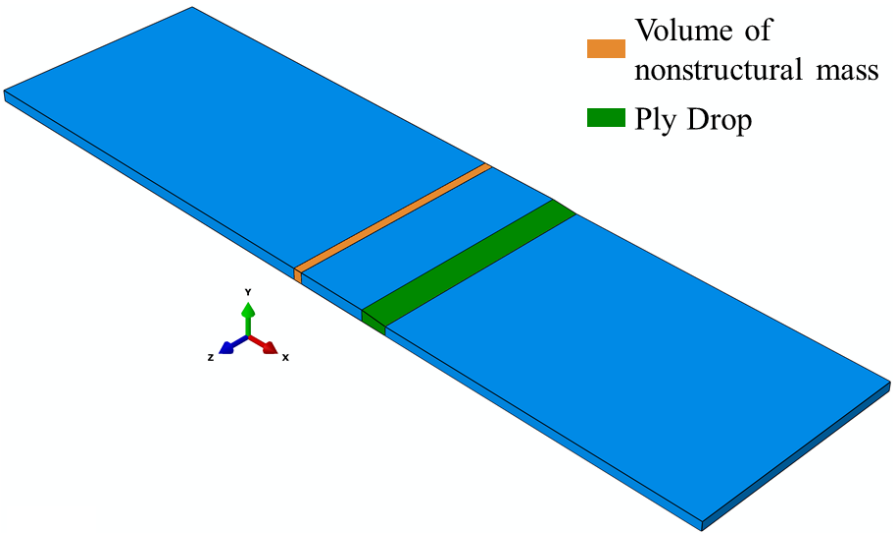

Figure 5.1: 3D geometry of the component

Another crucial aspect in the model development is capturing the actual shape of the ply drop region. This way a more accurate representation of both the dynamic response and the internal forces can be achieved. For this reason, a CFRP specimen was cut and polished around the ply drop. Its micrograph (Figure 5.2) was then used as a reference for simulating the specimen in the FE environment.

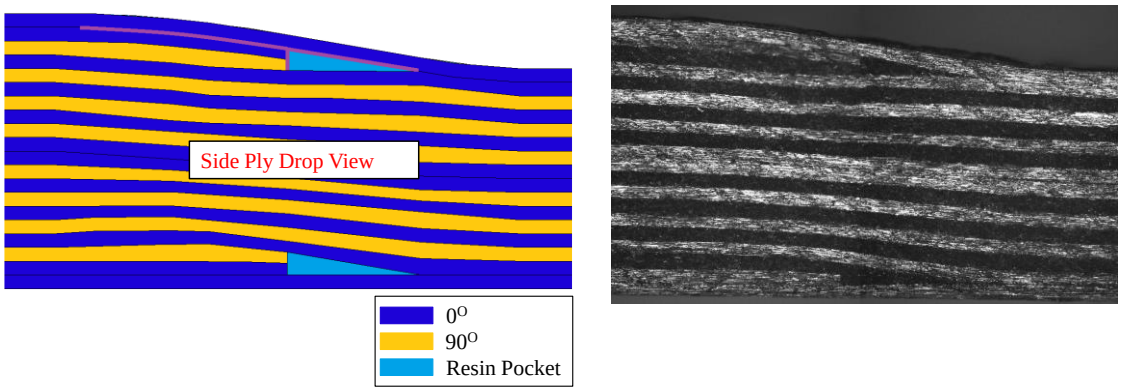

Figure 5.2: Left – FE ply drop geometry / Right – Micrograph employed to partition the FE model

As it was described in Chapter 3, the dynamic parameters (e.g. structural damping, resonance frequency) experience minor variation under the influence of different environmental temperatures. For this reason, it can be assumed that both the excitation frequency and the structural damping can be maintained constant (at 395 Hz and 0.0035), throughout the numerical investigation. The resonance frequency was extracted from the FE model and correlated to the experimental results. Furthermore, the damping value of the model (0.0035) coincides with the value extracted from the experimental data in Chapter 3. Hence, the material properties, for the numerical models are presented from Table 5.1 to Table 5.4.

Table 5.1: Physical and Mechanical Properties of UD laminate of IM7/8552

E_1 (GPa)	$E_2 = E_3$ (GPa)	$\upsilon_{12} = \upsilon_{13}$	υ_{23}	$G_{12}=G_{13}$ (GPa)	G_{23} (GPa)	ρ (kg/m^3)
164	10	0.3	0.45	5.56	3.45	1571

Table 5.2: Physical, Mechanical & Thermal Properties of epoxy resin 8552

E (GPa)	υ	ρ (kg/m^3)	κ (W/m°C)	C_P (J/kg°C)
5	0.3	1310	0.35	1000

Table 5.3: Thermal Properties of UD laminate IM7/8552

κ_1 (W/m°C)	$\kappa_2 = \kappa_3$ (W/m°C)	C_P (J/kg°C)	h (W/m^2°C)
5.4	0.95	857	10 – 80

Table 5.4: Dynamic Parameters

Structural Damping	Frequency [Hz]	Non – Structural Mass [kg]
0.003	395	15

5.3. Prediction of Damage Evolution

As it was discussed during the Literature Review, the Virtual Crack Closing Technique is commonly applied in order to provide information about the crack growth rate. Hence, it is possible to utilise this technique in order to attempt to simulate the occurrence of the Critical Event at various ambient temperatures conditions.

The interrupted tests, presented in Chapter 3, revealed the damage development sequence throughout an endurance test. Figure 5.2 also depicts how these data can be incorporated into the FE model, since the purple line represents the path followed by the crack under cyclic loading. The interrupted tests demonstrated that the crack will emerge as a transverse crack between the terminated plies and the resin pocket. Therefore, it is safe to assume that the damage will initiate where the resin pocket meets the transverse ply since the stress concentration at this is the highest; then it will propagate towards the outer ply.

The CT scan analysis also hinted that as soon as the transverse crack reaches the outer ply, the crack will extend towards the thicker section of the ply drop, possibly due to the higher strain concentration. However, after a few cycles, the crack is extended towards both the thin and the thick sections, forming a “T”. Fortunately, the propagation rate and direction can be deduced, using the VCCT.

5.3.1. The Virtual Crack Closure Technique

The VCCT dictates that a crack will extend towards the direction that the total energy released G_T exceeds the fracture toughness G_C of the actual mode mixity G_{II} / G_T. Therefore, its main objective is to measure the Strain Energy Release Rate (SERR) in order to estimate whether a major delamination will occur. After the initiation of the delamination, propagation follows the Paris Law while the crack growth rate depends on the relation between the G_T and G_C. Thus, the crack accelerates when the total energy available is close to the critical fracture toughness.

Russell and Street used an approach based in Fracture Mechanics and proposed that the Paris law between pure mode I and pure mode II can employed utilising a simple rule of mixture [83].

$$\frac{da}{dN} = C_m \left(\frac{\Delta G_I}{G_{Ic}} + \frac{\Delta G_{II}}{G_{IIc}} \right)^{n_m} \tag{5.1}$$

Where C_m and n_m are the Paris law parameters, G_I and G_{II} are the SERRs for mode I and mode II while G_{Ic} and G_{IIc} are the critical SERRs.

$$C_m = \frac{G_I}{G_T} C_I + \frac{G_{II}}{G_T} C_{II} \tag{5.2}$$

$$n_m = \frac{G_I}{G_T} n_I + \frac{G_{II}}{G_T} n_{II} \tag{5.3}$$

The crack experiences different R – ratios for mode I and mode II during a complete oscillation. Magi [68] pointed out that R = – 1 at mode II while R = 0 at mode I, even though reverse loading exists due to the resonance vibration. Furthermore, Matsubara et al. [84] argued that the ΔG_{II} definition lacks physical meaning. For this reason, they introduced the following relation which depends on the load range ΔP:

$$\Delta G_{II} = \Delta P^2 \cdot \left(\frac{G_{II}}{P^2}\right) \quad 5.4$$

$$= P_{max}^2 \cdot (1-R)^2 \cdot \left(\frac{G_{II}}{P^2}\right) \quad 5.5$$

$$= G_{IImax} \cdot (1-R)^2 \quad 5.6$$

Taking into account Eq. 5.6, the Paris law in Eq. 5.1 can be transformed into:

$$\frac{da}{dN} = C_m \left(\frac{G_{Imax}}{G_{Ic}} + \frac{4G_{IImax}}{G_{IIc}}\right)^{n_m} \quad 5.7$$

As a result, the propagation rate can be calculated for both crack tips of the "T" shape, using an iteration process on a FE environment, but it will only propagate towards the region where G_T is higher. The number of cycles clocked up can then be estimated for each iteration, by subtracting the life of the failed element by the residual life of the adjacent element sharing the crack. However, it is worth noting that the exact values of the crack propagation rate were considered beyond the scope of the aforementioned technique. Thus, this approach aims to investigate the development of delamination under different environmental conditions.

5.3.2. Delamination in a 2D Model

As it was discussed, the VCCT can be implemented on a synthetic dynamic FE environment and in particular using modal displacements. For this reason, a 2D model was built, incorporating the knowledge acquired by the CT scan analysis.

Among the options available, the *steady state dynamic* analysis was chosen since it has the capability to incorporate a structural damping coefficient while being computationally cheaper. In addition to this, Matlab scripts were developed, in order to conduct and control the iterative procedure. Following the requirements imposed by the experimental technique, during each iteration, the Matlab scripts had to maintain constant excitation frequency and vibration amplitude while extending the damage. In fact, Matlab was employed to generate the control algorithm for performing the FLL at constant excitation frequency.

Even though, the damage between the different instances (e.g. resin pocket, plies) was pre – imposed on the FE model, massless springs were applied at each node of the contact region between the instances; all along the crack path. This way the damage was propagated by removing the appropriate spring during one iteration. Only two springs were applied at each node, corresponding to the 2 axes of the 2D model. The springs are crucial for the VCCT analysis since they permit the extraction of nodal forces which can then be exploited by the VCCT. Thus, when a steady state analysis was concluded, the SERR was evaluated for both mode I and II while the springs at the onset of damage were removed. Additionally, the spring stiffness was chosen at 10^{13} N/m, which promotes a rigid bond between the contact areas since its magnitude is 6 times greater than the rigidity of the corresponding 0° ply. The full flow chart of the procedure is presented in Figure 5.3.

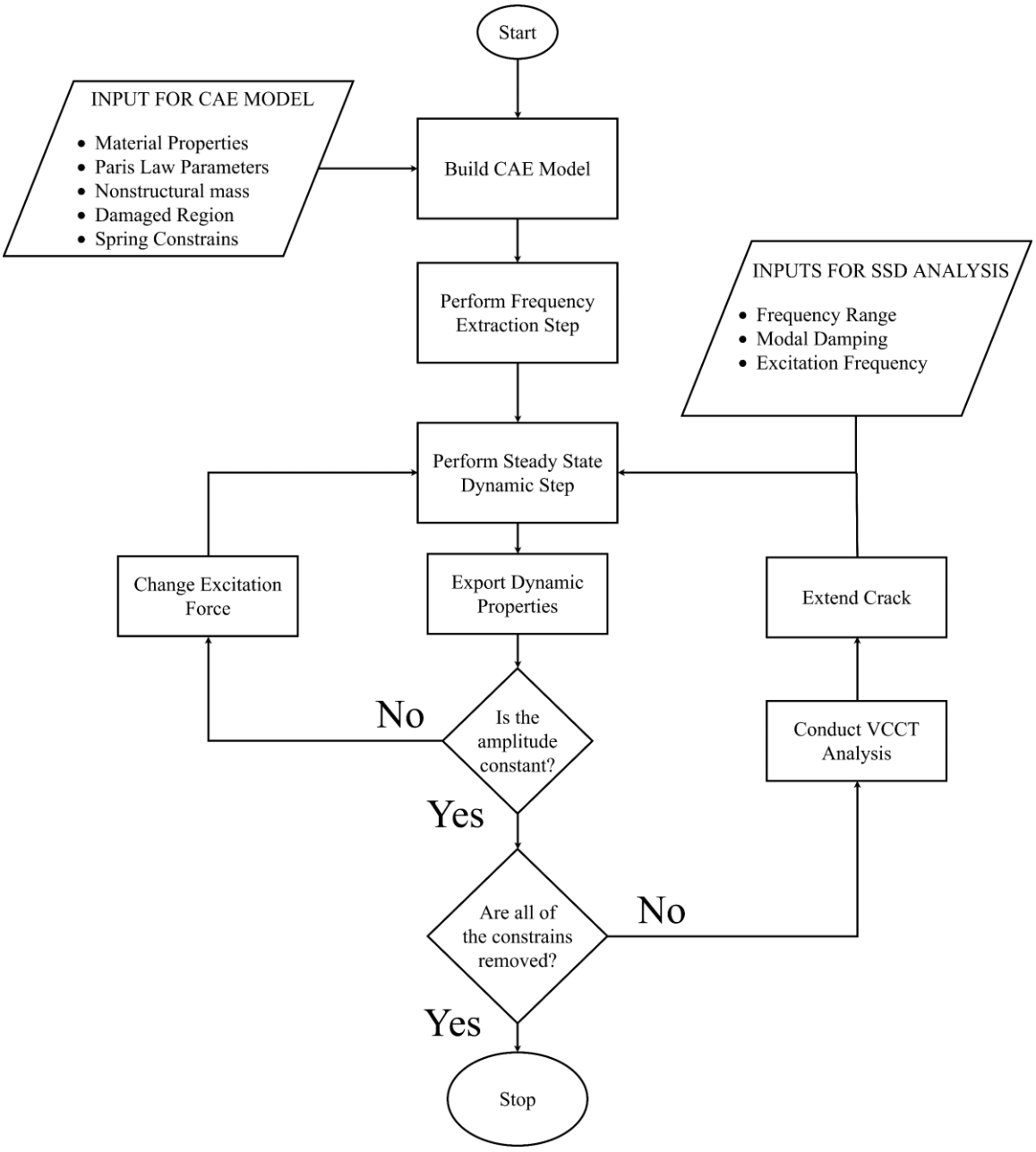

Figure 5.3: Flow Chart of the VCCT procedure

A major challenge presented itself in the face of the Paris Law parameters. Unfortunately, only a limited amount of information is available in the literature regarding the Paris law parameters of material in use (IM7 /8552), when exposed to various environmental temperatures. On the other hand, the proper investigation of these elements requires an in – depth experimental analysis which was considered beyond the scope of this study. For this reason, a decision was made to introduce a different CFRP material for the purpose of the VCCT analysis. Hence, the studies carried out by Asp [26] and Sjorgen [34], [85] were followed. The authors reported the Paris law parameters for a carbon / epoxy system, namely Hexcel HTA / 6376, at 2 environmental temperature levels (20 ℃ and 100 ℃). Moreover, for the purpose of the current study, a linear approximation was made in order to interpolate the results for a 3rd temperature level, at 60 ℃. Hence, Table 5.5 and Table 5.6 present the material and fracture properties of HTA / 6376, at 3 ambient temperature levels.

Table 5.5: Physical and Mechanical Properties of HTA/6376 [26], [34]

E_1 (GPa)	$E_2 = E_3$ (GPa)	$\upsilon_{12} = \upsilon_{13}$	υ_{23}	$G_{12}=G_{13}$ (GPa)	G_{23} (GPa)	ρ (kg/m^3)
120	10.5	0.3	0.51	5.2	3.4	1586

Table 5.6: Fracture mechanics properties of HTA/6376 [26], [34]

	20 ℃			60 ℃			100 ℃		
	G_C (J/m^2)	C	n	G_C (J/m^2)	C	n	G_C (J/m^2)	C	n
Mode I	260	1.2×10^{-7}	5.5	255	2.2×10^{-6}	4.9	249	4.2×10^{-6}	4.2
Mode II	1002	7.5×10^{-7}	4.4	852	8.3×10^{-7}	4.5	701	9.1×10^{-7}	4.6

5.3.3. Viscoelastic Temperature in a 3D Model

While the VCCT is able to capture the mechanical response of a composite laminate, subjected to cyclic loading; a different approach has to be adopted to simulate its thermal response. The internal heat generated during an endurance test is referred to the "*Self – Heating*" and it consists of two parts. The first part is the viscoelastic heat which is generated due to the viscoelastic properties of fibre reinforced polymer composite, while the second part is a combination of heat generated due to frictional forces in the delaminated region and the viscoelastic temperature. Furthermore, it can be easily understood that temperature distribution along the surface of a specimen cannot be captured through a 2D model, which simulates the through thickness geometry of a specimen; especially when different thermal 3D loads have to be considered. Thus, a 3D model is necessary in this scenario.

Lahuerta et al. [86] described a method, presented in Chapter 2, for simulating viscoelastic temperature of UD coupon under cyclic bending loads. They demonstrated that the viscoelastic heat of the components is related to their strain energy through the damping factor. It is therefore possible to develop a FE model which exploits this relation. In that respect, the strain energy can be extracted from a frequency extraction step and converted into heat input which can be imported into a heat transfer analysis. Figure 5.4 illustrates the flow chart of this procedure.

An important part of the thermal model can be traced down to the thermal properties of the system since they can affect the final results. Even though, Hexcel provides an extensive datasheet about the mechanical properties of the material system, its thermal properties are not as broadly studied. However, different sources present slightly different results [87], [88], [89]. As a consequence, a sensitivity analysis was conducted to identify the optimum values.

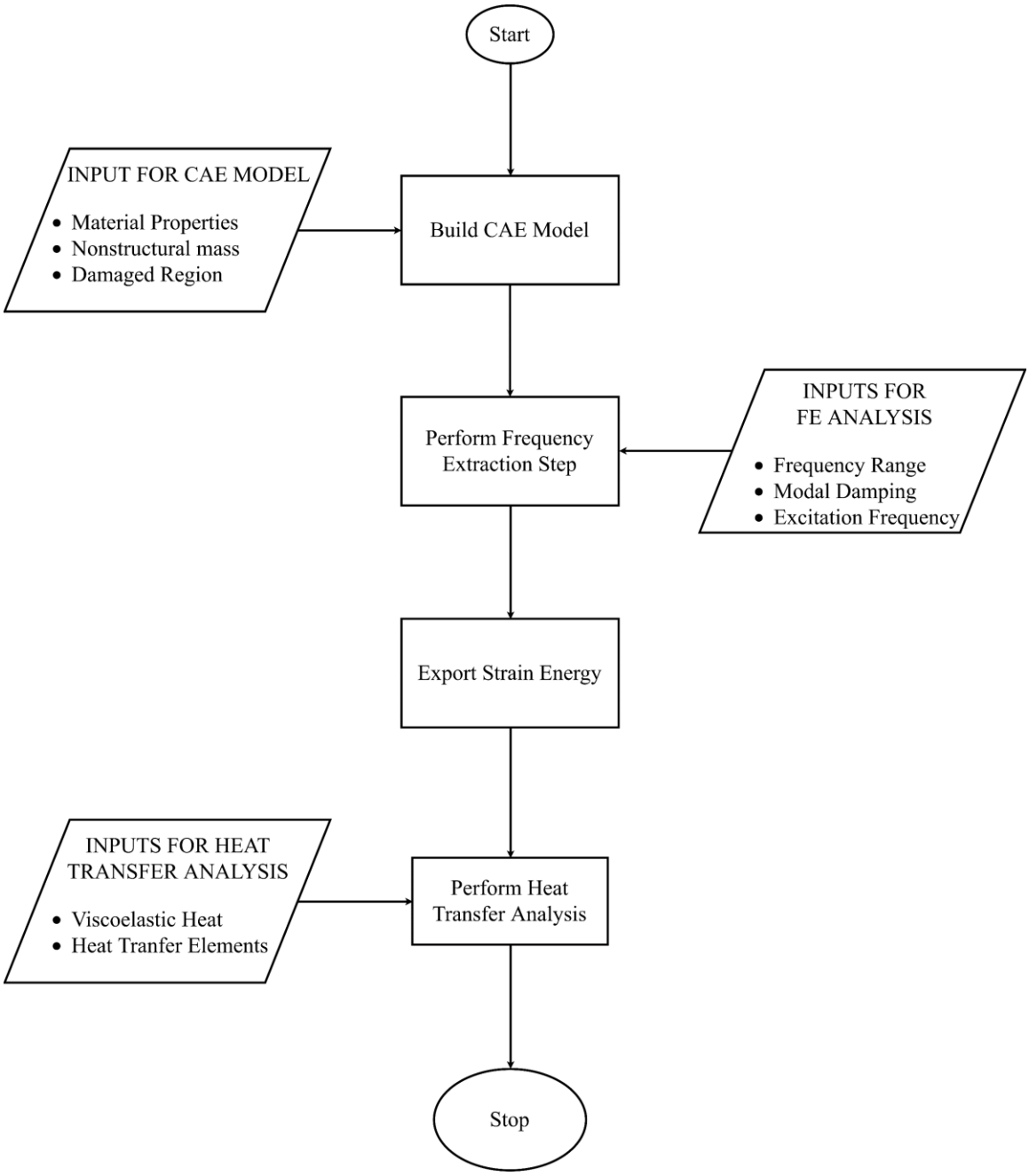

Figure 5.4: Flow Chart of the Viscoelastic Temperature Simulation Procedure

The through thickness thermal conductivity was the first property examined. Different studies have reported the thermal conductivity (κ) of CFRP between 3.9 to 6.6 W/m°C [87], [88]. Hence, the simulations were executed following the procedure given in Figure 5.3, for a constant vibration amplitude while assuming an isotropic thermal conductivity. The conductivity was alternated at each iteration, keeping the rest of the material properties constant. Figure 5.5a reports the maximum surface temperature of the specimen at different conductivities. It can be observed that with increasing conductivity, the endogenous temperature of a component decreases. However, the effects on the surface temperature are minor (< 1°C), for the conductivity range of interest.

Additionally, the transverse conductivity was analysed following the same procedure. In this case, an isotropic conductivity was assumed and the transverse values were alternated. It was reported that it can be placed between 0.75 – 1.13 W/m°C [88], [89]. FE analysis revealed that the influence of the transverse conductivity is less severe, but they follow a similar pattern (Figure 5.5b).

Another aspect of model, which is of great importance, is the Heat Convection Coefficient (h). The tests were run inside an environmental chamber where air flow was applied to control the surrounding temperature. This phenomenon can be simulated on a synthetic FE environment though the heat convection coefficient. Typical heat transfer coefficient values for free convection can vary from 10 – 350 W/m^2 °C, depending on the air velocity. Hence, for this set of simulations, only the values of convection were changed. Figure 5.5c demonstrates that the modelled component exchanges heat at a higher rate with the environment when the heat convection coefficient is increased.

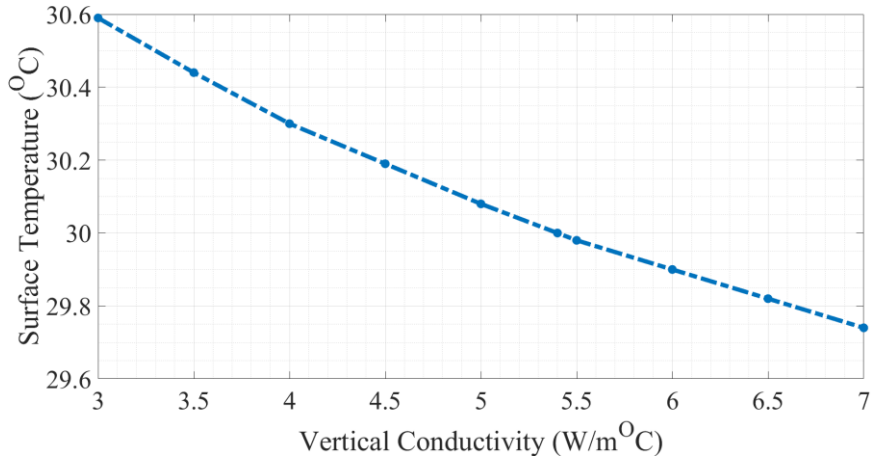

(a)

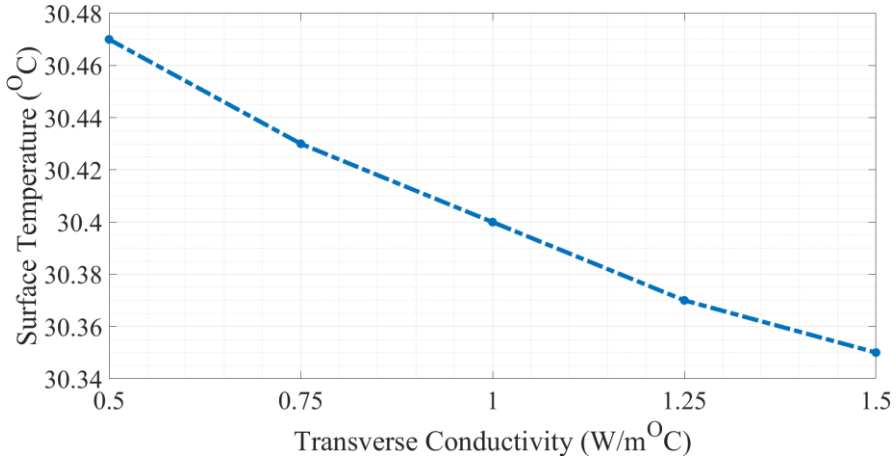

(b)

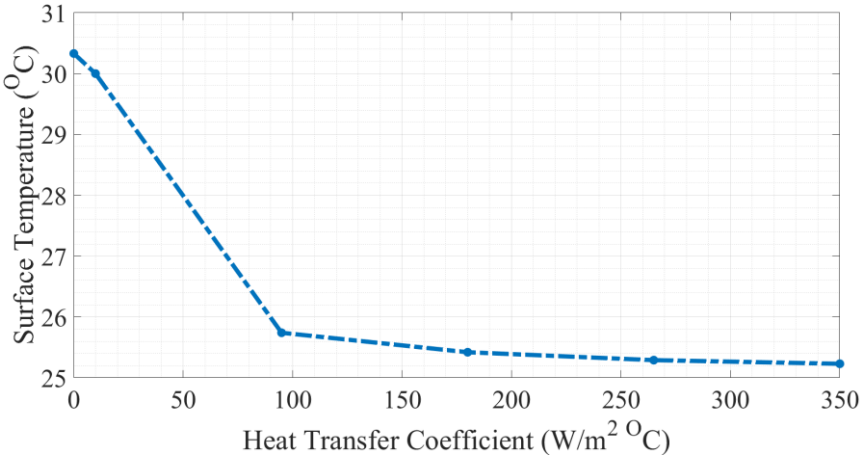

(c)

Figure 5.5: The effects of (a) through thickness conductivity, (b) transverse conductivity, (c) heat transfer coefficient over the self – heating temperature

Moreover, the effects of convection coefficients are not only limited to changes in the specimen's temperature. It was observed that the air flow can drastically change the surface temperature distribution shape. Figure 5.6 demonstrates that increased convection could lead to changes in the temperature distribution shape which indicates that the modelled environment is not similar to the experimental conditions. What's more, the analysis of the thermal images showed that the heat convection is greater at the edges of specimens; resulting in an oval shaped temperature distribution around the most stressed region (ply drop). This is another phenomenon that ought to be considered in the FE model in order to acquire the precise shape. For this reason, a higher convection value was chosen around the edges of the model to match experimental observations. On top of that, the air flow temperature can also be selected which is a great advantage since the model could find application into various environmental temperatures levels.

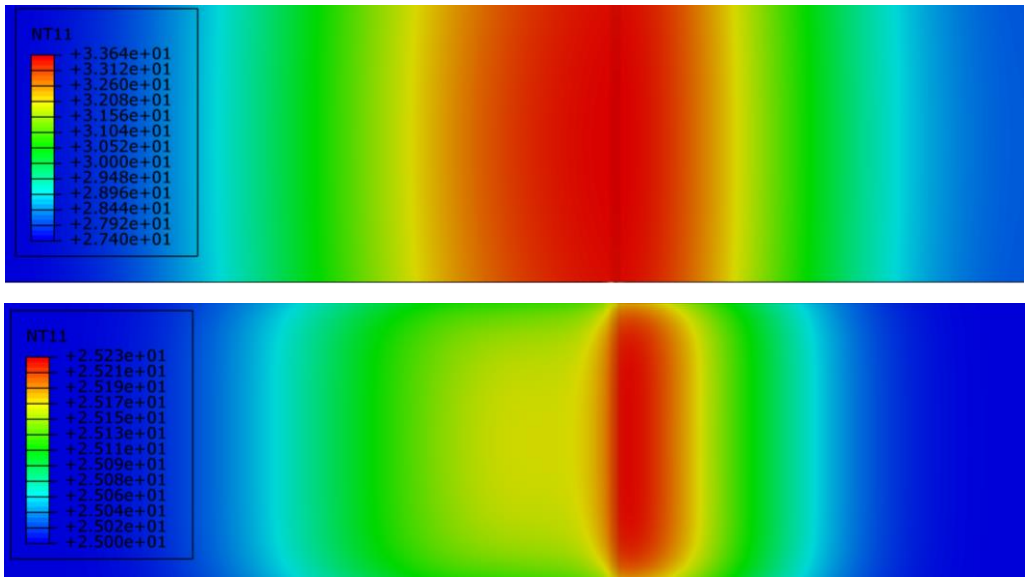

Figure 5.6: Temperature distribution at Low (top) and High (bottom) Flow Rates in the FE environment

In conclusion, a vertical conductivity of 5.4 W/m°C and a transverse conductivity of 0.95 W/m°C were chosen since they fall close the values proposed in the literature while

resulting into small variations in the final numerical results. Figure 5.7 and Figure 5.8 present a comparison between the experimental and simulated viscoelastic temperature distribution. One could notice that the analytical technique generally follows the experimental trends. The thermal images also imply that the heat dissipation at the edges of specimens is higher since the surface temperature is lower around area. Besides that, one clear advantage of this technique is that it reveals the through thickness temperature distribution of specimens which can be particularly challenging to investigate experimentally. In this case, it was observed that the temperature difference between the outer and inner layers is less than 0.5 ℃ since the most stressed region is located only two plies (25×10^{-5} m) below the surface.

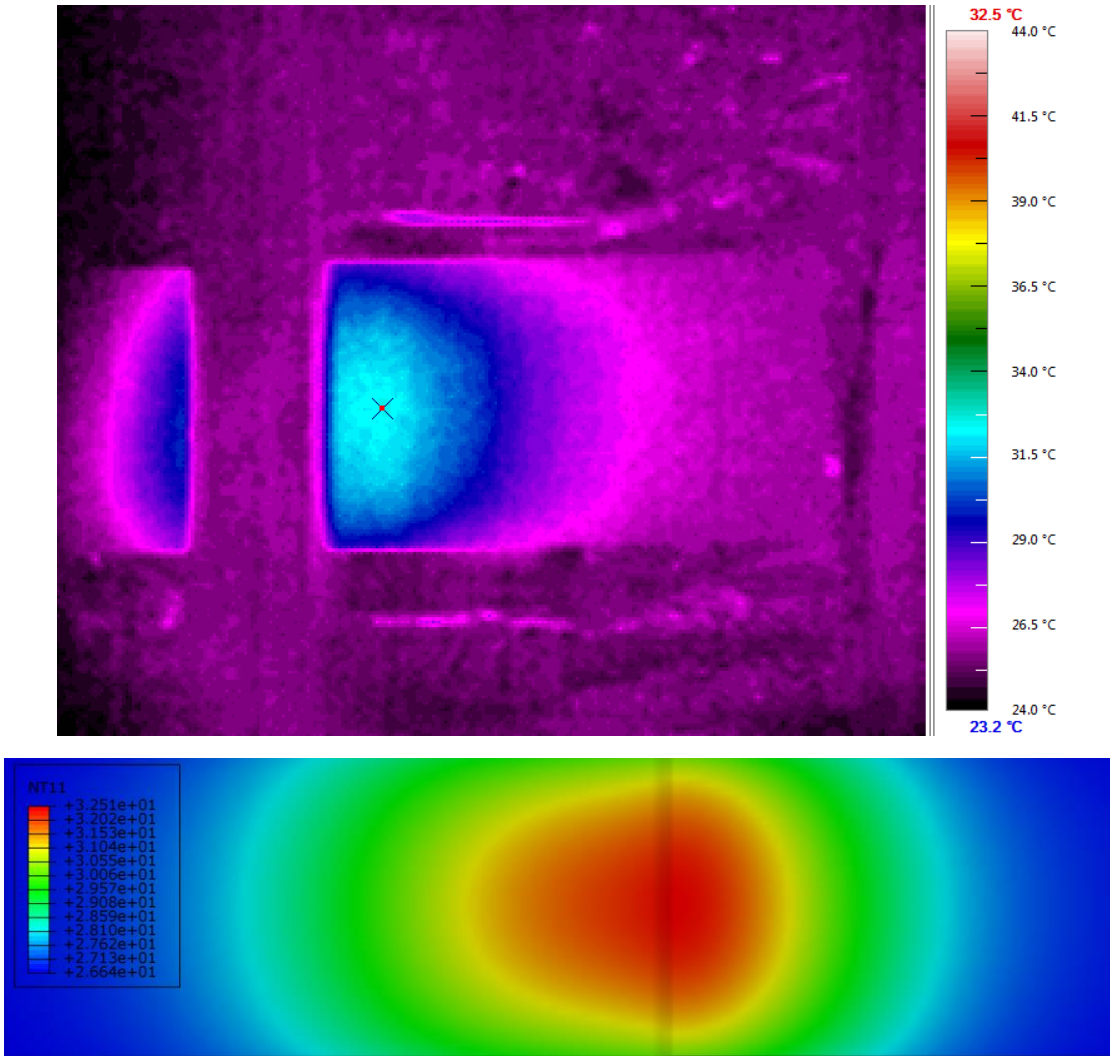

Figure 5.7: Comparison between the experimental (top) and FE (bottom) temperature distributions along the surface of a specimen

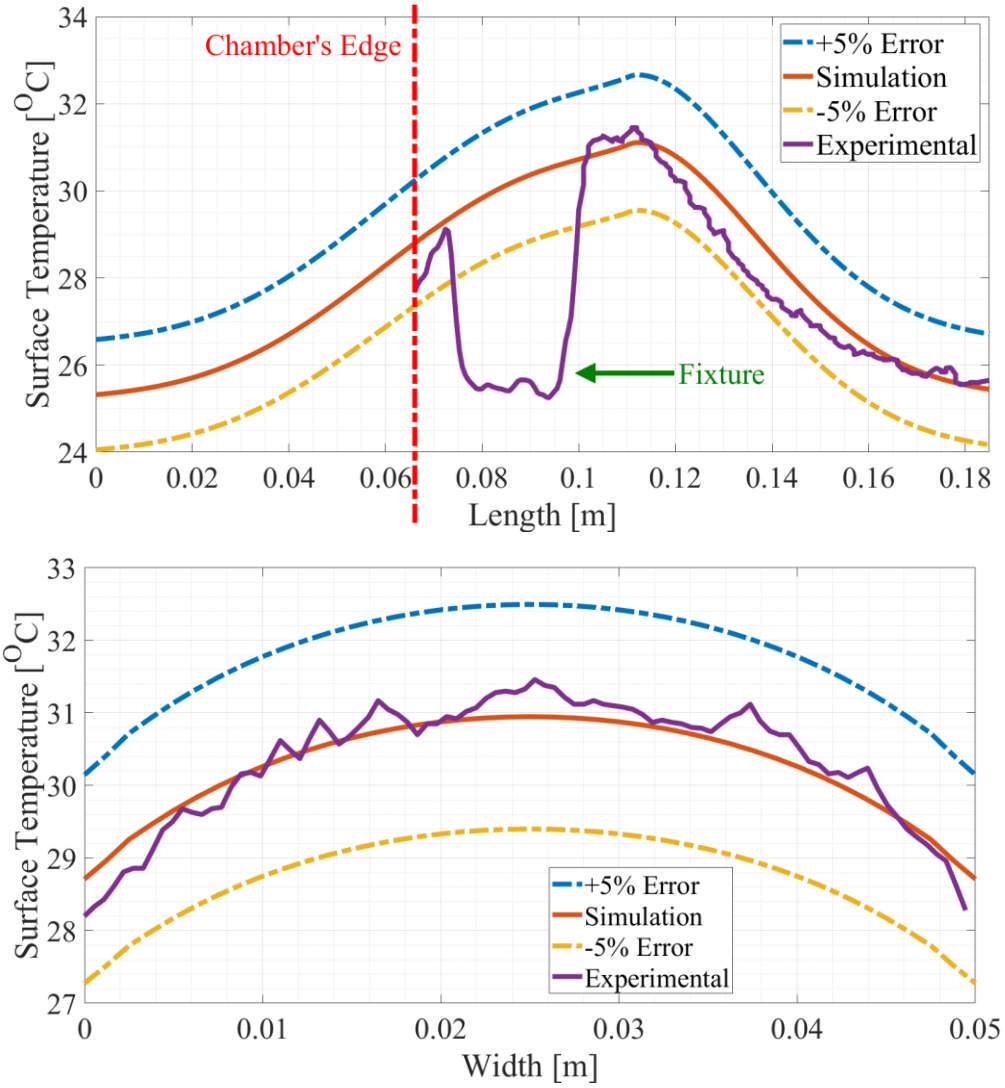

Figure 5.8: Numerical comparison between the experimental and FE temperature distributions along the length (top) and width (bottom) of a specimen

5.3.4. Simulation of Frictional Heat in 3D Model

The linear dynamic FE environment can therefore be exploited in order to evaluate the occurrence of the Critical Event as well as the endogenous heating of specimens; always considering the ambient conditions. Nevertheless, contact between the damaged regions cannot be simulated using linear dynamics. More specifically, heat developed due to ply by ply rubbing in the delaminated areas is governed by the frictional forces in the areas of contact. However, friction is an inherently a non – linear phenomenon and as such cannot be captured by linear steps. For this reason, a different approach had to be implemented.

Even though a non – linear dynamics analysis can be implemented in Abaqus, it is computationally so expensive that it renders the analysis impractical. For this reason, a different technique had to be investigated. It was decided that the optimum solution was to develop a multi – physics FE model which is capable of capturing the frictional heat emerging due to ply by ply rubbing at the damaged region. Following the procedure described in Figure 5.9, a linear steady state dynamic analysis still forms the basis of the model. The delamination was pre – introduced in the model according to the observations made by the CT scans and their respective thermal images (Figure 5.10). The damage can then be expanded in order to simulate the hot spot expansion in the thermal images. Despite that, the linear dynamics analysis is still unable to capture the contact between the delaminated plies. In fact, a static analysis was employed in order to overcome this obstacle. Hence, the modal displacements of the bending mode shape were extracted from the linear dynamic analysis and superimposed into a static step; introducing the same modal displacements. A static analysis supports the simulation of friction since it is a non – linear step and it can simulate the nodal friction forces between the top and bottom surfaces of the delaminated region. It can also evaluate the distance that two adjacent nodes, travelled with respect to each other; in this case the nodes between the top and bottom – delaminated – plies. Thus, the frictional work could then be estimated from the friction force and sliding movement of the two plies in the delaminated area. This frictional work is then utilised as an input in a heat transfer step.

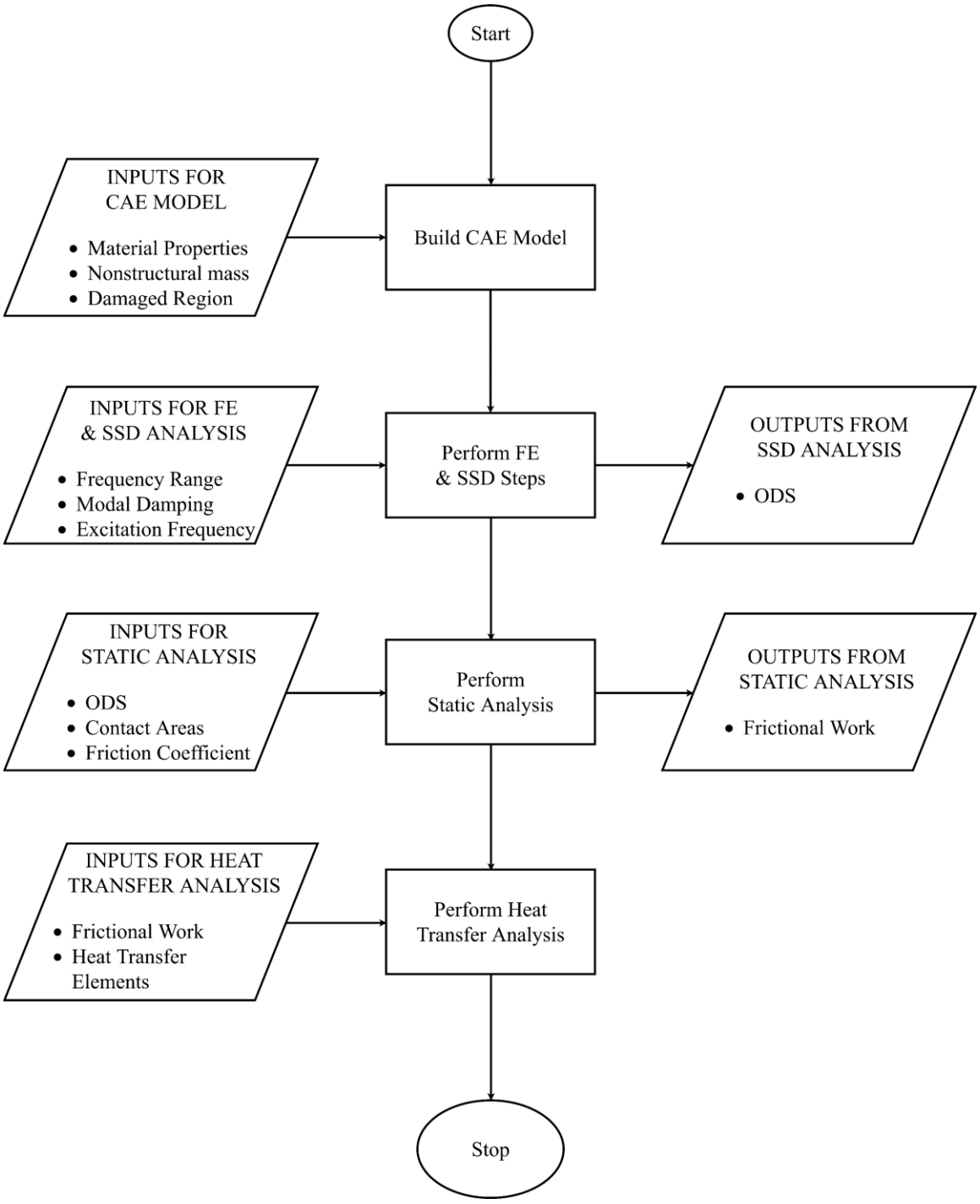

Figure 5.9: Flow Chart of the Frictional Temperature Simulation Procedure

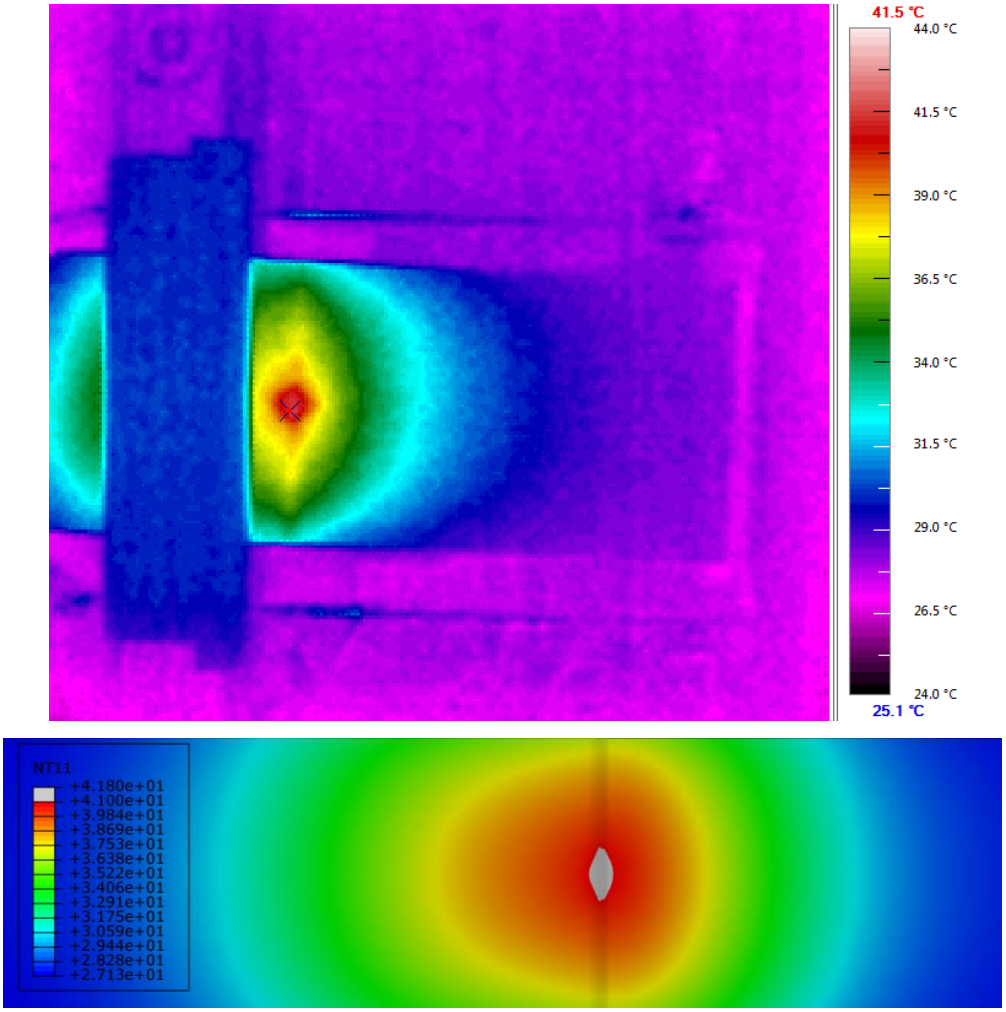

Figure 5.10: Comparison between the experimental (top) and FE (bottom) Hot – Spot temperature distributions along the surface of a specimen / the Simulated Hot – Spot is depicted by the grey area

Be that as it may, an aspect of great importance for a frictional heat model is the friction coefficient. One could understand that the experimental investigation of the friction coefficient is a subject which contains many challenges. An experimental study carried out by Schön [90] on a carbon / epoxy material system (HTA / 6376), reported that the peak coefficient of friction falls within 0.7 and 0.8. Fortunately, it possible to conduct a numerical sensitivity analysis, within this range, in order to examine the effects of different friction coefficient on the friction generated temperature, following the aforementioned

procedure. Figure 5.11 captures this behaviour, for simulation implemented at the same vibration amplitude while adopting the thermal conditions introduced for the viscoelastic temperature model. It can be observed that the temperature generated due to ply by ply rubbing could increase more than 1 ℃ under the influence of the friction coefficient. However, taking into account both the maximum temperature recorded during the interrupted tests and the literature data, it is believed that the optimum value of the friction coefficient is close to 0.75. Hence, this value can be employed for the investigated self – heating temperature of a CFRP specimen after the Critical Event.

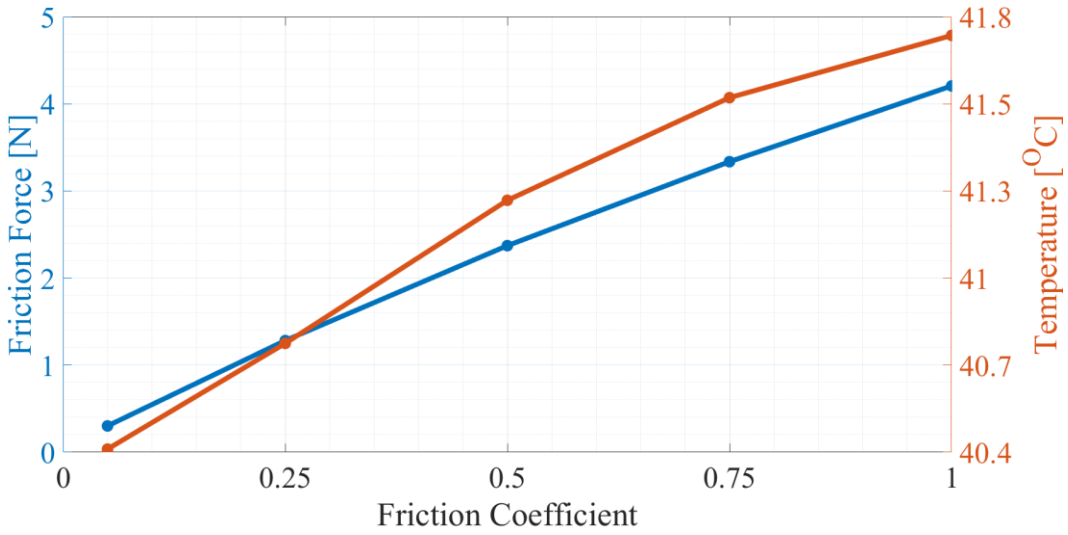

Figure 5.11: The effects of increasing Friction Coefficient over the Friction loads and temperature at the damaged region

5.4. Remarks

The experimental results acquired via the vibration testing technique paved the way for investigating the high cycle fatigue behaviour of carbon reinforced composites under various temperature conditions. It was reported that the Critical Event is influenced by the ambient temperature while introducing a connection between the thermal and mechanical responses of the testing coupons. However, it become apparent that the in – depth understanding of the fatigue behaviour can only emerge through the incorporation of both numerical and experimental results.

A first attempt at reproducing the experimental behaviour was made by exploiting the Virtual Crack Closure Technique. A method was introduced for simulating damage propagation at different environmental temperatures and in extend to study their effect on the occurrence of the Critical Event. This method attempts to produce further insights into the high fatigue behaviour of CFRP laminates.

On the other hand, the thermal response was less straight forward to reproduce due to the various variables that affect its behaviour. The thermal conditions inside the environmental chamber were transferred to the FE environment, combining the experimental and numerical results. As a result, a method for simulating the viscoelastic temperature of components was established. Furthermore, the self – heating temperature of specimens is also associated with the frictional heat generated due to ply by ply rubbing in the delaminated regions. For the purpose of this investigation, a multi – physics model was introduced.

In conclusion, the established numerical methods are not limited by the material or the geometry of the components but they have to closely translate the dynamic testing environment into the FE models. As a result, the models can be exploited in order to broaden the existing knowledge around CFRP composites while aiding the simulations of the experimental observations; such as developing a connection between the thermal and mechanical responses.

Chapter 6

A NUMERICAL EXAMINATION OF THE FATIGUE LIFE

The fatigue behaviour of composite components, subject to a combination of thermal and dynamic loads, is investigated exploiting the advantages of the Finite Element Analyses, described in Chapter 5. The experimental environment was simulated in order to better understand the physics that govern the fatigue damage development. In addition to this, the FE results were correlated against the experimental data. Finally, the experimental results were employed to develop an empirical relation, which takes into account the heat energy lost per cycle. The simulated mechanical and thermal responses of composite components, subjected to cyclic loading, were then related to the experimental observations.

6.1. Introduction

The tapering, such as reduction of thickness, is a widely used designing feature in various composite structures (e.g. fan blade roots) to achieve a desired geometry. These regions of discontinued geometric locations are achieved via of dropped plies which give rise to high interlaminar stresses [91]. In these scenarios, the load is transferred from the dropped plies to the resin pocket. Then, it is extended to the adjacent plies, forming a delaminated region. As it was explained by Khan in [91], the delaminations are driven towards the thin section of the laminate, only for steep thickness reduction. However, delaminations most commonly occur towards the thick section due to the high shear stresses. A FE approach is usually applied to simulate the delamination propagation within the damaged areas, due to the complex physics that governing the fatigue life of tapered laminates.

It is therefore considered crucial to capture the effects of stress raising features, like ply drops, when examining the failure mechanism of tapered laminates as their absence from analysis could lead to overestimation of the components' capabilities. While on an industrial scale the simulation of tapered components, such as wind turbine blades [92], call for a homogeneous approach; on a smaller scale, a ply – boundary modelling approach can be considered. This study aims to simulate the crack propagation in the ply – drop region since experimental investigation indicated fatigue damage is most likely to open in this area. In particular, it aims to exploit the modelling method described in Chapter 5, in order to gain a better understanding of the factors influencing the early growth of fatigue damage on tapered components and capture their failure mechanism.

An experimental investigation was carried out on CFRP tapered specimens to examine their fatigue resistance at resonance and at various ambient temperature conditions. Their associated failure regions were identified through a CT scan analysis of interrupted tests at predefined number of cycles. This chapter will discuss the results of a FE investigation, performed using high fidelity models of an image – based mesh; under similar loading and temperature conditions to the experimental environment. The experimental data were utilised in order to strengthen numerical approach as well as to assess the applicability of the proposed models to simulate the mechanical and thermal responses of FRPs having complex and realistic geometries.

6.2. The Mechanical Response by means of dynamic VCCT

A synthetic dynamic environment was established in ABAQUS in order to reproduce the experimental approach, along with the support of the Virtual Crack Closure Technique in an iterative manner. In a nutshell, the crack will propagate when the strain energy stored at the crack tip exceeds the fracture toughness of the material, G_C. The propagation at different temperature levels can then be studied by imposing different Paris Law / temperature dependent parameters in the numerical model.

6.2.1. The Effects of different Severity Levels

The first product of the dynamic VCCT analysis emerged in the form of the delamination locus. Following both the information available in the literature and the experimental observations captured by the X – ray Computed Tomography, the delamination will first propagate towards the thick side of the ply drop and then towards both the thick and the thin sides (Figure 6.1). This is considered as an initial indication that the VCCT model is able to simulate sufficiently, the damage growth pattern at dynamic loading conditions.

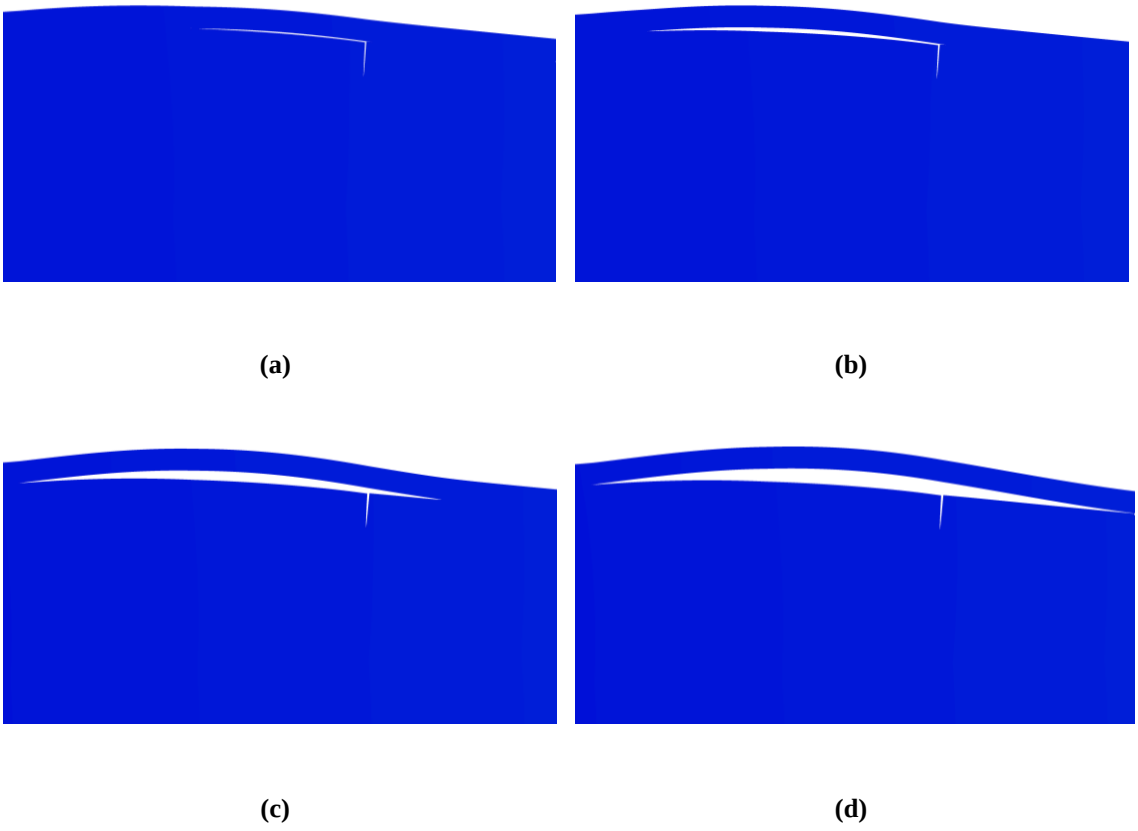

Figure 6.1: Typical Damage Evolution as captured by VCCT

A MATLAB script was used to perform an iterative process and control the vibration amplitude similar to the actual experimental procedure. Additionally, the script was

extending the damage according to the VCCT while evaluating the respective vibration phase drop at each step. Figure 6.2 captures the typical evolution in simulated phase following the aforementioned procedure. It can be observed that the phase traces three quasi – linear regions, similar to what was described in Chapter 4, for the experimental data. As a result, the simulated response seems to follow closely the experimental behaviour which supports the comparison between the two and can be used to further strengthen the vibration fatigue testing knowledge.

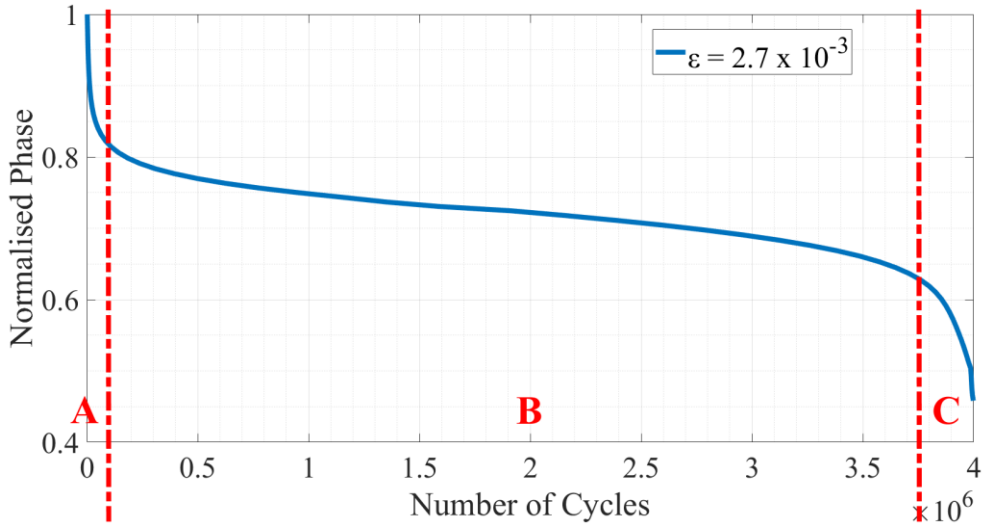

Figure 6.2: Typical Phase evolution as captured by VCCT

The experimental technique dictates that the applied strain should be the representative severity level since it varies with the application of different dynamic loads. In fact, it was experimentally observed that the vibration amplitude is an inadequate severity level.

Similar to this approach, the strain of the VCCT models was measured at a fixed point while different loads were applied in order to examine the system's behaviour at different severity levels. In particular, the simulated strain was measured at the same point across the various simulation that were performed to permit the comparison between the numerical results. Additionally, the point of measurement of the simulated strain coincided with the point at which the strain was measured during the experimental investigation.

In that respect, Figure 6.3 illustrates a comparison between the experimental and simulated data of the vibration phase for three strain levels. The discrepancy between experimental and simulated results is mainly attributed to the 2D prismatic geometry of the VCCT models. Despite that, the simulated data seem to have a good agreement with their experimental counterparts. Additionally, one can notice that the phase evolution of numerical results mimics the experimental behaviour, as it goes from low to high number of cycles. Nevertheless, the FE models report a slightly higher fatigue life with increasing strain while outlining different deterioration rates (slopes) in the respective region of the phase evolution. On top of that, they were also able to simulate the fatigue life at severity levels where experimental procedure had to declare the specimens undamaged, e.g. the blue line at the strain of 2.5×10^{-3}.

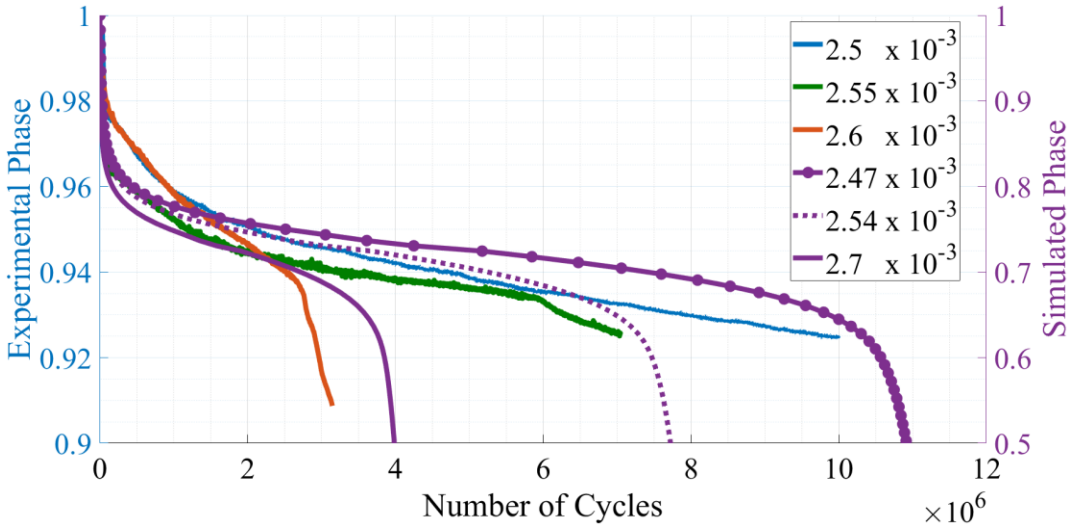

Figure 6.3: Comparison between Experimental and Simulated Phase evolutions at different severities and at 25 ℃

Further analysis on the VCCT results revealed that the amount of phase deterioration is related to the damage growth. Figure 6.4 presents how the phase evolution, at two severity levels, correlates to the damage opened at each step. One can notice that the Critical Event always occurs at the phase of 0.6365 regardless of the strain level and the number of cycles. This stage in the phase life corresponds to a prismatic damage area of

71 mm^2. Furthermore, this behaviour is also confirmed at an earlier stage in the phase evolution, at 0.7836, where the opened delamination corresponds to 34.7 mm^2. This phenomenon implies that the phase value corresponds to a specific amount of damage. In fact, this behaviour is to be expected since the stiffness deterioration is linked to both the damage opening and the phase decay. As a result, it can be assumed that the Critical Event corresponds to a Critical Damage Size beyond which the crack growth is considerably accelerated.

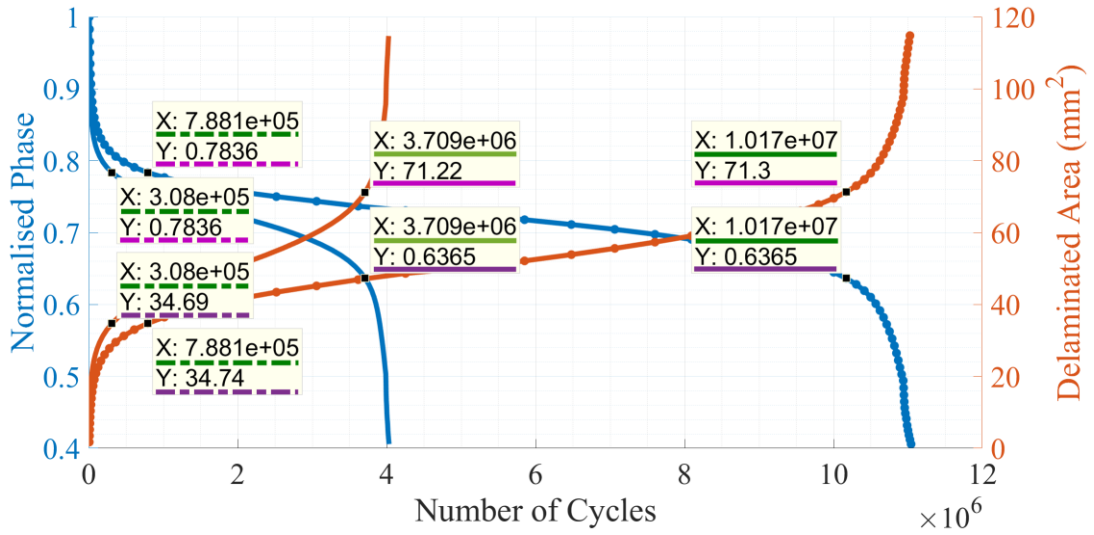

Figure 6.4: Comparison between the increase in Damage Area and Phase decay for two strain levels, as captured by VCCT

Nevertheless, the great strength of the VCCT model is its capability to produce information about variables of the system that could be very challenging to capture experimentally; by vibration testing. In that respect, Figure 6.5 shows the typical crack growth rate evolution during a dynamic endurance test simulation. It is apparent that the propagation rate decreases until a certain point (2 × 10^6 cycles). Beyond this stage, the growth will experience a slight acceleration until the Critical Event; where a significant acceleration in the crack opening rate is presented. Even though, the increase in acceleration can be considered minor until the Critical Event; it is important to mention that the point of 2 × 10^6 cycles coincides with the 50% opening of the pre – imposed

delamination towards the thick side. In Chapter 4, it was described how the different rates of decays in the quasi – linear region of the vibration phase life, could be exploited as a measure of the crack growth rate. The results of Figure 6.5 seem to support the proposition made in this section, suggesting that the region after the Critical Event is associated with a faster growth rate.

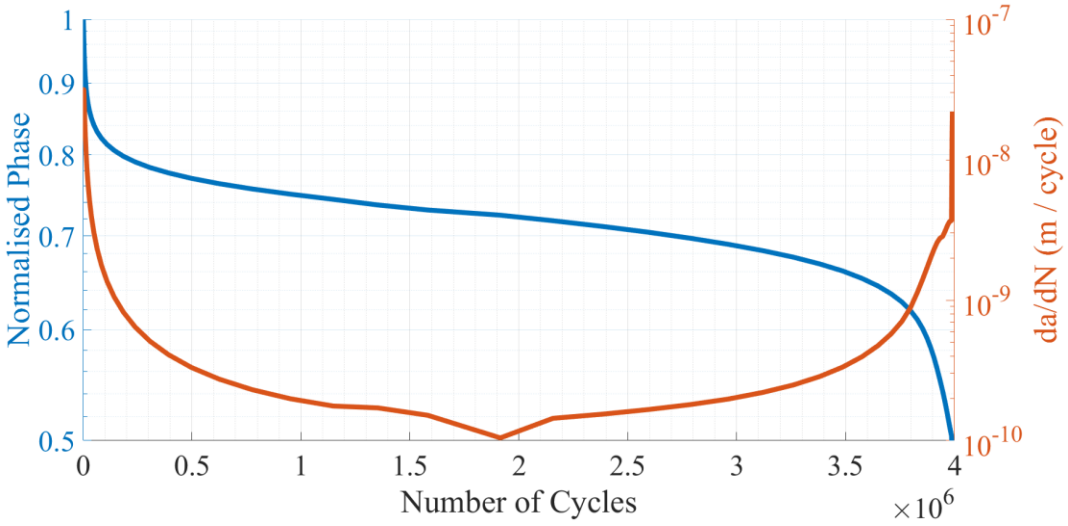

Figure 6.5: Typical response Phase and crack growth rate as captured by VCCT

Moreover, Figure 6.6 illustrates how this technique can be employed to simulate and study the influence of increasing severity; at the same ambient temperature level. The data collected from the simulation were employed to create a double logarithmic graph of damage growth rate against the Energy Release Rate (ERR). The ERR was normalised against the fracture toughness (G_C) in order to eliminate any variations caused by G_C. It is worth noting that Region A was excluded from Figure 6.6, since it corresponds to a transient state of the experiment.

Furthermore, Figure 6.5 and Figure 6.6 imply that the crack growth is slower in the initial stages of endurance testing, corresponding to a lower ERR. However, the damage growth accelerates under the effect of higher ERR, reaching a threshold limit. It is apparent that the severity will not affect the crack growth greatly, during vibration testing. This can be attributed to the fact that the threshold values are identical for the tests performed at the

same ambient temperature, since the strain dependency is more obvious at lower ERRs. In other words, the difference between the fracture toughness and the total strain energy is smaller under the effect of higher strain, resulting to rapid damage development.

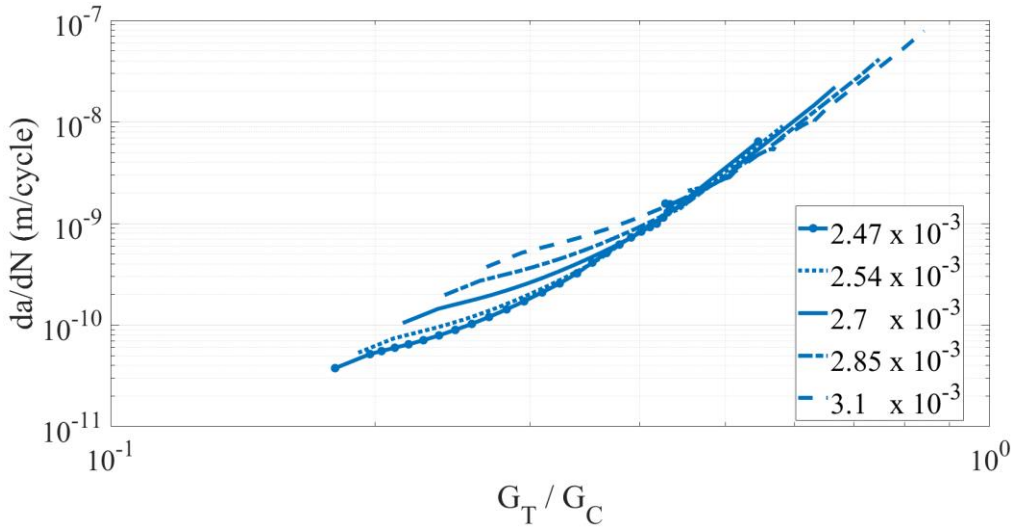

Figure 6.6: Comparison of the simulated crack growth rates at different severities

6.2.2. The Effects of different Environmental Temperature Levels

In the same manner, the VCCT models can support the analysis of the vibration fatigue testing under different ambient temperature conditions. The traces in Figure 6.7 demonstrate a comparison between the experimental and simulated mechanical responses, as they are described by the decay in vibration phase, at different exposure temperature environments but at the same strain level (2.6×10^{-3} for the experimental data and 2.7×10^{-3} for the simulated). It is evident that the VCCT is capable of reproducing the vibration fatigue life at different ambient temperatures. On top of that, it is even able to simulate the behaviour at various temperature conditions. For this purpose, Figure 6.7 plots the phase evolution at an ambient temperature level of 100 ℃ (at a strain of 2.7×10^{-3}), which is not represented by any experimental data). Despite that, the larger phase deterioration of the simulated data is again attributed to the 2D prismatic geometry of the FE specimen.

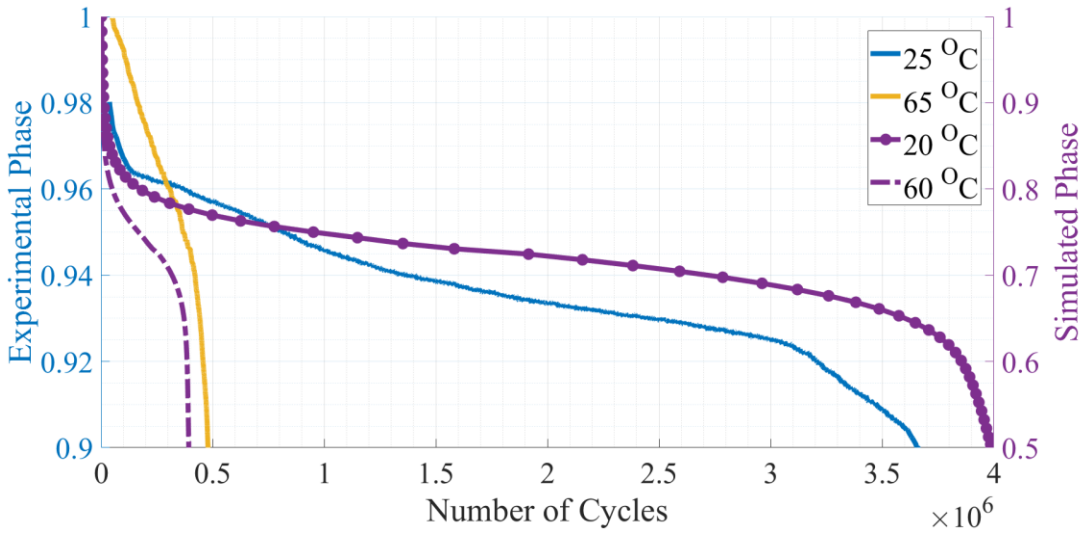

Figure 6.7: Comparison between Experimental and Simulated Phase evolutions at different ambient temperature levels and at the same severity (2.7×10^{-3})

Similar to the numerical approach that was employed to simulate the fatigue life at separate strain levels, Figure 6.8 accommodates the fatigue damage growth rates at three different temperatures. In this case, the simulations were conducted at the same strain level. It can be noticed that the vibration fatigue data can form straight lines which permits the application of a power fit; hence, following the Paris Law. The graphs trace similar patterns while presenting a considerably accelerated rate at 100 ℃, compared to 20 ℃. This behaviour illustrates that the specimens are significantly more prone to damage under harsher temperature environments since the energy required to open the crack at higher environmental temperatures is lower.

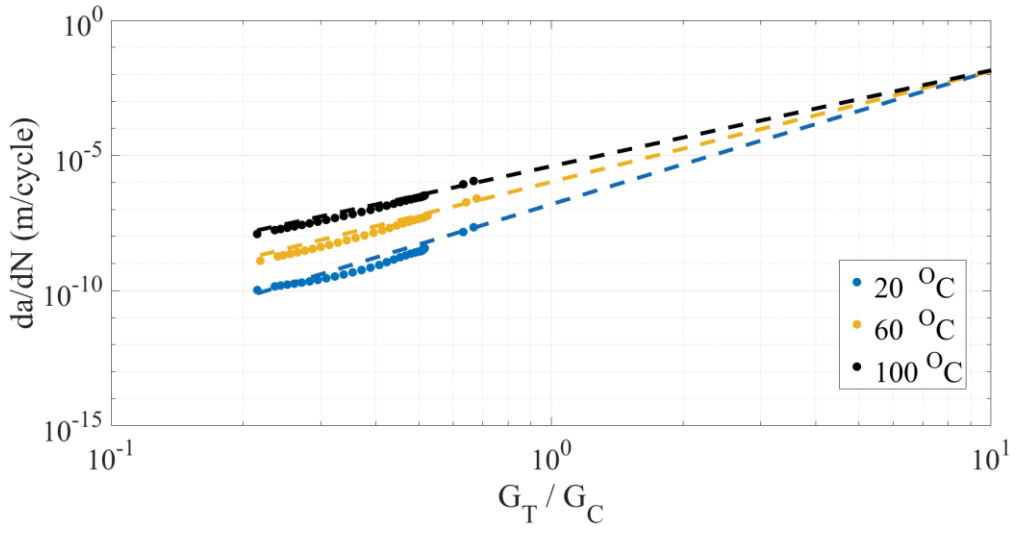

Figure 6.8: Comparison of the simulated crack growth rates at different ambient temperature levels

In the same fashion, the simulative fatigue life curves at different ambient temperature and severity levels can be outlined. Figure 6.9 contains the simulated SN Curves for three distinct ambient temperatures as well as for three separate strain levels. As it was expected both the environmental conditions and the strain levels imposed contribute the degradation of CFRP when subjected to high frequency vibration testing. It appears that the influence of the exposure temperature is less severe on the simulated curves compared with the experimental curves which were presented on Chapter 4; with a slope difference of 5.4×10^{-5} between 100 °C and 20 °C and a difference of 12×10^{-5} between 25 °C and 75 °C. This small difference in their inclinations can be attributed to the effect of the strain levels. It was discussed that it is possible to reproduce the fatigue life at lower ambient temperatures. Even then, a dissimilar behaviour is traced at more severe conditions. It is therefore believed that the combined effects of the strain level and the surrounding temperatures is not captured completely. Additionally, it can be expected that effect of the temperature conditions over the other variables of the system (e.g. crack growth rate), can only be amplified when taking the aforementioned discussion into account.

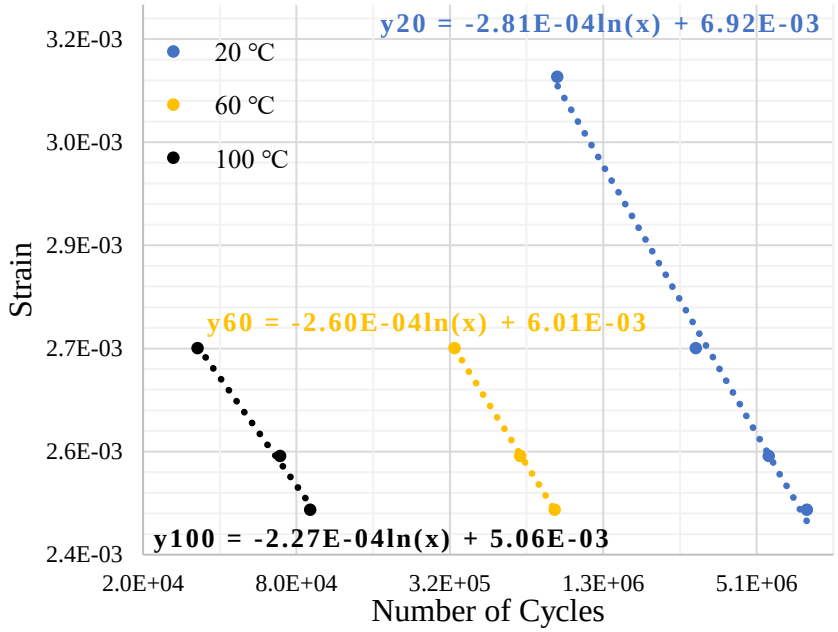

Figure 6.9: Simulated Fatigue Life curve at different ambient temperatures

Finally, the rate of change of the simulated response phase evolutions, before and after the Critical Event, can also be analysed following to the approach introduced in Chapter 4. Hence, the rate of change of the response phase for the quasi – linear regions B and C were extrapolated using a linear method (Figure 6.10). The top graph depicts the inclination of the phase evolution before the Critical Event, for separate ambient temperatures and strain levels. This figure illustrates the acceleration in stiffness degradation due to the opening of delamination; in relation to both ambient temperature and strain level. On the other hand, the rate of change of phase after the Critical Event is presented in Figure 6.10. The harsh temperature conditions impose a rapid change in the phase at this stage which corresponds to a more pronounced crack growth rate. In line with the observations made throughout the experimental investigation, these figures seem to confirm that the stiffness degradation is translated into the simulated phase decay. When taking Figure 6.5 into consideration, it is obvious that the slower phase drop prior to the Critical Event, corresponds

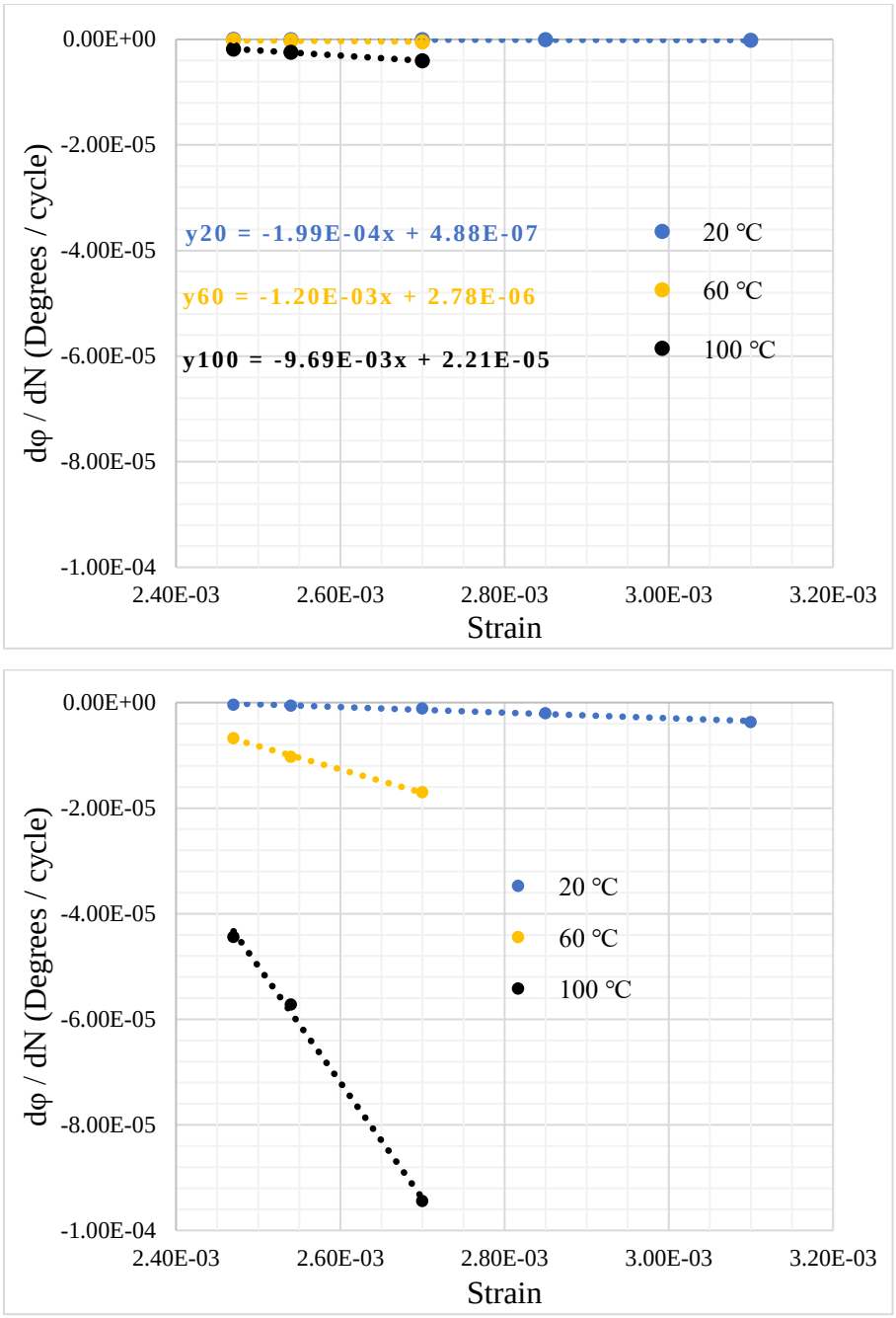

Figure 6.10: Simulated Rate of Change of Phase at different ambient temperatures / Top – Before the Critical Event (Region B) / Bottom: After the Critical Event (Region C)

to slower crack growth rate. Similarly, the rapid phase decay after the Critical Event coincides with a higher propagation rate. It is, however, worth noting that the VCCT considers a constant self – heating temperature during the life of the "simulated endurance test" which implies that the rate of change of the response phase is not influenced by the further acceleration of the propagation rate as a result of the rise in the internal temperature.

6.2.3. Suspension of Fatigue Damage

The strength of the VCCT model in revealing insights into high frequency testing in ways that are challenging to investigate experimentally, was discussed earlier. It is therefore logical to exploit this in order to study more complicated vibration fatigue behaviours. In Chapter 4, an experimental method was described which was capable of delaying the Critical Event, under the application of different localised heat loads. The experimental data hinted that the extension in the fatigue life was the result of the suspension in the damage propagation rate.

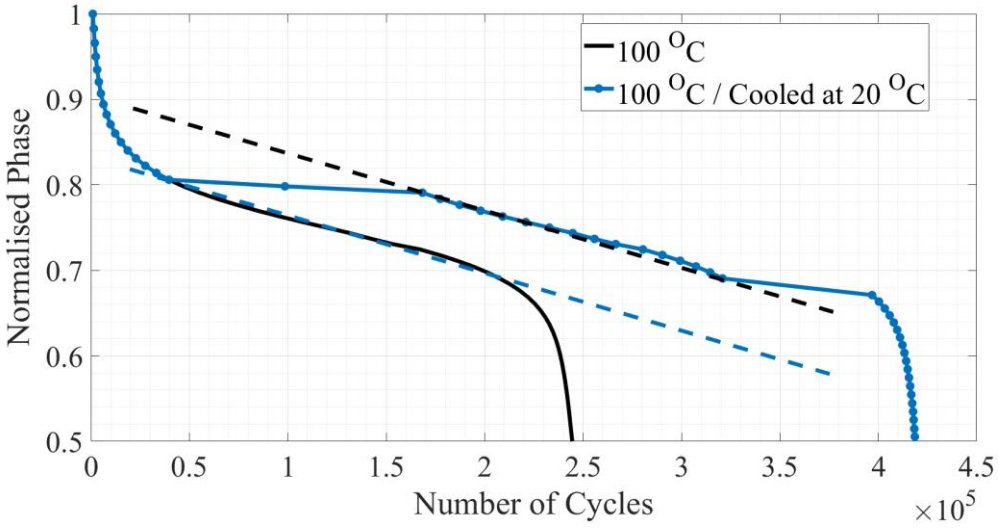

Figure 6.11: Simulated Fatigue Damage Suspension Tests at the same ambient temperature and strain levels / Response Phase evolutions of the Cooled Test compared to original

It is therefore possible to simulate the experimental procedure by changing the specific temperature dependant parameters of the system. Actually, the simulation was initiated at 100 °C, followed by a period during which the parameters were changed to simulate a 20

℃ ambient temperature. After 1×10^5 cycles, the parameters adjusted back for 100 ℃ and the simulation was allowed to continue, normally. Figure 6.11 presents a comparison between the phase evolution of the aforementioned FE simulation and the original phase decay at 100 ℃ and at the same severity. The cooled simulation traces a less intense decline in the response phase evolution during the cooling period. Thereafter, the phase experiences a deterioration identical to the original simulation which coincides to what was observed during the experimental study. A region of a different slope can also be observed towards the end of the simulation. As it is illustrated by Figure 6.11, this region corresponds to only one of the VCCT iteration and coincides to the Critical Event. For these reasons, it is regarded of low importance for the initial purpose of the simulation which was to reproduce the suspension of damage.

Previous VCCT analyses proposed that the rate of change in the decay of phase is directly related to the damage growth rate. As such, it can be confirmed what was suggested by the experimental analysis; that the growth rate is suspended during localised cooling. As a result, the fatigue life of the specimen is extended.

6.3. The Thermal Response by means of multi – physics FE Models

Unlike to what was discussed for the Virtual Crack Closure Technique, fewer references are available in the literature for the simulation of self – heating temperature evolution of specimens at vibration fatigue conditions. For this reason, a more conventional approach was employed. The viscoelastic heating was established through the estimation of the elastic strain energy of the system while the hot – spot temperature was simulated separately, through the evaluation of the frictional work on the damage area. After that the energy generated was used as a heat input to a heat transfer analysis. Various exposure temperatures can then be considered through the application of different boundary conditions in the heat transfer analyses.

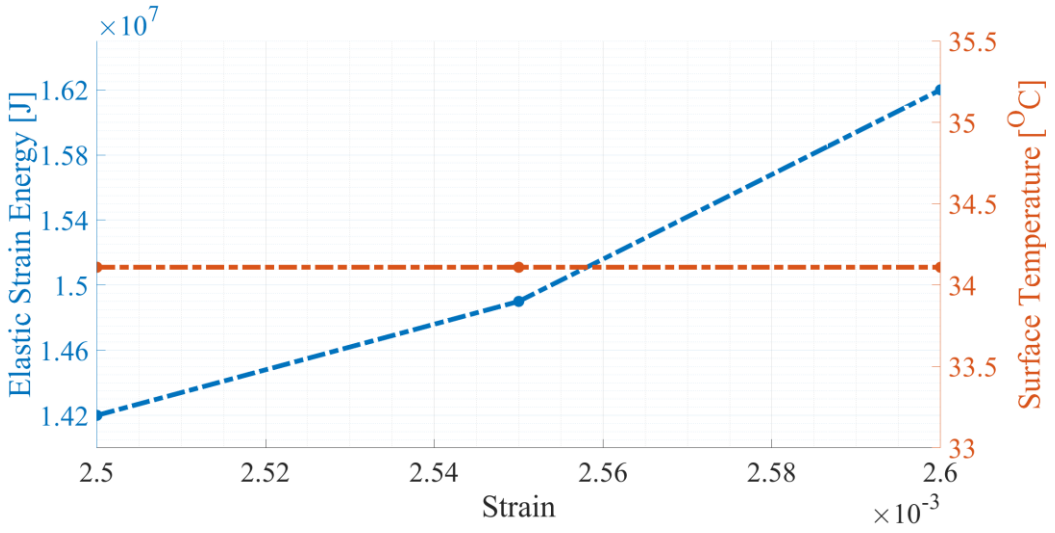

Figure 6.12: The change in the Elastic Strain Energy and its respective viscoelastic Temperature due to the increase in the applied strain

6.3.1. Self – Heating on Pristine Specimens

The first observation facilitated from the viscoelastic heat model referred to the influence of applied strains over the viscoelastic temperature distribution of fibre reinforced polymer composites. Chapter 4 illustrated how the equilibrium temperatures (Point A – where no damage has occurred) of coupons, is unaffected by the severity of the test. Figure 6.12 depicts the increase of the elastic strain energy of a specimen at the three separate strain levels; which coincide to the severities of the VCCT models. While the strain energy is subjected to an increase of 14 %, its effect over the maximum viscoelastic temperature is negligible, which is in accordance with the experimental observations. It is therefore safe to assume that the strain range of interest is not sufficient to influence the viscoelastic temperature of specimens.

In addition to this, the impact of the ambient temperatures can also be simulated. Figure 6.13 portrays the change in the maximum viscoelastic temperature distribution as a result of the increase in the exposure temperature levels. The ambient temperature levels of 20 ℃, 60 ℃ and 100 ℃ corresponds to the VCCT temperatures while the environmental temperature levels of 25 ℃, 65 ℃ and 75 ℃ agree with the experimental investigation. The FE results seems to be in line with the maximum temperature data, measured by the IR Camera; while being able to simulate the behaviour under various environmental temperature conditions. In general, the viscoelastic temperature appears to follow a linear relation with the ambient temperature.

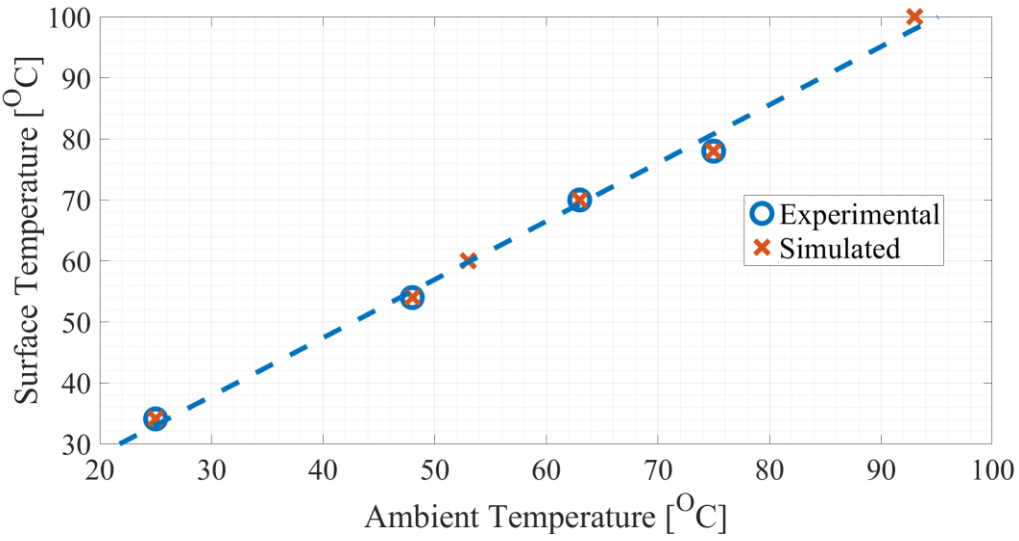

Figure 6.13: Viscoelastic Temperature change due to the ambient Temperature

6.3.2. Self – Heating on Delaminated Specimens

In a similar manner the impact of the frictional heat over the self – heating temperature can be investigated. Figure 6.14 depicts the influence of applied strain on the maximum friction force in the delaminated region, and as a result, on the self – heating temperature. It can be observed that the temperature varies less than 0.3 °C for the strain range of interest. Figure 6.12 and Figure 6.14 have therefore confirmed the experimental observation which hinted that the equilibrium and Critical Event temperatures (Points A and C) are almost unaffected by the variations in strain levels. This behaviour can only be attributed to the fact that the self – heating temperature is predominantly governed by the fatigue damage size. Thus, when the investigation is performed at the same ambient temperature conditions, the same damage size will result in the same increase in temperature.

However, it is worth noting that the Figure 6.14 plots the maximum surface temperature as it would be capture by an IR camera. The temperature at the crack tip is slightly higher as it is located 2 plies below the surface. This implies that components of different shapes should have distinct surface temperature distributions. For example, a thicker coupon may

have a smaller increase in its surface hot – spot temperature which may not be captured by an IR camera, altogether. In that sense, the FE model is able to capture information that can be challenging to observe experimentally.

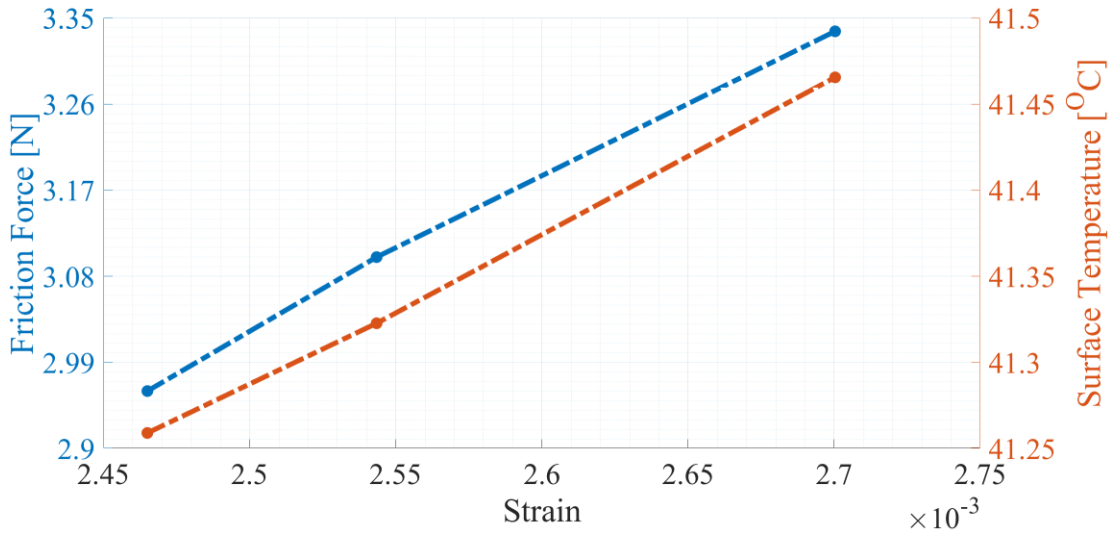

Figure 6.14: The change in the Friction Force and its respective frictional Temperature due to the increase in the applied strain

6.3.3. Self – Heating and Damage Evolution

During the period of the test prior the Critical Event, the CT scans proposed that micro – damage has already been developed; even if the thermographic analysis was not able to capture any Hot – Spot, during this period. It can therefore be assumed that the viscoelastic heating is the dominant source of self – heating before the Critical Event since the delaminated area seems to be unable to produce substantial frictional heat to produce a hot spot. Nevertheless, it is essential to replicate, as much as possible, the actual size and shape of delamination at various stages of the fatigue life, in order to capture changes in the mechanical response and internal strain energy. For this reason, the five interrupted tests were exploited in order to aid the introduction of damage geometries into a 3D FE model

which are similar to the experimental data and they correspond to different moments of the fatigue life before and after the Critical Event.

The “maximum Elastic Strain Energy” can be extracted from a linear dynamic step and corresponds to the strain energy from a fully reversible process. Unfortunately, this energy does not accurately represent the non – reversible process of the vibration fatigue testing since it does not take into account the rate of heat dissipation due to the advancement of the number of cycles. However, the energy dissipated per cycle can be calculated by the product of the loss factor and the computed maximum strain energy.

To this end, an empirical relation was developed as very limited information could be found in the literature. In fact, a “correction factor” or “loss factor” had to be employed, in each step, in order to quantitatively approximate the experimental results. Each of the steps of Figure 6.15 can be correlated to a different interrupted test since its imposed delamination geometry corresponds to a distinct damage size, extracted from an interrupted test. As a result, it also coincides with a unique number of cycles. Figure 6.15 displays the growth of the Elastic Strain Energy (fully reversible process) as a result of the damage propagation as well as the calibration function employed; at an ambient temperature of 25 °C. The number of cycles used in this figure corresponds to the number of cycles of the respective interrupted tests. It is apparent that the strain energy of the tapered specimen simulated, is not affected significantly by the development of micro – damage before the Critical Event. On the other hand, the strain energy seems to be more affected by the damage size after the Critical Event which can only amplify the events taking place at this stage (e.g. crack propagation rate).

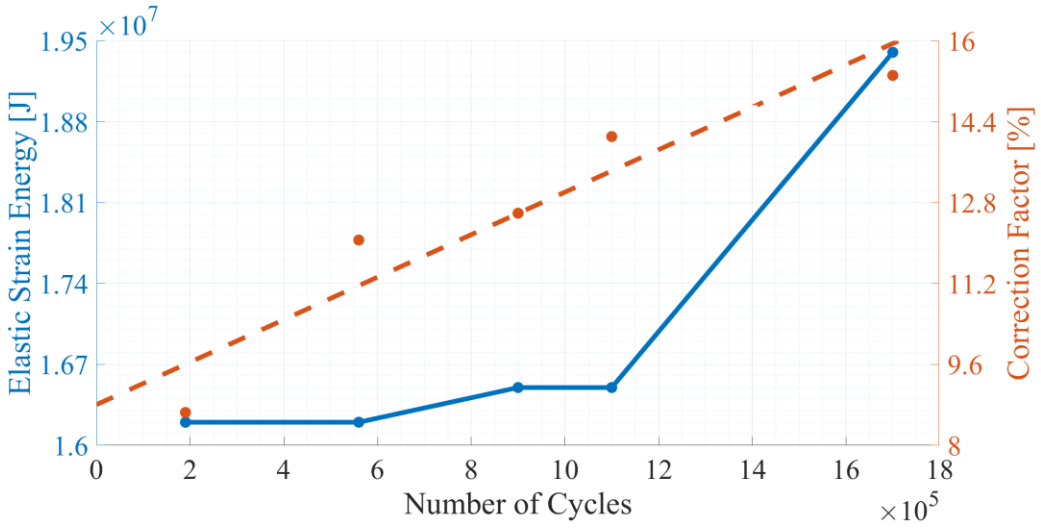

Figure 6.15: The change in the Elastic Strain Energy and its respective Correction Factor due to damage propagation

The energy of the frictional heat can then be superimposed in order to simulate the hot – spot temperature. Actually, a delamination size even greater than the one proposed by the final interrupted test was introduced in the FE model; aiming to confirm that the model can also simulate the behaviour at the final stages of the fatigue life. Figure 6.16 shows the temperature distribution along the simulated specimen as a result of the combined effect of frictional work and viscoelastic heat. One can notice how the hot – spot size and temperature is enhanced due to the propagation of fatigue damage. Finally, Figure 6.17 sketches the simulative results for the thermal and mechanical responses at 25 ℃.

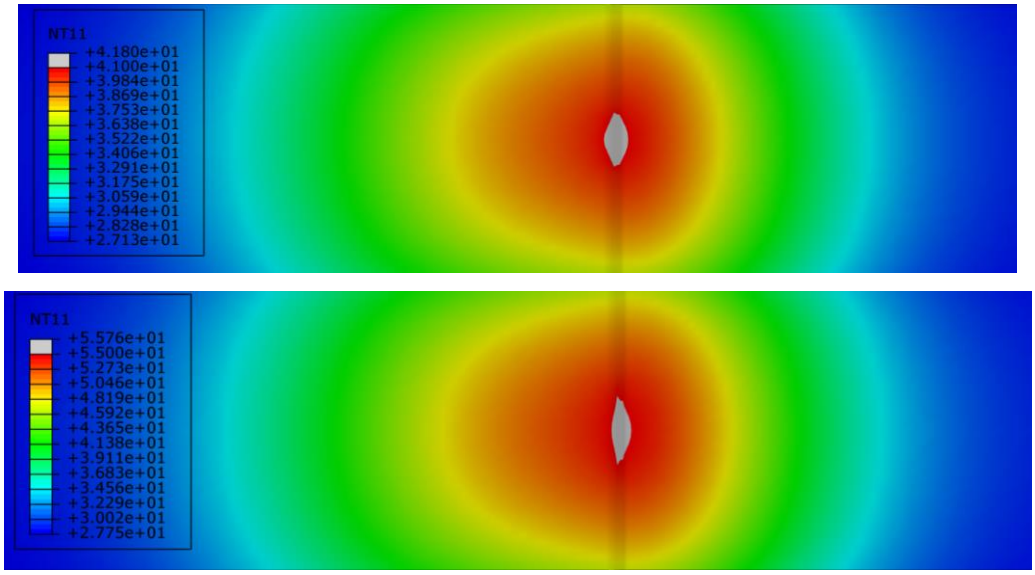

Figure 6.16: The increase in the Hot – Spot due to the damage propagation / the Hot – Spot is depicted by the grey area

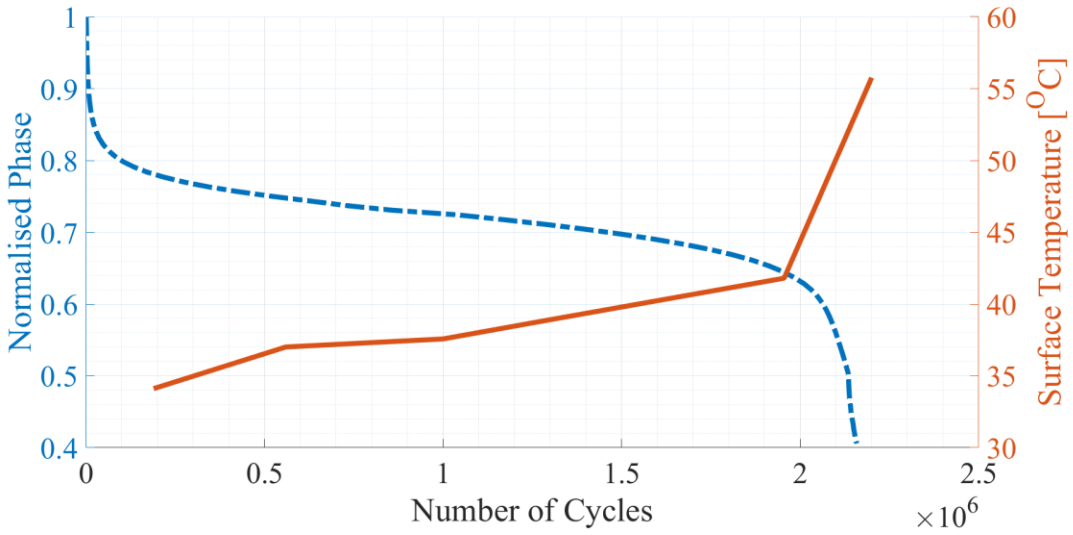

Figure 6.17: Simulated Phase and Self – Heating Temperature Evolutions (based on the interrupted tests) at 25 °C

6.4. The relationship between the Thermal and Mechanical Responses

It can therefore be appreciated that the increase in self – heating temperature is governed primarily by the damage size. The different strain and ambient temperature levels can only contribute towards the accelerated accumulation of a particular damage size. It is therefore possible to apply the aforementioned empirical relation against various severities since their effect is minimal. Nevertheless, this model does not consider the contribution of the higher ambient temperatures. The rate of accumulation of viscoelastic heat differs according to the surrounding thermal conditions. Thus, the empirical relation established is not able to capture accurately the influence of the accumulation of number of cycles in harsher environments. This obstacle was overcome through in – depth analysis of the experimental results and the development of a new empirical relation which is based on the interrupted tests as well as on the phase – self – heating temperature curves presented in Chapter 4.

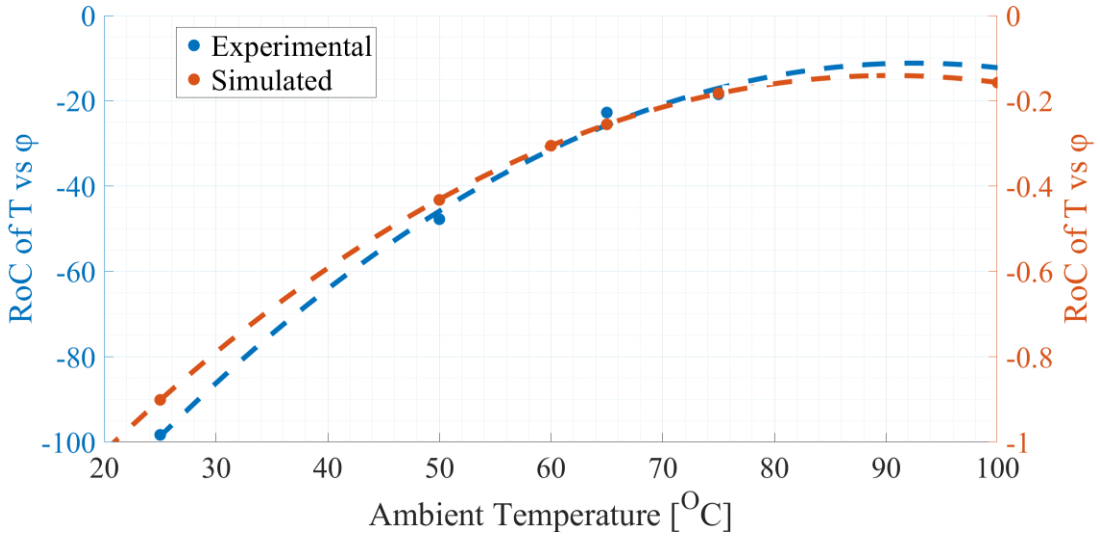

Figure 6.18: Experimental and Simulated Rate of change of the "Self – Heating over Phase" curves

The first step for the development of the new empirical relation is depicted in Figure 6.18. Chapter 4 described how the phase – self – heating temperature (PvT) curves form linear patterns while their rate of change (RoC) is mainly affected by the ambient

temperatures. Figure 6.18 presents the "reverse" RoC of those curves. Thus, the RoC of the self – heating temperature against the response phase was extracted, for the available elevated temperature tests. This way, it is possible to relate the phase decay with the increase of the internal temperature while taking into account the ambient conditions. It is therefore possible to simulate the change in slopes due to the ambient conditions.

Furthermore, it has been illustrated that the simulated phase decay can be correlated with its experimental counterpart thought the use of the VCCT, when they are both excited at the same strain level. Figure 6.19 shows how the phase, extracted by the final interrupted test, can be associated to the simulated phase decay. It is clear that the simulated phase decay is greater than the experimental. However, the specific moments of the evolution of the simulated phase can be correlated to each interrupted test as well as to their respective terminal self – heating temperatures, which were captured thought the IR Camera (Chapter 4). Hence, the simulated phase – self – heating temperature (PvT) curve can be sketched for the 25 °C, utilising the results from both VCCT and the thermal model (Figure 6.17).

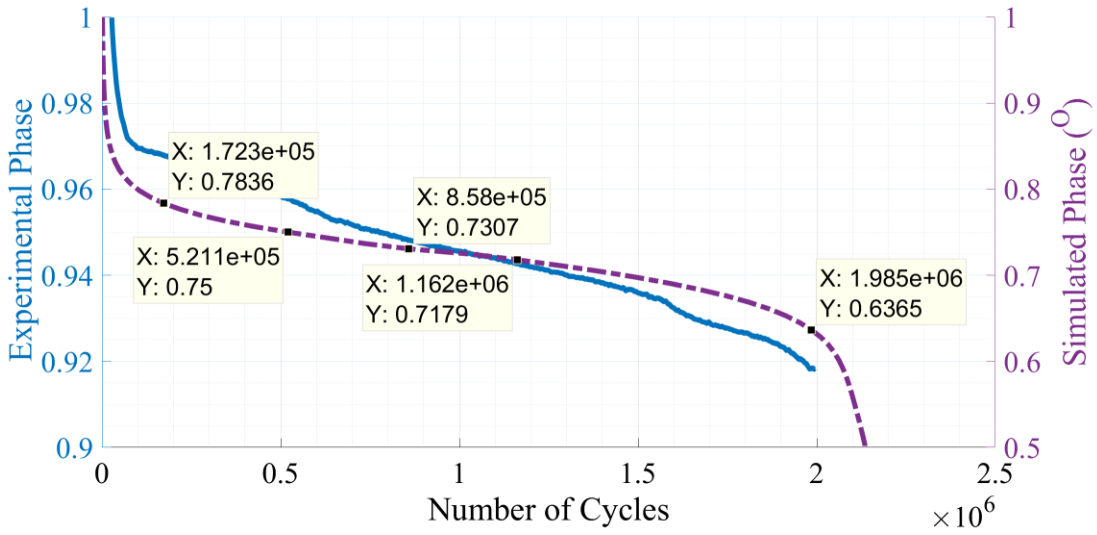

Figure 6.19: A comparison between the final interrupted test and its simulated counterpart

In addition to these, it was discussed extensively how both the response phase and the self – heating temperature of a testing coupon are mainly governed by the fatigue damage. This implies that a specific amount of damage should always result in a specific increase

in self – heating temperature under similar environmental conditions. This is due to the fact that the damage size is driven by the amount strain energy of the system and not by the ambient conditions. Hence, the phase values of Figure 6.19, were also used for creating the PvT curves at elevated temperatures.

In conclusion, the following were obtained:

- FE models were able to simulate the PvT curve.
- A method was developed which simulated the change in the inclination of the PvT curves due to the environmental temperatures.
- A method was developed which correlated the simulated phase decay and the self – heating temperature.

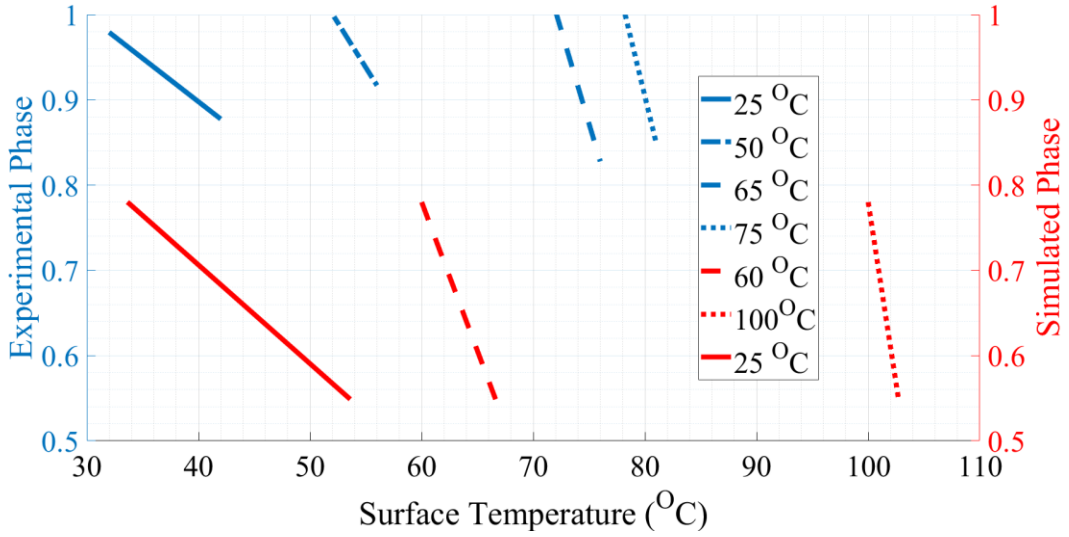

Figure 6.20: A comparison between the Experimental and Simulated "Phase over Self – Heating Temperature" Curves

This information can then be used to develop an empirical relation to simulate the self – heating temperature at elevated temperatures while taking into account the impact of the advancing number of cycles. The results regarding this set of simulations can be summarised in Figure 6.18 and Figure 6.20. The simulated curves follow closely the experimental observations. As a matter of fact, the graphs trace similar linear patterns of analogous rates of change. What is more, the model managed to simulate the behaviour at

an ambient temperature of 100 °C, where the experimental investigation was not possible. This implies that the model is capable to simulate the behaviour at a wide range of temperatures.

6.5. Discussion on the vibration Fatigue Testing

6.5.1. The Critical Event

So far, the vibration fatigue of composite laminates was investigated using both experimental and numerical approaches. All these tests generated data that could greatly expand the current knowledge about high frequency vibration fatigue. Nevertheless, we have yet to discuss the nature of the Critical Event. In particular, what is the source of the Critical Event?

Previous studies on resonance testing, successfully captured and introduced the Critical Event for the first time [50], [68]. However, the data acquired for the purpose of the current study can be combined to provide a better understanding of the natural phenomenon behind the Critical Event. As it was discussed previously, the strength of a FE model can be attributed to the fact that it can expand over the limitations of the high frequency vibration testing and it is able to capture information that can be challenging to observe experimentally.

On such set of parameters is the localised behaviour at the root of the crack. Figure 6.21 presents the typical opening forces and their resulting displacements, at the crack tip during the vibration fatigue life, as simulated by VCCT. The data are relative to the characteristic modes of separation (mode I and II). Additionally, the figure traces a comparison between the typical opening forces / displacements and the fatigue life as it captured by the phase decay. The first thing that can be noticed, is that the mode I opening force is becoming more dominant as the damage grows, which gives rise to an increasing mode I displacement at the crack tip.

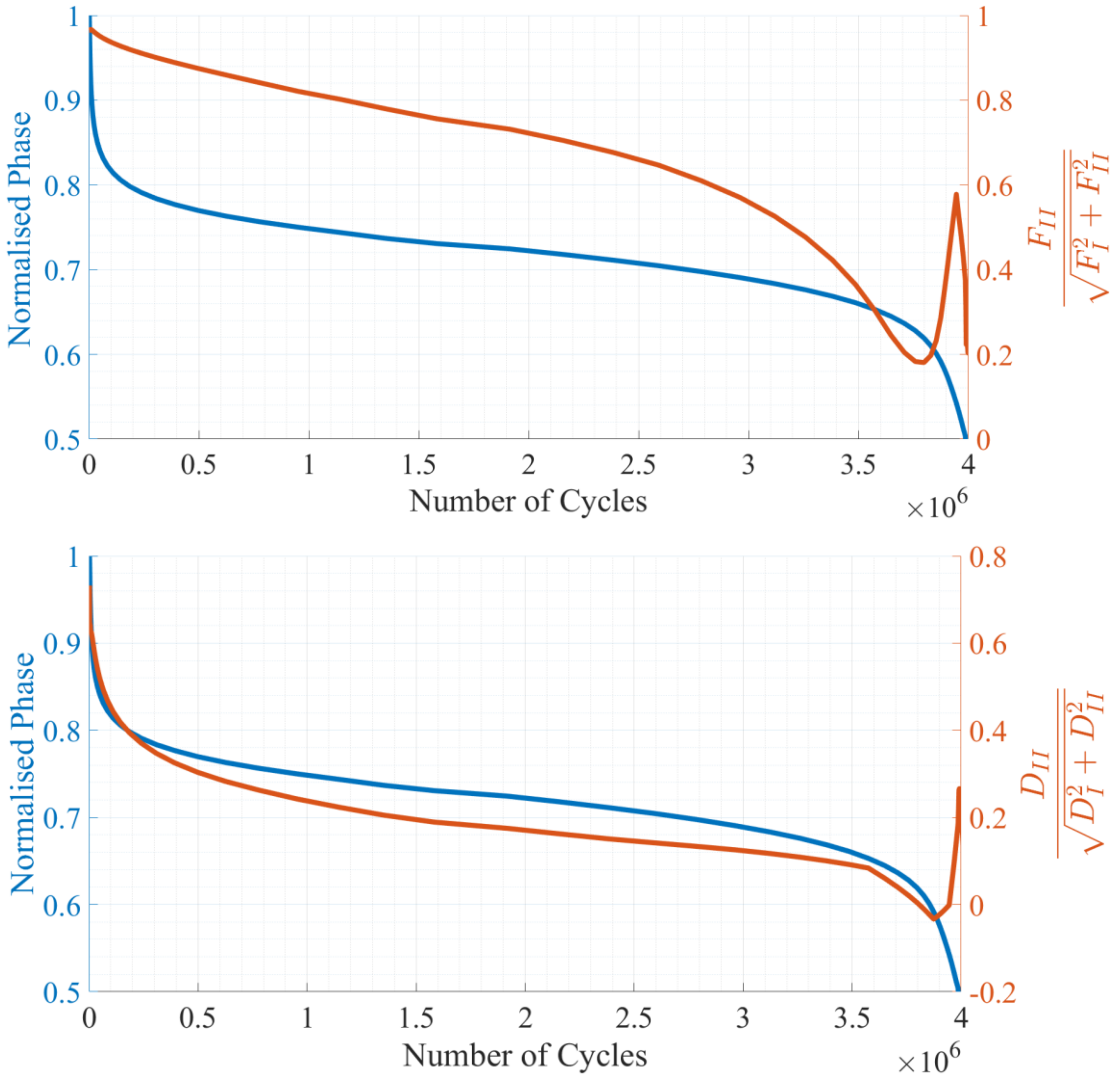

Figure 6.21: Typical Phase and Modes of Separation Responses as captured by VCCT / Top – Mode Mixity Force Ratio / Bottom – Mode Mixity Displacement Ratio

In the previous section, it was also discussed for the first time that the Critical Event corresponds to a Critical Damage Size, which remained unchanged across the different numerical scenarios that were investigated. In fact, Figure 6.21 indicates that mode I is the dominant mode of separation at the moment of the Critical Event. Thus, the mode I force drives the crack to open mainly in mode I. Hence, the relative minimum at the force ratio graph is followed by a relative minimum at the displacement ratio graph.

Figure 6.22 presents the behaviour of the ply over the crack, at different stages in the fatigue life. The lines plotted at Figure 6.22, correspond to different number of cycles which coincide to an early stage in the fatigue life (2.16×10^6), the Critical Event (3.8×10^6) or the peaks presented in Figure 6.21 (3.96×10^6, 4.03×10^6 and 4.04×10^6). It is worth noting that Figure 6.22 appears to be inclined since it follows the mode shape of the specimen during this stage of the vibration cycle.

In other words, the behaviour observed, in Figure 6.21 during the Critical Event, implies that the Critical Damage Size corresponds to the damage area required for plies above the crack to buckle and force the crack to open. Prior to this moment, excessive buckling was not present at the plies (Figure 6.22). Thereafter, the rate of propagation accelerates rapidly under the effect of an increasing mode II. Another minimum in the force ratio graph can be observe but the resulting displacement ratio is not as low as the first one, since the delaminated area is much larger at this stage and mode II seperation is significantly increased. However, it can be assumed that this behaviour can further support the accelerated damage propagation.

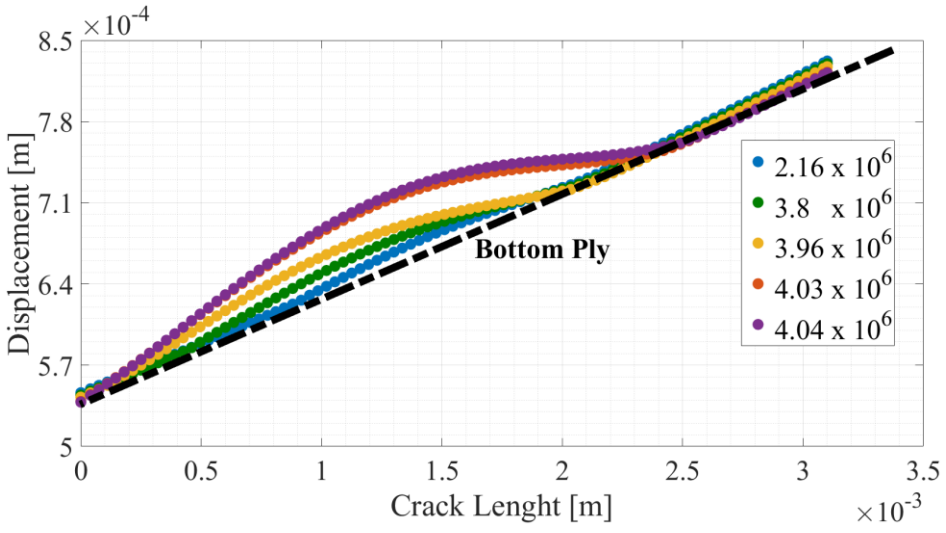

Figure 6.22: Nodal Displacement at different stages of the simulated fatigue life (Number of Cycle)

6.5.2. Crack Growth Propagation Rate

As it can be easily understood, there are multiple cases during which the extraction of experimental data under high frequency testing is rather challenging, even though during low frequency testing can be a trivial task to extract the same properties.

The search for improved ways to extract important information from a structure subject to vibration testing, is the logical step forward. One representative case of this scenario is the extraction of the material properties of a laminate specimen. It was shown how the crack growth rate can be employed in order to extract the Paris Law parameters and simulate the fatigue life of composite components. In addition, Figure 6.4 illustrated that the phase is strongly dependent on the damage size. It is therefore logical to assume that the rate of change of vibration phase can be correlated to the crack growth rate.

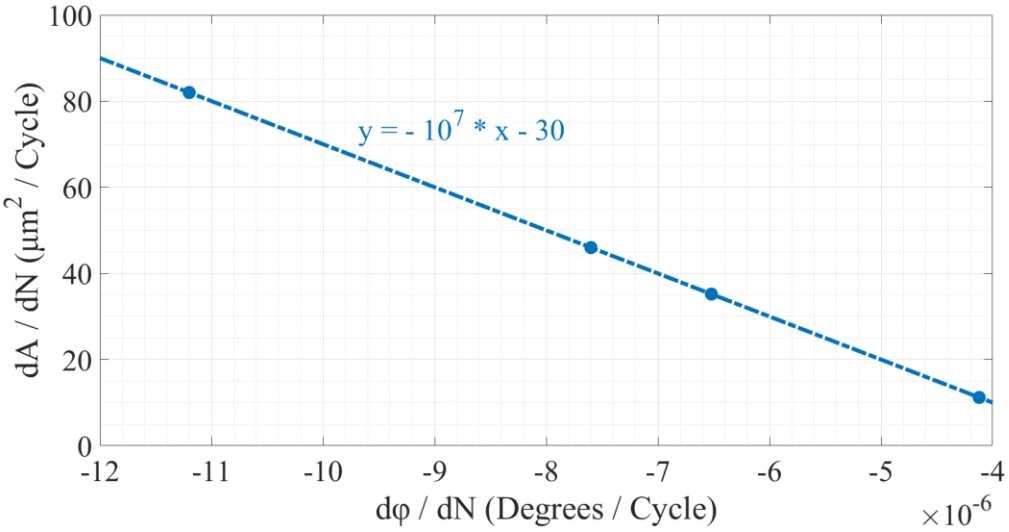

Figure 6.23: Damage Growth Rate against Response Phase Decay

The interrupted tests were employed once again to confirm this hypothesis. Figure 6.23 traces the relation between the damaged area and the respective phase decay. The CT scan analysis revealed that the damage will open along the length and the width of the specimen during endurance testing; at the same time. For this reason, Figure 6.23 presents the damaged area instead of the crack length. It is apparent that the vibration phase is linearly related to the damage size.

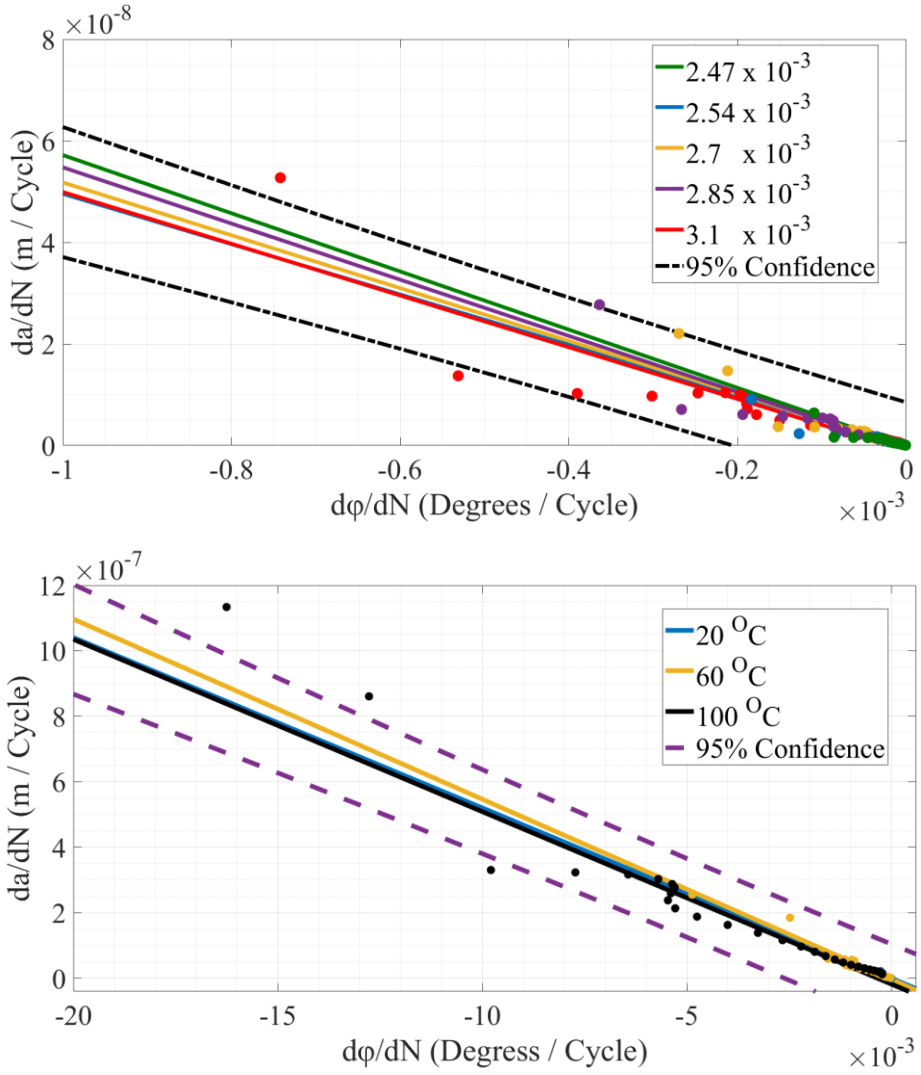

Figure 6.24: Simulated Damage Growth Rate against Response Phase Decay / Top – Same ambient Temperature but different strain levels / Bottom – Different ambient Temperatures but same severity

Unfortunately, the interrupted tests investigated the behaviour only at one ambient Temperature and for a single strain level. Once again, the VCCT can be exploited to provide a better insight in the phase – damage relation. Figure 6.24 holds the relation between the phase decay and the crack growth rate, as simulated for different ambient temperature and strain levels. It is clear that phase – crack relation is not affected greatly by the surrounding temperature or the applied severity. In fact, Figure 6.24 demonstrates a linear relation for all the cases that were studied; similar to the experimental observations of Figure 6.23. It is worth noting that linear forecasts were employed alongside the fitted lines in order to aid the better comparisons between the simulated results, since higher severities and harsher environmental conditions could lead to accelerated crack growth rates. Hence, lower propagation rates could be too small to plot alongside the cases that wield rapid damage opening, without the use of forecasts. However, for completion reasons, the actual simulated data are also presented in Figure 6.24. Additionally, the few outliers that are apparent on this figure correspond to the final steps of the fatigue life (after the Critical Event) where the crack growth rate is not as stable.

In conclusion, it is apparent that the data presented on this section hint that phase decay could be exploited in order to capture the crack growth rate, during vibration fatigue testing. Then, a numerical model can be exploited to establish a Paris Law for the material system that is investigated.

6.6. Remarks

The FE methods established in Chapter 5, were employed in order to strengthen the knowledge about the physics that governs the fatigue damage development of carbon reinforced composites subjected to elevated temperature conditions. For this reason, fatigue tests simulations were performed in a synthetic FE dynamic environment exploring the effects of different mechanical and thermal loads. The numerical results were correlated against their experimental counterpart.

It became quickly apparent that the Virtual Crack Closure Technique was able to successfully reproduce the path followed during damage opening under high frequency vibration loading, while being also able to trace a response phase decay, characterised by a Critical Event; similar to its experimental counterpart. Moreover, it was noticed that the simulated fatigue lives at various severities are in line with the experimental data. As a result, the VCCT indicated that it is able to simulate the fatigue life at a various range of applied cyclic loads. In a similar manner, the VCCT approach was also able to capture the fatigue life of CFRP laminates, by means of phase deterioration, supporting the development of simulated SN Curves. It was therefore able to anticipate the increase in stiffness deterioration due to the higher ambient temperatures.

The strength of the VCCT however lies with its capability to provide insight over multiple variables of the systems which could be challenging to track experimentally, during a high frequency vibration test. As such, it was possible to study the crack growth rate under different conditions. As it was expected, the propagation is accelerated when subjected to higher severities but the phenomenon is more profound under different surrounding temperatures.

In general, it was observed that the damage accumulation follows a Paris Law behaviour even under vibration testing at different ambient temperature conditions. Additionally, the crack growth rate increases as the test evolves which corresponds to the increase of the strain energy release rate. This information confirms the behaviour that was indicated through tracking the phase decay experimentally (Figure 4.17). It was hinted that

the crack growth rate is lower before the Critical Event and higher after that, corresponding to an increased and decreased phase deterioration before and after the Critical Event, respectively. As a result, the simulated phase traces the same patterns.

With the simulated data being confirmed by the experimental analysis, the VCCT was then applied into more complicated scenarios. More specifically, it was employed as a proof of concept in order to show that the fatigue life can be extended under the application of different thermal loads; following the experimental observations. Even though a prismatic 2D model was considered, it seemed that the experimental behaviour was successfully reproduced.

On the other hand, the thermal response of a tapered CFRP specimens was captured through the implementation of a multi – physics FE model. The numerical approach revealed that the equilibrium and Critical Event temperatures are only affected by the ambient temperature conditions. In fact, the combined investigation of the VCCT and the thermal model revealed that both the thermal and mechanical responses a predominantly dominated by the fatigue damage size. This observation along with the establishment of an empirical relation, which considers the energy lost per cycle to simulate the thermal life at various temperature conditions lead to the connection between the two; through the use of FE models.

Finally, it was shown that the Critical Event is characterised by a dominant mode I separation which is the result of buckling in the plies above the delaminated area. Additionally, it was demonstrated that the phase decay could be exploited to provide in situ monitoring of the damage propagation during high frequency vibration testing. Thus, it was indicated that simultaneous experimental and numerical investigations could be employed to establish a Paris Law for the material system that is under consideration.

Chapter 7

CONCLUSIONS

7.1. The novelties

As stated in the title, this thesis offered an examination regarding the vibration fatigue of composites under various environmental temperature conditions. Even though, the literature review highlighted that multiple studies had already investigated the effects of ambient temperatures, it also arrived in the conclusion that the combined effect of vibration and thermal loads were never employed in the past; for the analysis of the fatigue behaviour in composites. As a result, the objectives of this project were:

1. First and foremost to develop an experimental technique for the investigation of vibration fatigue of composites, at different exposure temperatures; exploiting a failure criterion (Critical Event) that had already been introduced for resonance testing.
2. To utilise the aforementioned technique in order to examine, for the first time, the influence of the elevated ambient temperatures, over the Critical Event
3. To simulate the mechanical response of the composite laminates that was observed during the experimental investigation. Additionally, this project introduced a method for simulating the rise in self – heating temperature of the specimens during high frequency testing while always taking into account the ambient conditions.
4. To demonstrate the feasibility of the FE models, correlating the experimental and the numerical results.

The new experimental method was addressed in Chapter 3, where many parameters were studied and presented in order to establish a repeatable vibration testing procedure which incorporates the effects of ambient thermal loads. Therefore, the ground was set for the examination of structural degradation of composite components during resonance testing. This Chapter aimed to be a guidance for the endurance testing of specimens, when

subjected to similar experimental conditions; thus, identifying the weak and strong points of the experimental procedure.

Chapter 4 offers to the literature an extensive data set, acquired using the aforementioned testing procedure. In fact, CT scan analysis employed, for the first time, in specimens that had undergone vibration testing in order to examine the damage accumulation. In contrary to what was proposed by previous studies, CT scan data revealed that the damage occurs well before the Critical Event. Thus, the results hinted that the Critical Event corresponds to a Critical Damage size beyond which the resistance to damage is minimised. Moreover, both the mechanical and thermal responses, of a composite specimen, can be separated into three distinct quasi – linear regions:

- Test initiation (Transient State)
- Test Evolution – before the Critical Event
- Test Conclusion – after the Critical Event

Experimental results suggested that in each of these regions, the rate of decay (for the mechanical response) and the rate of increase (for the thermal response) are proportional to the crack growth rate.

For this reason, an investigation was performed in order to examine the relation between the mechanical and thermal responses. It became quickly apparent that the two responses are linked linearly and their relation is dependent solely on the ambient temperature conditions. This dependency hints that the fracture toughness of the material is mainly influenced by the ambient temperatures, since the responses of the specimen are related strongly to the crack growth rates.

In addition to these, the experimental results revealed that the vibration fatigue lives of composite laminate, deteriorate under the effect of harsher environmental temperatures. On can therefore easily understand why a different experimental scenario was employed, as a proof of concept, aimed to suppress the damage propagation through localised cooling. It was revealed that the damage accumulation can successfully suspended, utilising this method.

The next objective was described in Chapter 5. Even though the experimental analysis hinted numerous different phenomena (e.g. the Critical Damage size), the high frequency testing can set certain limitations in the information that can be captured experimentally. In particular, experimental parameters (e.g. crack growth rate, frictional heat) are principally challenging to extract during resonance testing. For this reason, a necessity emerged in order to simulate the mechanical and thermal responses of a coupon. Chapter 5 introduced a VCCT based method to simulate the dependency of the Critical Event during different ambient thermal loads.

Additionally, the thermal response was also simulated, too. For this purpose, a novel multi – physics numerical model was developed, aiming to reproduce the self – heating temperature evolution during vibration testing. This was not a trivial task, since the self – heating temperature is attributed to the combined effect of viscoelastic and frictional heat. Hence, the two heat sources were simulated, employing novel numerical models while paying close attention to important material parameters (e.g. friction, thermal conductivity) which are not commonly discussed in literature.

Chapter 6 accommodated more than just a presentation of the numerical results, acquired by the aforementioned methods. In fact, it illustrated how a semi – empirical relation, that takes into account the energy lost per cycle, can be employed to simulate the increase of the self – heating temperature during vibration testing. The relation lead to a good correlation between the experimental and numerical results, when carefully considering parameters such as the friction forces, heat dissipated due to convection and the surrounding temperature conditions.

Furthermore, interesting information were gathered from the simulation of the mechanical response, too. The VCCT results seemed to follow closely the experimental behaviour. In fact, it was presented that the simulated Critical Event at elevated temperatures, follows an identical behaviour to the experimental observations. The simulated fatigue life, at harsher temperature conditions, was characterised by an accelerated phase decay. This method was then employed for simulating more complicated

behaviours; confirming that the propagation of damage can be suspended through the application of localised thermal loads.

The two numerical methods were then employed to simulate the relation between the mechanical and thermal responses. It was illustrated that the two responses can be linked linearly, following once again the experimental observations, closely.

Furthermore, it was confirmed that the fatigue damage size at the moment of the Critical Event, corresponds to a Critical Damage size; which remains unaffected by the ambient temperature or even the applied level of severity. In particular, it was demonstrated, for the first time, that the Critical Damage Size is the source of intense buckling at the plies over the delaminated area. The simulations also revealed that this phenomenon will lead to a dominant mode I separation, resulting to acceleration in the crack propagation.

Finally, the relation between the phase decay and the accumulation of damage was explored, both experimentally and numerically. It was observed that the two are linked linearly. Thus, it was hinted that the crack growth rate can be captured, in situ, exploiting the phase decay during the resonance endurance testing.

7.2. Future Work

All things considered, this investigation has a few aspects that can be improved, following the comments provided in the end of each chapter.

First of all, this study introduced a novel testing method for characterising the fatigue life of CFRPs under dynamic and thermal loads. However, the robustness of the experimental technique can only be validated when different scenarios are exploited. In particular a wider range of environmental temperatures, including sub – zero temperatures, should be explored in order to provide a better insight on the fatigue behaviour of composites. Alongside these, the examination of different environmental effects (e.g. moisture) should also be considered. Most importantly, it is crucial to expand the knowledge around the damage suspension through the application of different thermal

loads. Moreover, it could also be interesting to study how different material systems react under vibration fatigue testing in order to acquire a better understanding about the testing methodology. Additionally, the study of specimens which incorporate different stress raisers (e.g. cut ply) could enhance our understanding about the phase decay and its connection to the damage accumulation.

Studying the accumulation of damage in IM7 / 8552 is also important. An extensive test campaign needs to be performed to establish the threshold values at numerous temperature and strain conditions. Once a wide data set has been developed, the propagation of damage can be analysed from an in – depth CT scan analysis of interrupted test at different ambient temperature environments. Thus, the failure mechanisms at various temperatures can be revealed. Moreover, the examination of the damage evolution can lead to the identification of a damage size threshold which corresponds to the Critical Damage Size and its respective percentage of phase decay; as indicated by the numerical analysis. The author would suggest that the first step towards the successful completion of this rigorous testing campaign is to eliminate the challenges that come with the vibration testing method (e.g. the dependency of strain gauges to ambient temperatures).

Another interesting aspect for further investigation is the in – situ damage monitoring. As indicated by the current project, the crack growth rate can be monitored through the deterioration in the response phase. As a result, a dedicated study could make the necessary changes in the current experimental procedure in order to trace the damage opening during vibration testing. In fact, it could also be possible to capture other important information during high frequency testing. As a matter of fact, previous studies have shown that the strain energy can be evaluated through the bending moment of the delaminated area which could also be exploited for vibration fatigue testing. Additionally, as it was indicated, simultaneous experimental and numerical investigations could be employed to establish a Paris Law for the material system that is under consideration.

On the numerical side, multiple steps forward are still necessary. It is essential to evaluate the Paris Law parameters, for various temperatures, in order to be able to simulate the mechanical response of IM7 / 8552 specimens. For completion purposes, the VCCT

should also be employed to simulate the mechanical response, on a 3D model. Nevertheless, there are more challenges associated with the simulation of the self – heating evolution. The first step would be to evaluate the temperature / orientation dependent parameters (e.g. thermal conductivity). The friction coefficient should also be considered, even though, the experimental investigation of friction forces in a delaminated area could be extremely challenging. Another aspect of great importance is the loss factor. In particular, an extensive study regarding the evolution of Strain Energy should be employed alongside an analysis of thermal images to acquire the dissipated energy at different conditions.

What suggested in this section, describe the authors point of view forward and they are not meant to define a precise procedure. Instead, they should be considered as an indication of possible interesting future research work.

BIBLIOGRAPHY

[1] G. Slayter, “Method of making glass wool”, 1939.

[2] W. Schütz, “A history of fatigue”, *Eng. Fract. Mech.*, vol. 54, no. 2, pp. 263–300, 1996.

[3] U. Plumbridge W. J. (University Engineering Department, Cambridge, “Fatigue-crack propagation in metallic and polymeric materials”, *J. Mater. Sci.*, no. 7, pp. 939–962, 1972.

[4] O. Kolednik, “Fracture Mechanics”, *Wiley Encycl. Compos.*, vol. 37, pp. 171–183, 2012.

[5] G. R. Irwin, “Analysis of Stresses and Strains Near the End of a Crack Traversing a Plate”, *J. Appl. Mech.*, pp. 361–364, 1957.

[6] M. P. Paris, P. C.; Gomez and W. E. Anderson, “A rational analytic theory of fatigue”, *Trend Eng.*, vol. 13, pp. 9–14, 1961.

[7] J. L. Dew-Hughes, D.; Way, “Fatigue of fibre - reinforced plastics: a review”, *Composites*, pp. 167–173, 1973.

[8] K. Reifsnider, “Fatigue behavior of composite materials”, *Int. J. Fract.*, vol. 16, pp. 563–583, 1980.

[9] R. Talreja, “Damage and fatigue in composites - A personal account”, *Compos. Sci. Technol.*, vol. 68, pp. 2585–259, 2008.

[10] Z. Hashin, “Analysis of cracked laminates: a variational approach”, *Mech. Mater.*, vol. 4, no. 2, pp. 121–136, 1985.

[11] J. A. Nairn, “The Strain Energy Release Rate of Composite Microcracking: A Variational Approach”, *J. Compos. Mater.*, vol. 23, no. 11, pp. 1106–1129, 1989.

[12] J.A.Nairn and S.Hu, “The initiation and growth of delaminations induced by matrix microcracks in laminated composites”, *Int. J. Fract.*, vol. 57, pp. 1–24, 1992.

[13] R. Talreja, “Internal variable damage mechanics of composite materials”, in *Yielding, Damage, and Failure of Anisotropic Solids*, J. P. . Boehler, Ed. London: Mechanical Engineering Publications, 1990, pp. 509–533.

[14] M. Alvarez, “Characterization of impact damage in composite laminates”, Bromma, 1998.

[15] V. Z. Parton, *Fracture Mechanics: From Theory to Practice*. Gordon and Breach Science Publishers, 1992.

[16] R. B. Pipes and N. . Pagano, “Composite Laminates Under Uniform Axial Extension”, *J. Compos. Mater.*, vol. 4, pp. 538–548, 1970.

[17] C. Mittelstedt and W. Becker, “Free-Edge Effects in Composite Laminates”, *Appl. Mech. Rev.*, vol. 60, no. 5, p. 217, 2007.

[18] A. Committee, “Standard Terminology Relating to Fatigue and Fracture Testing”, *ASTM Int.*, vol. E1823, no. 13, pp. 1–25, 2014.

[19] F. Magi, “Vibration fatigue testing for identification of damage initiation in composites”, PhD Thesis, University of Bristol, 2016.

[20] M. D. Sangid, “The physics of fatigue crack initiation”, *Int. J. Fatigue*, vol. 57, pp. 58–72, 2013.

[21] M. J. Salkind, “Fatigue of composites”, *Compos. Mater. Test. Des. (2nd Conf), ASTM STP 497, Am. Soc. Test. Mater.*, pp. 143–169, 1972.

[22] M. Quaresimin and M. Ricotta, “Fatigue behaviour and damage evolution of single lap bonded joints in composite material”, *Compos. Sci. Technol.*, vol. 66, no. 2, pp. 176–187, 2006.

[23] G. D. Sims, “Fatigue test methods, problems and standards”, in *Fatigue in Composites*, B. Harris, Ed. Whoodhead Publishing Limited, 2003, pp. 36–62.

[24] M. May and S. R. Hallett, “A combined model for initiation and propagation of damage under fatigue loading for cohesive interface elements”, *Compos. Part A Appl. Sci. Manuf.*, vol. 41, no. 12, pp. 1787–1796, 2010.

[25] M. May and S. R. Hallett, “An assessment of through-thickness shear tests for initiation of fatigue failure”, *Compos. Part A Appl. Sci. Manuf.*, vol. 41, no. 11, pp. 1570–1578, 2010.

[26] L. E. Asp, “The effects of moisture and temperature on the interlaminar delamination toughness of a carbon/epoxy composite”, *Compos. Sci. Technol.*, vol. 58, no. 6, pp. 967–977, 1998.

[27] C. Beland, S.; Komorovski, J. P.; Roy, “Hygrothermal influence on the interlaminar fracture energy of graphite/bismaleimide modified epoxy composite (IM6/5245C)”, in *International Conference on Composite Materials VI*, 1987, pp. 305–303.

[28] A. J. Russell, “Micromechanisms of interlaminar fracture and fatigue”, *Polym. Compos.*, vol. 8, pp. 342–351, 1987.

[29] Russell, Street, “ASTM STP 876: Moisture and temperature effects on the mixed-mode delamination fracture of unidirectional graphite/epoxy”, *Delamination Debonding Mater.*, pp. 349–370, 1985.

[30] H. Horiguch. K. Shindo, Y. Wang, R. Kudo, “Double Cantilever Beam Measurement and Finite Element Analysis of Cryogenic Mode I Interlaminar Fracture Toughness of Glass-Cloth/Epoxy Laminates”, *J. Eng. Mater. Technol.*, no. 123, pp. 191–197, 2000.

[31] N. S. Okad., T. Hond., “Evaluation of Epoxy Resin by Positron Annihilation for Cryogenic Use”, *Adv. Cyrogenic Eng.*, pp. 1137–1144, 1994.

[32] S. Hartwig, G. Knaak, “Fibre-epoxy composites at low temperatures”, *Cryogenics (Guildf).*, no. 24, pp. 639–647, 1984.

[33] M. B. Kasen, “Cryogenic properties of filamentary-reinforced composites: an update”, *Cryogenics (Guildf).*, no. 21, pp. 323–340, 1981.

[34] A. Sjögren and L. E. Asp, “Effects of temperature on delamination growth in a carbon/epoxy composite under fatigue loading”, *Int. J. Fatigue*, vol. 24, no. 2–4, pp. 179–184, 2002.

[35] J. R. Gregory and S. M. Spearing, “Constituent and composite quasi-static and fatigue fracture experiments”, *Compos. Part A Appl. Sci. Manuf.*, vol. 36, no. 5, pp. 665–674, 2005.

[36] G. Charalambous, G. Allegri, and S. R. Hallett, “Temperature effects on mixed mode I/II delamination under quasi-static and fatigue loading of a carbon/epoxy composite”, *Compos. Part A Appl. Sci. Manuf.*, vol. 77, pp. 75–86, 2015.

[37] G. Charalambous, G. Allegri, and S. R. Hallett, “Temperature effects on mixed mode I/II delamination under quasi-static and fatigue loading of a carbon/epoxy composite”, *Compos. Part A Appl. Sci. Manuf.*, vol. 77, pp. 75–86, 2015.

[38] D. Di Maio and F. Magi, “Development of testing methods for endurance trials of composites components”, *J. Compos. Mater.*, vol. 49, no. 24, pp. 2977–2991, 2015.

[39] O. Kovářík, “Resonance bending fatigue testing with simultaneous damping measurement and its application on layered coatings”, *Int. J. Fatigue*, 2015.

[40] J.-K. J. Youngjung Ke, Seung-Ho Kim, Jung-Ho Han, “Resonant Fatigue Testing of Full-Scale Composite Helicopter Blades”, *ECCM 15th*, no. June, pp. 1–4, 2012.

[41] S. H. Han, D. G. An, S. J. Kwak, and K. W. Kang, “Vibration fatigue analysis for multi-point spot-welded joints based on frequency response changes due to fatigue damage accumulation”, *Int. J. Fatigue*, vol. 48, pp. 170–177, 2013.

[42] P. Lorenzino and A. Navarro, “The variation of resonance frequency in fatigue tests as a tool for in-situ identification of crack initiation and propagation, and for the determination of cracked areas”, *Int. J. Fatigue*, vol. 70, pp. 374–382, 2015.

[43] K. G. McConnell, *Vibration testing - Theory and Practice*. John Wiley & sons, Inc., 1995.

[44] T. J. Adam and P. Horst, “Experimental investigation of the very high cycle fatigue of GFRP [90/0]scross-ply specimens subjected to high-frequency four-point bending”, *Compos. Sci. Technol.*, vol. 101, pp. 62–70, 2014.

[45] D. Backe, F. Balle, and D. Eifler, “Fatigue testing of CFRP in the very high cycle

fatigue (VHCF) regime at ultrasonic frequencies", *Compos. Sci. Technol.*, vol. 106, pp. 93–99, 2015.

[46] B. J. Lazan, "Fatigue failure under resonant vibration conditions", no. March, p. 58, 1954.

[47] F. Just-Agosto, A. Peralta, B. Shafiq, and D. Serrano, "A vibration technique to obtain fatigue", *ICCM17proceedings*, 2009.

[48] W. Gu, J.; Sol, H.; Van Paepegem, "The study of resonance fatigue testing of test beams made of composite material", in *PACAM XI*, 2009.

[49] A. Pickard, "High Cycle Endurance of Carbon Fibre Reinforced Plastic: Delamination Prediction and Measurement", University of Bristol, 2012.

[50] F. Magi, D. Di Maio, and I. Sever, "Damage initiation and structural degradation through resonance vibration: Application to composite laminates in fatigue", *Compos. Sci. Technol.*, vol. 132, pp. 47–56, 2016.

[51] J. S. Earl and R. A. Shenoi, "Hygrothermal ageing effects on FRP laminate and structural foam materials", *Compos. Part A Appl. Sci. Manuf.*, vol. 35, no. 11, pp. 1237–1247, 2004.

[52] A. Katunin, "The conception of the fatigue model for layered composites considering thermal effects", *Arch. Civ. Mech. Eng.*, vol. 11, no. 2, pp. 333–343, 2011.

[53] A. Katunin and A. Gnatowski, "Influence of heating rate on evolution of dynamic properties of polymeric laminates", *Plast. Rubber Compos.*, vol. 41, no. 6, pp. 233–239, 2012.

[54] A. Katunin and D. Wachla, "Self-heating based vibrothermography - A non-destructive testing method for polymeric composite structures", *AIP Conf. Proc.*, vol. 1981, no. July, 2018.

[55] A. Katunin, "Thermal fatigue of polymeric composites under repeated loading", *J. Reinf. Plast. Compos.*, vol. 31, no. 15, pp. 1037–1044, 2012.

[56] A. Katunin, "Self-heating effect in laminate plates during harmonic", *Sci. Probl. Mach. Oper. Maint.*, vol. 44, no. 2, pp. 73–84, 2009.

[57] A. Katunin, "Influence of the Self-Heating Effect on Fatigue of Polymeric Laminates", no. June, pp. 24–28, 2012.

[58] A. Katunin and K. Krukiewicz, "Physicochemical analysis of self-heating of glass-epoxy composites cured by novolac", *Chemik*, vol. 66, no. 12, pp. 1326–1331, 2012.

[59] A. Katunin and W. Hufenbach, "Frequency dependence of the self-heating effect in polymer-based composites", *... Achiev. ...*, vol. 41, pp. 9–15, 2010.

[60] A. Katunin, "Critical self-heating temperature during fatigue of polymeric composites under cyclic loading", *Compos. Theory Pract.*, vol. 1, pp. 72–76, 2012.

[61] A. Katunin, "Analytical model of the self-heating effect in polymeric laminated rectangular plates during bending harmonic loading", *Maint. Reliab.*, no. 4, pp. 91–101, 2010.

[62] Y. Miyano, M. K. McMurray, N. Kitade, M. Nakada, and M. Mohri, "Loading rate and temperature dependence of flexural behaviour of unidirectional pitch-based CFRP laminates", *Composites*, vol. 26, no. 10, pp. 713–717, 1995.

[63] Miyano, Nakada, "Prediction of flexural fatigue strength of CRFP composites under arbitrary frequency, stress ratio and temperature", *J. Compos. Mater.*, vol. 31, no. 6, pp. 619–638, 1997.

[64] A. Vassilopoulos, *Fatigue life prediction of composites and composite structures*. Whoodhead Publishing Limited, 2010.

[65] J.R.Rice, "A Path Independent Integral and the Approximate Analysis of Strain Concentration by Notches and Cracks", *J. Appl. Mech.*, vol. 35, no. 2, p. 379, 1968.

[66] T. K. Hellen, "On the method of virtual crack extensions", *Int. J. Numer. Methods Eng.*, vol. 9, no. 1, pp. 187–207, 1975.

[67] R. Krueger, "Virtual crack closure technique: History, approach, and applications", *Appl. Mech. Rev.*, vol. 57, no. 2, p. 109, 2004.

[68] F. Magi, D. Di Maio, and I. Sever, “Validation of initial crack propagation under vibration fatigue by Finite Element analysis”, *Int. J. Fatigue*, vol. 104, pp. 183–194, 2017.

[69] D. Di Maio, “Experimental validation of composites under endurance measurements using a contact-less pulsed air-jet exciter”, in *1st Int. conference on composites dynamics*, 2012, no. DYNACOMP, p. 3.

[70] F. Magi, D. Di Maio, and I. Sever, “Development of a testing method for vibration fatigue at resonance”, *20th Int. Conf. Compos. Mater.*, no. July, pp. 19–24, 2015.

[71] Hexcel, “HexPly 8552 Data Sheet”, pp. 1–6, 2016.

[72] M. A. Gehringer, “Application of controlled displacement stepped sine testing to a nonlinear pin-jointed structure”, *IMAC XII*, p. 3, 1992.

[73] L. Toubal, M. Karama, and B. Lorrain, “Damage evolution and infrared thermography in woven composite laminates under fatigue loading”, *Int. J. Fatigue*, vol. 28, no. 12, pp. 1867–1872, 2006.

[74] E. Z. Kordatos, K. G. Dassios, D. G. Aggelis, and T. E. Matikas, “Rapid evaluation of the fatigue limit in composites using infrared lock-in thermography and acoustic emission”, *Mech. Res. Commun.*, vol. 54, pp. 14–20, 2013.

[75] J. Montesano, Z. Fawaz, and H. Bougherara, “Use of infrared thermography to investigate the fatigue behavior of a carbon fiber reinforced polymer composite”, *Compos. Struct.*, vol. 97, pp. 76–83, 2013.

[76] R. Steinberger, T. I. Valadas Leitão, E. Ladstätter, G. Pinter, W. Billinger, and R. W. Lang, “Infrared thermographic techniques for non-destructive damage characterization of carbon fibre reinforced polymers during tensile fatigue testing”, *Int. J. Fatigue*, vol. 28, no. 10 SPEC. ISS., pp. 1340–1347, 2006.

[77] L. Vergani, C. Colombo, and F. Libonati, “A review of thermographic techniques for damage investigation in composites”, *Frat. ed Integrita Strutt.*, vol. 8, no. 27, pp. 1–12, 2014.

[78] N. G. Stephen, “On energy harvesting from ambient vibration”, *J. Sound Vib.*, vol. 293, no. 1–2, pp. 409–425, 2006.

[79] V. I. . K. S. B. Ratner, “Self-heating of plastics during cyclic deformation”, *Mekhanika Polim. 1*, vol. 3486, no. June, pp. 63–68, 1996.

[80] J. M. Kenny and M. Marchetti, “Elasto-plastic behavior of thermoplastic composite laminates under cyclic loading”, *Compos. Struct.*, vol. 32, no. 1–4, pp. 375–382, 1995.

[81] F. Lahuerta, T. Westphal, A. Oil, and R. P. L. Nijssen, “Self-heating forecasting for thick laminate specimens in fatigue”, February 2016, 2014.

[82] R. Růžek, M. Kadlec, and L. Petrusová, “Effect of fatigue loading rate on lifespan and temperature of tailored blank C/PPS thermoplastic composite”, *Int. J. Fatigue*, vol. 113, no. April, pp. 253–263, 2018.

[83] Russell and Street, “Predicting interlaminar fatigue crack growth rates in compressively loaded laminates”, *Compos. Mater. fatigue Fract.*, pp. 162–178, 1989.

[84] G. Matsubara, H. Ono, and K. Tanaka, “Mode II fatigue crack growth from delamination in unidirectional tape and satin-woven fabric laminates of high strength GFRP”, *Int. J. Fatigue*, vol. 28, no. 10 SPEC. ISS., pp. 1177–1186, 2006.

[85] A. Sjögren, L. Asp, E. Greenhalgh, and M. Hiley, “Interlaminar Crack Propagation in CFRP: Effects of Temperature and Loading Conditions on Fracture Morphology and Toughness”, *Compos. Mater. Testing, Des. Accept. Criteria*, pp. 235-235–18, 2009.

[86] F. Lahuerta, T. Westphal, and R. P. L. Nijssen, “Self-heating forecasting for thick laminates testing coupons in fatigue”.

[87] C. Fiber, “HexTow ® IMA IM7 Datasheet”, vol. 000, pp. 1–2, 2016.

[88] M. T. Saad, S. G. . Miller, and Torrence Marunda, “Thermal Characterization of IM7/8552-1 Carbon - Epoxy Composites”, in *Proceedings of the ASME 2014*

International Mechanical Engineering Congress and Exposition, 2014, pp. 1–8.

[89] Furkan Ismail Ulu, "Measurement of Multidirectional Thermal Conductivity of IM7-G/8552 Unidirectional Composite Laminate", North Carolina A&T State University, 2015.

[90] J. Schön, "Coefficient of friction and wear of a carbon fiber epoxy matrix composite", *Wear*, vol. 257, no. 3–4, pp. 395–407, 2004.

[91] B. Khan, K. Potter, and M. R. Wisnom, "Suppression of delamination at ply drops in tapered composites by ply chamfering", *J. Compos. Mater.*, vol. 40, no. 2, pp. 157–174, 2006.

[92] P. Agastra and J. F. Mandell, "Testing and simulation of damage growth at ply drops in wind turbine blade laminates", *Int. SAMPE Symp. Exhib.*, 2010.